STUDY THE EFFECT OF TOPOGRAPHY DESIGN ON CELLULAR BEHAVIOUR

GOH SEOK HONG

(B. ENG (Hons), Nanyang Technological University)

A THESIS SUBMITTED

FOR THE DEGREE OF DOCTOR OF PHILOSOPHY

DEPARTMENT OF BIOMEDICAL ENGINEERING

NATIONAL UNIVERSITY OF SINGAPORE

2015

DECLARATION

I hereby declare that this thesis is my original work and it has been written by me in its entirety. I have duly acknowledged all the sources of information, which have been used in the thesis.

This thesis has also not been submitted for any degree in any university previously.

Goh Seok Hong

21 August 2015

ACKNOWLEDGEMENT

I would like to express my gratitude and thanks to Dr. Evelyn K.F. Yim and Dr. Low Hong Yee, for their guidance and encouragement throughout these 5 years. Their support and motivation made this thesis possible. Their enthusiasm for science and research inspires me to become a better scientist.

I would also like to thank Dr. Catherine Le Visage and her group in INSERM for their valuable advice and help in my experiments. I am also thankful to Ms Wang Xiaoning and Ms Toh Chin Min from Flow Cytometry Laboratory Unit (NUS, NUMI) for their valuable input and help in flow cytometry for my experiments.

I am also grateful to be a part of the Regenerative Nanomedicine lab. Thanks to all the members, whom have encourage and help me in one way or another. My time in the lab and doing experiment will not be so fulfilling and fun without their company.

Special thanks to the following people whom have made significant contribution to my PhD project in these 5 years. Firstly, I would like to thank my mentor, Dr. Teo Kim Kiat for his time and patience for imparting his skills and knowledge on the biological experiment techniques to me. His insightfulness during discussion enlighten me to see things in different perspective. Next, I would like to thank Ms Marie Cutiongco for her constructive input during project discussion and support in the experiment related to poly (vinyl alcohol) PVA vascular graft project (Chapter 3). I would also like to express my gratitude to Mr Marek Kukumberg for his support in samples fabrication and his valuable contribution in the endothelial cell

screening on various topographies (Chapter 4). Lastly to Mr Daniel Wong and Ms Dawn Neo for volunteering their time for my experiments.

I would also like to thank my colleagues and friends at IMRE, Ms Lim Su Hui, Ms Man Shu Mei, Mr Andrew Ng, Mr Vincent Lim, Ms Ivy Wong and Ms Laura-Lynn Liew. Thank you for being my listening ears when I need someone to talk to.

Lastly, I would like to thank my family and friends for their endless love and encouragement. Their moral support is my source of energy and strength to pursue and complete my PhD study.

TABLE OF CONTENT

SUMMARY

While the importance of topographical cues in directing cellular behaviours are increasingly evident, there is a lack in systematic study to understand and identify the role of topographical designs on cellular behaviours. In this thesis, it is hypothesized that topography can change cellular responses on biomaterials and each topographical design has its individual role in modulating cellular behaviours. This thesis focus on topographical designs for cellular behaviours applicable towards vascular engineering and drug and gene delivery. Firstly, topographical modification was investigated to improve cell responses on poly (vinyl alcohol) (PVA) hydrogel that has poor cell adhesion property. Novel 2 dimensions and 3 dimensions patterning of PVA were successfully demonstrated. I*n vitro* and *in vivo* studies showed improved cell adhesion on patterned PVA. Specifically, 2 μm gratings significantly increased endothelial cell density *in vitro* and maintained graft patency *in vivo* as compared to the unpatterned control. It is apparent that understanding the effect of topographical designs on cellular behaviours can aid in effective selection of topography for different cell responses. Thus, there is a need for a systematic and high throughput screening platform. Multi-architecture (MARC) chip was used to screen and identify more topographical design that modulate various cellular behaviours. For application towards vascular engineering, cell adhesion and proliferation are essential in promoting *in situ* endothelialisation for long term graft patency. Whereas for gene delivery, cell transfection influence the overall efficiency of gene therapy. Screening with MARC chip demonstrated that endothelial cells behaviour, including cell adhesion, proliferation and transfection, can be modulated by topography. In

particular, lenses, hierarchical, nano size gratings and U-gratings topographies were identified to modulate endothelial cells (EC) behaviour. Notably, this is the first demonstration that shows that topography can modulate cell transfection in endothelial cells. The effect of topography on cell endocytosis and cell transfection was further investigated in the last part of the thesis for its potential in drug and gene delivery application. The topography with curvature contains 2 set of topographical design, curvature in z direction and spatial orientation. To understand the effect of each design set, the spatial orientation, similar to the pillars and gratings topography, was selected to be further investigated. In addition, cell types that are more relevant for drug and gene delivery are selected for the study. For instance, stem cells are typically resistant to conventional transfection mechanisms; cancer cells have been a challenging therapeutic target for selective drug and gene uptake. The investigation using molecular internalization showed that the topographical effect were cell type dependent. The effect of topography on endocytosis was observed in human mesenchymal stems cells (hMSCs) but not breast cancer cells (MCF-7). In particular, endocytic activity of hMSCs was enhanced significantly when cultured on 2 μm pillars topography and 200 nm pillars topography can better enhanced hMSCs transfection efficiency. The difference in dominating topographical design is speculated to be effect of topography feature size, activating of different endocytosis pathway. Overall, the study shows that topographical design is essential to control specific cellular responses on biomaterials.

LIST OF TABLES

LIST OF FIGURES

LIST OF ABBERIATIONS

2D	2 dimensions
3D	3 dimensions
bFGF	Basic fibroblast growth factor
CD 31	Platelet EC adhesion molecule
CD 34	Hematopoietic progenitor cell antigen
DAPI	4', 6-diamidino-2-phenylindole
DMEM	Dulbecco's modified eagle's media
DNA	Deoxyribonucleic acid
EC	Endothelial cells
ECM	Extracellular matrix
EPC	Endothelial progenitor cells
eSEM	Environmental scanning electron microscope
FA	Focal adhesions
FBS	Fetal bovine serum
FITC	Fluorescein isothiocyanate
GFP	Green fluorescent protein
HBSS	Hanks' balanced salt solution
HEPES	4-(2-hydroxyethyl)-1-piperazineethane sulfonic acid
hMSCs	Human mesenchymal stem cells
HUVEC	Human umbilical vein endothelial cell
IPN	Interpenetrating polymer network
KS	Kaposi's sarcoma-like
MARC	Multi-architecture
MW	Molecular weight
NIL	Nanoimprint lithography
PA	Poly(acrylamide)
PC	Polycarbonate
PDMS	Polydimethylsiloxane
PEG	Poly(ethylene glycol)
PFA	Paraformaldehyde
PMMA	Poly(methyl methacrylate)
PS	Polystyrene
PVA	Poly(vinyl alcohol)
RC	Radius of curvature
SE	Standard error of the mean
SEM	Scanning electron microscope
Si	Silicon
siRNA	Small interfering ribonucleic acid
STMP	Sodium trimetaphosphate
T_g	Glass transition temperature
TNS	Trypsin neutralization solution
VEGF	Vascular endothelial growth factor
VEGFR2	Vascular endothelial growth factor receptor 2
vWF	Von Willebrand factor

Chapter 1 Introduction

1.1 Background and motivation

1.1.1 The lack of systematic study to identify the role of topography

The importance of extracellular topographical cues in modulating cell behaviours have become increasingly evident in recent studies. Topographical effect on cellular behaviours like cell adhesion, proliferation, differentiation and migration are widely studied and extensively reviewed [1-3]. The collection of topographies studied is widespread, from random to ordered pattern array, isotropic to anisotropic orientation, micron- to nano-size feature, regular to irregular shape geometry and simple to multiple layer patterns. Yet, there is a lack of systematically studies in the role of topographical design in modulating cellular behaviours. Finding a correlation between topographical designs and cellular behaviours in different reports is challenging due to the usage of different cell types, materials and experimental conditions which diminish the significance of research findings. Thus, a platform to identify the role of topography is necessary to provide the key in understanding, controlling and applying topographical cues in the field of tissue engineering and regenerative medicine. In this thesis, a platform will be created to identify the design role of topographies in cellular behaviours with applications in vascular engineering and drug and non-viral gene delivery as the examples.

1.1.2 The lack of endothelial lining on synthetic vascular graft

Driven by the number of increasing patients suffering from cardiovascular disease, researchers in the field of vascular engineering are urgently looking for the ideal vascular graft to solve the patency problem that is, especially

prominent for graft diameters smaller than 6 mm. The lack of endothelialisation causes the loss of the ability to control inflammation, thrombosis and fibrinolysis, thereby leading to graft occlusion [4]. Thus, different strategies were applied to achieve endothelialisation in synthetic graft. Forced seeding of the graft with endothelial cells (EC) prior to implantation [5] and, chemical surface modification [6] with adhesion protein or growth factors to attract and proliferate circulating endothelial progenitor cells (EPC) and EC are widely employed to enhance endothelialisation. Since topographical cues were demonstrated to enhance EC adhesion and proliferation [7], it is another promising approach to improve endothelialisation. Yet, topography has not been widely applied for application in vascular graft. Therefore, it is necessary to understand the topographical designs role in modulating EC behaviour to improve endothelialisation and ultimately aid to maintain vascular graft patency.

1.1.3 Low transfection efficiency in non-viral gene delivery

Efficient delivery of nucleic acid-based drugs is desirable for gene therapy applications. However, toxicity and immunogenic response against viral vector based gene delivery [8] hinders its use in gene therapy. Non-viral gene delivery is a safer approach but is limited by low transfection efficiency of gene expression [9]. Thus, improving the efficiency of non-viral gene delivery is now one of the main focus of gene therapy research. Creating delivery vehicles with high transfection rate is one of the approaches to overcome the delivery barrier. Modification of the chemistry, size, surface charge and shape of delivery vehicles can influence transfection efficiency and are widely explored [10, 11]. Most of the time, the delivery vehicles are injected into the

targeted area and subsequently internalized by the surrounding cells. Meanwhile, substrate-mediated transfection requires the immobilisation of delivery vehicles on the surface before cell interaction. Besides modification of the delivery vehicles, a substrate medicated transfection also utilizes the effect of the underlying substrate to play a role in transfection efficiency. Although the effect of topography is widely studied for other cell behaviours, its implications in endocytosis and transfection is poorly understood. Up until now, there are only a few reports on the use of topography in enhancing substrate-mediated transfection [12-14]. Investigating the effect and design parameters of the topography could greatly progress the non-viral gene delivery system to the next generation.

1.2 Thesis hypothesis

In this thesis, it is hypothesized that topographical design of biomaterials surfaces can direct cellular behaviours and different topographical design parameters, such as curvature and feature size, have its individual role in modulating cellular behaviours.

1.3 Project objectives and aims

The objective of the study is to search and identify the design parameters of topography for specific cellular behaviours applicable towards vascular engineering and drug and non-viral gene delivery. To achieve this goal, the study was further divided into the 3 sub-objectives.

Objective 1: To identify topography to improve EC adhesion with poly (vinyl alcohol) (PVA) hydrogel required for vascular engineering application

Patterning of PVA in 2 dimensions (2D) and 3 dimensions (3D) was explored using casting, nanoimprint lithography (NIL) and dip-coating. The effect of topography on human endothelial cell line, EA.hy926, was investigated *in vitro* on 2D PVA film and *in vivo* using rat model in 3D PVA tubular graft.

Objective 2: To screen and identify design parameters in topography for human umbilical vein endothelial cells (HUVEC) adhesion, proliferation and transfection using Multi-architecture (MARC) chip for high throughput screening

Multi-architecture (MARC) chip was used as a platform to screen and identify potential design parameters of the topographies that modulate cellular behaviours. Forty-five topographies were screened for modulation of HUVEC adhesion, proliferation and transfection. Selected topographies were subsequently investigated for individual study to verify the observation in the MARC chip.

Objective 3: To identify the design role of feature size and spatial orientation for cellular internalization and transfection through non-viral gene delivery

The effect of feature size (micron versus nano) and spatial orientation (anisotropy versus isotropy) of topographical cues on cellular internalization using lipofectamine 2000 was investigated on patterned poly(methyl methacrylate) (PMMA) substrate using different cell types: fibroblast (COS 7); cancer cell line (MCF 7); and adult stem cells (human mesenchymal stem cells, hMSCs). The effect of topography lipofectamine-assisted transfection on hMSCs was investigated to identify potential design parameters for non-viral gene delivery.

Chapter 2 Literature review

2.1 Exploring different patterning techniques

Introduction of micro and nanopatterning technology from the semiconductors and microelectromechanical system industries created new breakthroughs for the field of biology, especially in the field of tissue engineering. Patterning techniques like photolithography [15], electron beam lithography [16], soft lithography [17, 18] and NIL [19, 20] have been used in the field of biotechnology and tissue engineering. These patterning techniques allow the fabrication of various topographies to facilitate studies on topography-directed cellular behaviours. The criteria for choosing suitable patterning techniques for biological and tissue engineering applications include fast patterning process, compatibility with most biomaterials, inexpensive equipment and simple process flow. Thus, understanding the advantages and disadvantages of each patterning technique will aid in selecting a suitable platform for patterning various polymeric-based biomaterials. A summary of the advantages and disadvantages of commonly used patterning techniques is provided in Table 2.1.

Table 2.1: Advantages and disadvantages of different patterning techniques.

Patterning Techniques	Advantages	Disadvantages
Photolithography	• High throughput	• Requires a photomask • Sub-micron size patterning resolution • Patterning resolution limited by light diffraction • Requires specialized equipment
Electron beam lithography	• Nano-size patterning resolution • Mask-less technique	• Low throughput • Requires specialized equipment • Time consuming

		• High cost
Soft lithography	• High throughput • Requires non-specialized equipment • Allows patterning on curved substrates	• Requires a mold/ template • Limited feature height profile; not suitable for high-aspect ratio structures • Sub-micron size patterning resolution
Nanoimprint lithography	• High throughput • Nano-size patterning resolution • Low cost	• Requires a mold/ template • Requires specialized equipment

Generally, patterning technology can be classified into template or non-template techniques. Electron beam lithography belong to non-template techniques while photolithography, soft lithography and NIL require templates for patterning. Among these techniques, electron beam lithography has the highest patterning resolution but the process is time consuming [21] and requires expensive equipment, making it the least favourable technique. Photolithography refers to the patterning of UV-sensitive materials using a template. Although this process is a batch patterning process that allows high throughput patterning, cleanroom facilities requirement and the use of organic solvent limits its biological applications. On the other hand, soft lithography and NIL are widely used and will be discussed in more details in the following chapters.

2.1.1 Soft lithography

Soft lithography is the most common technique adopted by researchers in biology due to its simplicity, low cost and versatility in patterning organic, inorganic and biological materials like proteins [22]. Soft lithography refers to a set of fabrication techniques based on printing and molding materials using

elastomeric stamps with the patterns of interest [17, 18, 23]. Figure 3.1 showed some common soft lithography techniques commonly used in biology.

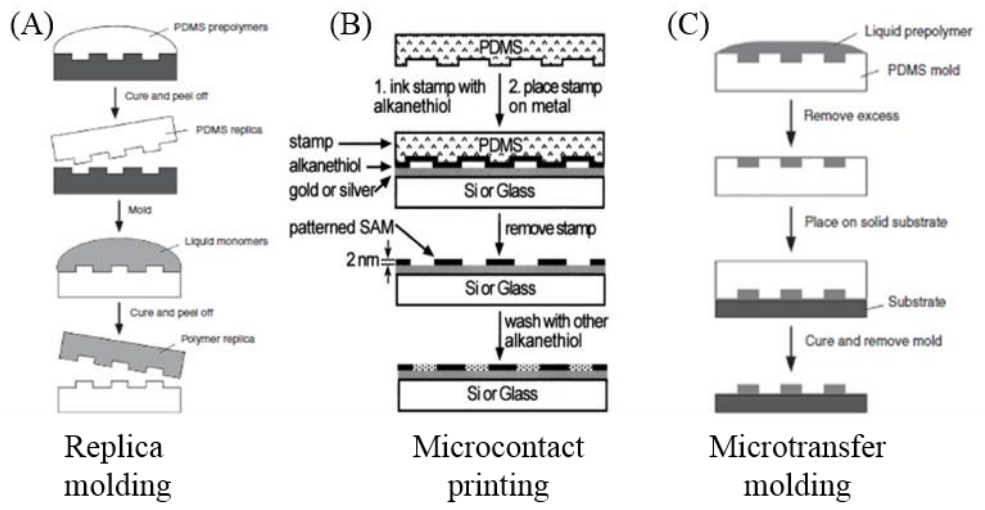

Figure 2.1: Illustration soft lithography techniques used in biology. (A) Replica molding, (B) Microcontact printing (C) Microtransfering molding. (Images obtained from Geissler et al. [23] and Whitesides et al. [17].

Replica molding is the process of curing a liquid precursor on a substrate and replicating the topographic information from it [24]. Microcontact printing is the process of printing material to the receiving substrate based on the affinity of the 2 materials [17]. Microtransfer molding makes use of an elastomeric mold to replicate topographical features on a substrate [25]. All these techniques are commonly used to either pattern polymer or to print biological molecules on other surfaces.

So far, soft lithography has been a very useful tool that has contributed significantly to the early investigations of topographical effect on cellular behaviours using biocompatible materials like polydimethylsiloxane (PDMS). This process is limited by the template used for replication and mechanical property of its elastomer molds limiting the resolution to >30 nm [26]. Since it

is a relatively simple process and does not require cleanroom facilities, it is an attractive method of patterning for biological application.

2.1.2 Nanoimprint lithography (NIL)

NIL was first introduced by Chou *et al.* [27] in 1995 and for the past decade, the field has progressed rapidly. NIL has a simple working principle as illustrated in Figure 2.2.

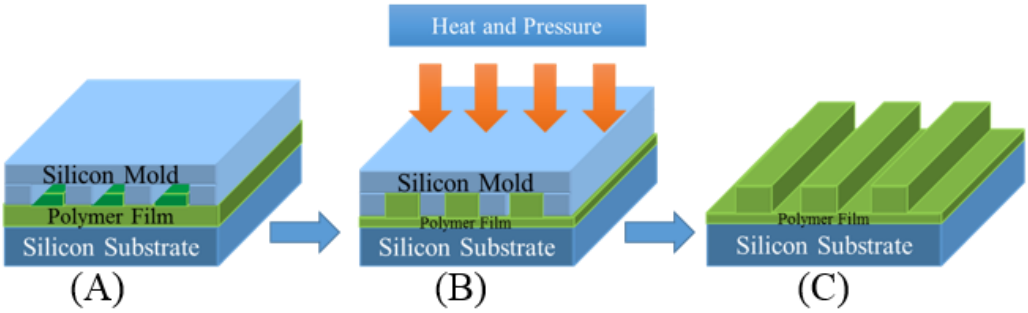

Figure 2.2: Illustration of basic NIL process.

First, the polymeric material to be imprinted on is spin-coated on a blank silicon (Si) /glass substrate. The mold is placed above the substrate, with the patterned surface facing down. Then, the setup is placed under pressure and heat or UV (depending on the crosslinking or curing condition of materials) for a certain period of time. The time required for the NIL process depends on the volume required to fill the mold with the polymeric material and the temperature used must be greater than the glass transition temperature (T_g) of the polymer. When the polymer is at a temperature above its T_g, the polymer is in its rubbery-state that allows the polymer to reflow and fill up the patterns on the mold. The setup is cooled down to a temperature below the polymer T_g and the mold is detached from the polymer. Using these simple steps, high resolution patterning of up to 5 to 10 nm feature size can be achieved [28, 29].

Subsequently, UV-NIL, step- and flash-NIL and roll-to-roll NIL [30] were developed to provide options for UV-sensitive polymers and high-throughput patterning processes for manufacturing.

NIL is an attractive patterning method due to its simple, high-throughput, versatile and low-cost characteristics. NIL also has a few advantages over soft lithography. Firstly, high resolution patterning is easily achieved using NIL in contrast to soft lithography. Secondly, NIL also allows a wide range of materials to be fabricated using UV- and thermo-curable materials. Thirdly, complex structures fabricated like hierarchical structures could be fabricated using NIL [31, 32], as shown in Figure 2.3. The above advantages make NIL a suitable technique to use in patterning materials for biological applications.

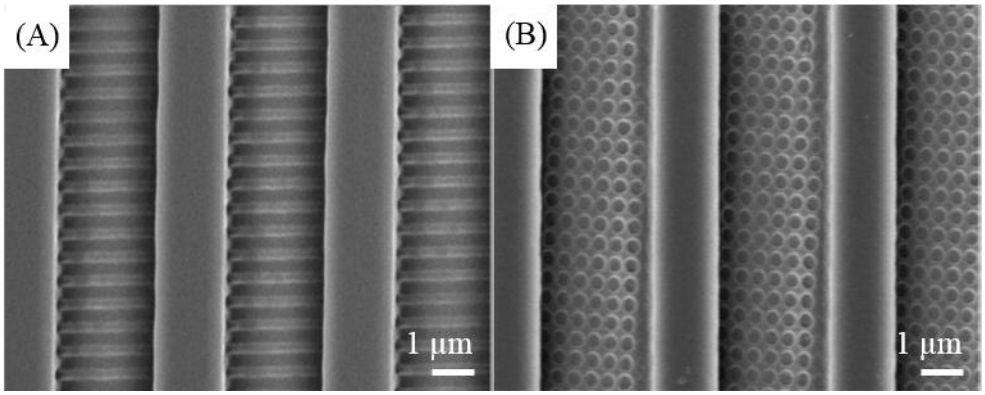

Figure 2.3: Scanning electron microscope (SEM) images of 3D hierarchical nanostructures SU-8. (A) shows 2 µm gratings as the primary structures with perpendicular 250 nm gratings in the recessed area of the patterns. (B) 2 µm gratings as the primary structures with 200 nm pillars in the recessed area of the patterns [31].

2.1.3 Techniques for hydrogel patterning

Hydrogels are suitable materials for biological applications. The low elastic modulus, tunable mechanical properties and high water content of hydrogels mimic native soft tissues, making it an attractive of material for soft tissue engineering. As the importance of topography on cellular behaviours surface,

patterning of hydrogel was also developed. Different patterning techniques have been demonstrated on various hydrogels such as poly(acrylamide) (PA) [33] and poly(ethylene glycol) (PEG) [34]. For example, PA hydrogel has been patterned via soft lithography using PDMS mold. Gratings of 100 µm and 2 µm was replicated on the surface of the PA gel with good dimension fidelity [33]. Mircopatterning of PEG-based hydrogel with 100 µm wells was also achieved using soft lithography. In this particular example, the patterning of hydrogel was carried out when the hydrogel was partially crosslinked and the polymer was left to cure before demolding was carried out [34].

Instead of thermal or physical-based crosslinking, patterning of hydrogel via UV crosslinking is also commonly adopted due to well-established photolithography techniques. Using photolithography, PEG hydrogel modified with various acrylate group was able to achieve a pattern resolution of 7 µm structure [35]. Similar work was carried using heparin-PEG [36] and hydroxyethyl methacrylate [37] where minimum feature size of 30 µm and 20 µm was obtained. Many new techniques have surfaced to achieve resolution beyond photolithography for UV-sensitive materials, and Lee *et al.* [38] used UV-NIL to pattern high resolution 500 nm square wells on PEG diacrylate hydrogel. Using (Hydroxyethyl) methacrylate , 500 nm gratings was achieved [39]. Although high pattern resolution can be achieved by using photocrosslinkable hydrogel, the usage of photoinitiator and free radical generation may case cytotoxicity. Overall, hydrogel patterning is limited by 2D patterning, micron-size resolution and usage of cytotoxic materials. Development of novel hydrogel patterning process will be required to achieve

3D patterning and nano-size feature resolution without the use of harmful chemicals for future application.

2.1.3.1 Patterning of PVA hydrogel

PVA is a synthetic polymer that has been used in a variety of biomedical application. The non-cytotoxic, non-immunogenic and biocompatibility of PVA makes it an attractive polymer to explore in biomedical devices.

Different PVA hydrogel fabrication approaches have been explored. Physical crosslinking using repeated cycle of thawing and freezing, chemical crosslinking using formaldehyde or glutaraldehyde or modification of PVA with photocrosslinkable functional groups have been demonstrated to form PVA hydrogel that is stable in an aqueous environment. However, limitation in hydrogel patterning hinders the physical modification of PVA hydrogel for improved cellular response during biological application.

Patterning of aqueous PVA hydrogel that remains stable in aqueous conditions is challenging because of the low water evaporation rate that leads to bubble formation and pattern shape deformation, thus reducing patterning yield and fidelity. Photolithography [40] and soft lithography [41] have been reported to pattern PVA hydrogel. As demonstrated by Poriciel *et al.*, PVA films with topography feature size as small as 100 µm can be achieved using methyl pyrindinium methyl sulphate as a photoinitiator [40]. Cheng *et al.* uses soft lithography using PVA resin to create PVA microfluidic unit for cell culture [41]. However, the purity and physical characteristics of the patterned PVA hydrogel is unknown, creating doubts on its possible application as medical implants. The highest resolution achieved was demonstrated by Jensen *et al.*

[42] using sodium sulphate-induced curing process which achieved 1 μm cubes topography.

Overall, current PVA patterning methods are limited to micron feature size and the addition of cytotoxic chemical photoinitiator. This limitation in patterning capability hinders the use of PVA and hydrogel for cell-surface interaction, creating a technical gap for usage of hydrogels for soft tissue application. Thus, in this thesis, development of the patterning method of aqueous-based PVA will be explored in 2D and 3D modalities. This development in patterning techniques can then be applied to other aqueous-based hydrogel for their progress in medical device applications.

2.2 Effects of topography cues on cellular behaviours

In the native environment that cells reside, topographical cues are often present in the extracellular matrix (ECM) or when cells are in contact with other cells layers. Similar to the tissue culture substrate or scaffold, basement membranes act as a substrate for cells to interact and adhere throughout the body. The basement membrane contains various ECM components necessary for cells' survival and interaction by providing a complex three-dimensional substrate with micro- and nano-structure. Evidence of these structures was found in various animals and human tissues, including human vascular endothelial basement membranes [43-47]. Regardless of the type of tissue and host, common topography structures like grooves, holes, ridges, and protrusions were reported by various groups, as shown in Figure 2.4.

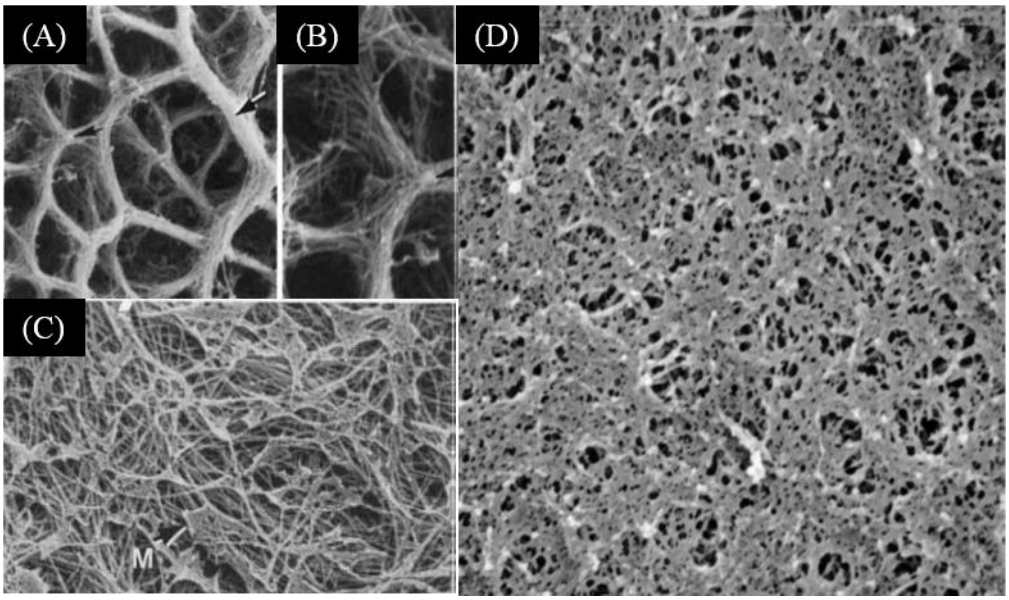

Figure 2.4 Basement membrane of various tissues of different hosts observed using SEM. (A-C) Dermal collagen fibrils that underlays the basal lamina after proteolytic degradation of the structure [43], (D) corneal epithelial basement membrane of rhesus macaque [45].

Cells are able to sense topography through the process of mechanotransduction and this is done through the engagement of different integrin receptors. Upon adhesion, integrin-based adhesion complexes are formed, linking integrin receptors with to the cytoskeletal network. Focal adhesions (FA) is one type of the integrin-based complexes assembled after adhesion acting as a cellular mechnosensor [48]. A series of events after cell-substrate interaction, including FA maturation and activation of the Rho-family cascade and myosin II [48, 49], will be triggered and lead to a change in the cellular behaviours.

Various cellular behaviours like cell adhesion [50-52], morphology [53, 54], proliferation [51, 55], differentiation [56-58] and endocytosis [14] are modulated by topography. The ability to use topography to precisely control cellular behaviours is an essential milestone to bring tissue engineering into reality. Thus, knowing the design role of topography in modulating different

cellular behaviours is very important. In the available literature, there are some common topographies that are regularly studied for their effects on cellular behaviours such as gratings, pillars and holes topography. A summary of the effect of these topography will be discussed in the following chapters.

2.2.1 Effect of anisotropic topography on cellular behaviours

Anisotropic topography refers to patterns that have a direction vector, such as gratings and grooves topography. Directional cellular behaviours like cell migration, alignment and elongation are widely studied using this group of topography. Grating topography were also shown to promote differentiation of cell lineages that have a native spindle-like or elongated morphology like neurons [58] or EC[59]. A summary of some of the recent studies showing the effects of anisotropic topography on cellular behaviours are shown in Table 2.2.

Table 2.2: Summary of effects of anisotropic topography on cellular behaviours.

Topography	Cell type	Material	Effects on cellular behaviours	Reference
Gratings	hMSCs	PDMS	• Enhanced cell elongation • Enhanced cell alignment • More pronounced cell alignment and elongation with smaller sized gratings • Differentiation into neuronal lineage with neurogenic factors	[53]
Lines	NIH3T3	ORMOCER (organic – inorganic hybrid polymer)	• Enhanced cell elongation (parallel lines) • Enhanced cell alignment (parallel lines)	[60]
Grooves	Human keratinocytes	Polycaprolactone film	• Enhanced cell alignment • Decreased gene	[61]

			• expression of matrix metalloproteinase 24 and 26 after day 7 • Increased integrin β5 gene expression	
Grooves	Primary cardiac fibroblast (Rat)	PA with varying stiffness	• Enhanced cell alignment on substrate with stiffness between 18 to 143 kPa • No difference in cell elongation on substrate with varying stiffness ranging from 18 to 143 kPa • Enhanced cell elongation observed on substrate with stiffness of 1 kPa	[62]
Gratings	HUVEC	Silk fibroin films	• Enhanced cell alignment • Decreased cell proliferation (600 nm gratings)	[63]
Gratings	Adipose-derived stem cells	Quartz	• No difference in cell attachment • Decreased cell proliferation • Increased cell elongation • Up-regulation of endothelial markers • Enhanced differentiation of cells towards endothelial lineage	[59]
Grooves	Astrocytes	PDMS	• Enhanced cell alignment, mitochondrial activity, adenosine triphosphate release and calcium activities • Decreased cell proliferation by ~ 35% • Enhanced cell alignment and nucleus deformation with increased groove height (250 nm to 500 nm)	[64]
Grooves	PC 12	Polystyrene	• Enhanced cell alignment and axonal outgrowth • Increased axonal outgrowth with	[65]

			increased groove width and pitch size	
Grooves	Schwann cells	PCL/PLA	• Enhanced cell elongation and alignment • Increased elongation and decreased cross over with V shaped and sloped grooves as compared to squared shape grooves • Decreased cell attachment • Decreased cell proliferation	[66]

2.2.2 Effect of isotropic topography on cellular behaviour

Isotropic topography refers to patterns that do not have a direction vector, such as pillars and wells topography. Unlike anisotropic topography, cell alignment and elongation is usually not studied in these topographies. In most cases, cell proliferation, adhesion and differentiation is studied. Pillars topography is also used to study the traction force exerted by the cells to probe the substrate-sensing mechanism [67]. A summary of some of the recent studies showing the effect of isotropic topographies on cellular behaviours are shown in Table 2.3.

Table 2.3: Summary of effects of isotropic topography on cellular behaviour.

Topography	Cell type	Material	Effects on cellular behaviour	Reference
Posts	Human bone marrow-derived connective tissue progenitors	PDMS	• Enhanced cell proliferation on posts with diameter of 10 µm and aspect ratio of 0.5 to 4. • Increase in cell density after 9 days on 10 µm pillars	[68]

Posts	Bone marrow-derived connective tissue progenitors	PDMS	• Enhanced early cell growth • Enhanced cell proliferation at day 30 • Enhanced osteogenic differentiation	[69]
Holes and pillars	MSC	Polycaptolactone films	• No change in cell proliferation (nano holes and nano-pillars) • Enhanced MSC chondrogenesis	[70]
Pillars	LRM 55 astroglial cells	Si	• Enhanced cell adhesion • Polarised cytoskeleton on pillars	[71]
Circles	NIH3T3 fibroblasts, HeLa, Primary hepatocytes	PDMS	• Enhanced cell attachment on pillars with diameter < 3 µm • Decreased cell attachment on pillars with diameter > 4 µm	[72]
Pillars	HUVECs and endothelial colony forming cells	SiO_2	• Decreased cell attachment with height > 6 µm • Decreased cell spreading with height > 6 µm	[73]
Pits	Rat fibroblast	PCl	• Decreased cell adhesion and area • Reduced FA number and size	[74]
Dimples	Murine peritoneal macrophages	PDMS	• No change in cell alignment observed • Enhanced elongation observed on dimples with 2 µm and 5 µm diameter • No change in macrophages activation on topography	[75]
Pits and islands	OCT-1 osteoblast like cells	Poly (L-lactide) Polystyrene	• Enhanced cell adhesion on pits and islands • No change in cell proliferation	[76]
Pits	Fibroblast	Quartz	• Enhanced cell proliferation on pit with 7 µm diameter • Increased cell proliferation with	[77]

			increased pit pitch • Enhanced cell migration on pit with 7 µm diameter • Decreased cell migration on pit with 25 µm diameter	

2.2.3 Effect of topography with curvature on cellular behaviours

In this thesis, topography with curvature refers to topography with radius of curvature (RC) in the z direction. Some examples of these topographies include concave and convex lenses, half cylinder gratings, U-gratings and fibers topographies as illustrated in Figure 2.5. Unlike the circular pillars topography that has its RC in the x-y plane, the topography with curvature has its RC in the z direction. For example, convex lenses is isotropic topography with RC in z direction while fibers is anisotropic topography with RC in z direction. While these topographies may be named differently in different study, this specification above allows clear identification of topographies of similar topographical design.

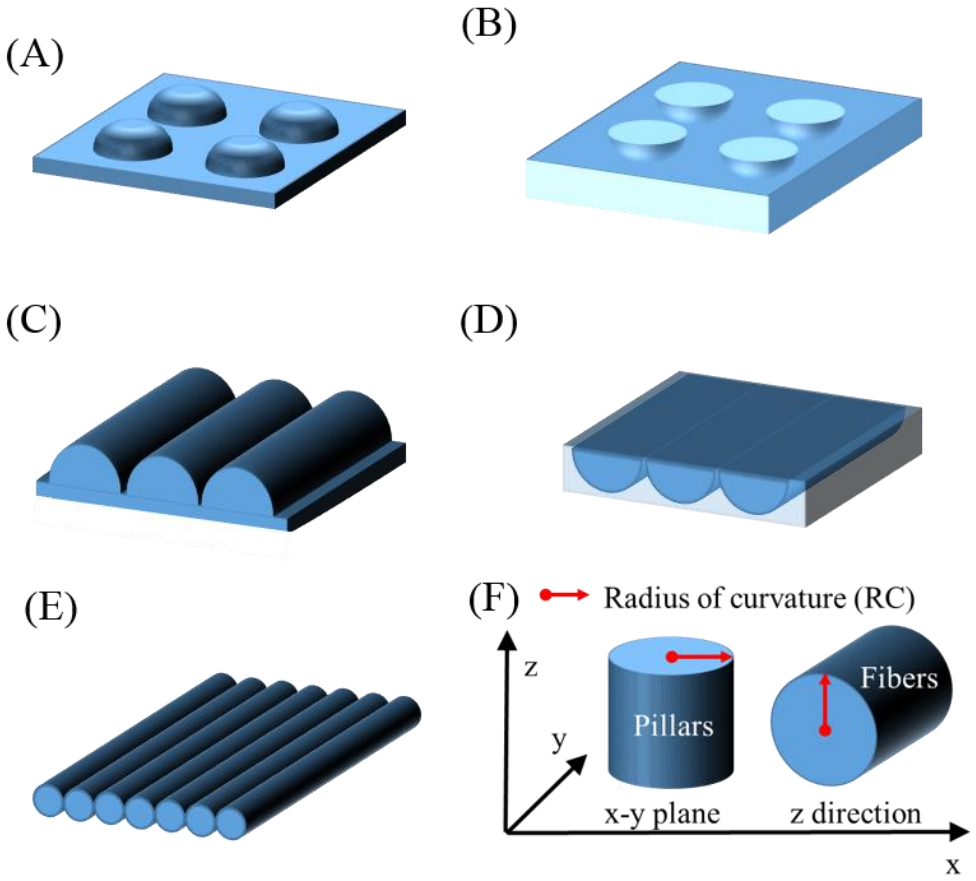

Figure 2.5: Illustration of topography with curvature. Isotropic topographies with RC in z direction are (A) convex lenses topography and (B) concave lenses topography while anisotropic topographies with RC in z direction are (C) half cylinder gratings topography (D) U-gratings topography and (E) fibers topography. (F) Difference between topography with RC in x-y plane such as pillar and anisotropic topography with RC in z-direction such as fibers topography.

The effect of topography with curvature had been studied on various cellular behaviours like migration, alignment, morphology and differentiation. Lower cell migration and longer FA clusters were observed on cells seeded on topography with increased RC as fibers diameter reduced [78]. In another study, differentiation of myoblast to myotube was significantly enhanced after culture on sinusoidal gratings as compared to square gratings [79]. Studying the cellular movement on concave and convex lenses with 200 nm diameter and 50 µm depth or height, cells were observed to avoid the concave lenses

and preferred to climb the convex lenses topography. Higher cell death was also observed in cells residing in the concave lenses microstructure [80]. These evidences demonstrated the effect of curvature on cellular behaviours.

2.3 Other factors influencing cellular behaviours

Aside from topography, other factors like cell type and substrate material could contribute to the contradicting cellular behaviours observed on similar topographies. Meyle *et al.* [81] reported that culturing various cell types on silicon dioxide with 1 µm width gratings yield different levels of cell alignment. They observed 100% alignment for human fibroblast, 20% alignment for monocytes, macrophages and no alignment for keratinocytes and neutrophils. In another article, titanium dioxide with 70 nm width gratings have differing effects on HUVEC and smooth muscle cells proliferation. HUVEC displayed an increase in proliferation as compared to the unpatterned control, while smooth muscle cells showed a lower proliferation rate [55]. The use of materials with different elastic moduli also varies the cellular responses. For instance, a matrix with low modulus promote neurogenic differentiation while a high modulus matrix promotes osteogenic differentiation of mesenchymal stem cells [82]. In another study, endocytosis and proliferation increase with higher substrate modulus while cell apoptosis increase with decreasing modulus [83]. These studies showed that cellular behaviours could be influenced by factors other than topography.

2.4 Endothelialisation for vascular tissue engineering application

2.4.1 Occlusive vascular diseases and its treatment

Coronary artery disease and peripheral arterial disease are common occlusive vascular diseases that are characterized by blockage of important blood vessels

supplying the heart and the lower limbs. These type of diseases are usually due to the process of atherosclerosis which results in the accumulation of plaques in the blood vessels [84].

Treatment for the disease for patients with more severe arterial occlusion, surgical treatment like angioplasty, stenting and vascular graft replacement is given. Angioplasty involves the use of an inflatable balloon to widen the blood vessel. This procedure often works hand-in-hand with stenting to hold the compressed plaque to the vessel wall and maintain blood vessel patency. Arterial bypass or replacement surgery involves the use of a vascular graft to create a new route for blood flow.

To date, the gold standard for vascular conduits is to use autologous saphenous vein grafts. Unfortunately, the vein is not always available due to morbidity or from previous usage. Hence, synthetic graft made of expandable polytetrafluoroethylene and polyethylene terephthalate are commonly used as a replacement. However, they are severely limited by mechanical mismatch, resulting in thrombosis and intimal thickening. Other than graft property mismatch, graft failure often occurs due to the lack of EC lining in the lumen of the graft. The presence of EC lining is necessary to improve and maintain the patency of the graft. The EC lining mimics the native vessel environment by providing dynamic control over homeostasis, interaction with blood and shear stress and regulation of the inflammatory response, vessel permeability, thrombosis and fibrinolysis of a blood vessel [4, 85]. The problem of rapid synthetic graft failure is most prevalent in vascular grafts with diameters smaller than 6 mm. Thus, it is important to develop a small diameter vascular graft (for diameter < 6mm) with capacity for endothelialisation and artery-

matching mechanical properties to provide good patency and reduce intimal hyperplasia.

2.4.2 Endothelialisation

Two main strategies have been used to achieve endothelialisation in the graft lumen, pre-seeding of cells to the lumen of the graft before implantation [5] and stimulation of *in situ* endothelialisation via chemical and physical surface modification of the luminal surface that encourages EC adhesion, migration and proliferation [6].

2.4.2.1 Seeding of EC to the lumen of the graft

One of the methods of endothelialisation in the graft lumen is by pre-seeding an EC layer or incorporating EC in the graft before implantation. In one of the earliest experiments conducted by Herring *et al.* [86], EC seeding together with anti-platelet agents show a significant improvement in patency of expanded polytetrafluoroethylene graft when compared to unseeded controls. In addition, they and Suavage *et al.* [87] had shown that areas with EC layer remained thrombus-free. Having identified the importance of EC to maintain synthetic vascular graft patency, different cell seeding techniques were studied and developed including gravitational seeding [88, 89], hydrostatic seeding [90] , biological glue, electrostatic force seeding [91, 92] and magnetic field seeding [93]. However, loss of greater than 95 % of pre-seeded EC occurs upon the first 24 hours of implantation due to the shear force of blood flow [94], lack of endothelialisation on an uneven surface [95] and thrombogenicity reaction on rough surface [96]. Although the use of magnetic field seeding technique seems promising, the safety of using of cells loaded with magnetic nanoparticles needs further evaluation.

In addition, pre-seeding cells on vascular graft is still limited due to long culture time needed to obtain the cell layer, high cost, and its suitability for clinical application [97, 98].

2.4.2.2 In situ endothelialisation via biochemical surface modification

In this approach, biochemical cues like growth factors, biofunctional molecules and drug and gene loaded nanoparticles are used to modify the surface of the lumen to promote EC and EPC migration, adhesion and proliferation. Protein molecules like heparin, fibronectin, collagen and vitronectin have been found to enhance EC adhesion [99].

For more targeted adhesion, immobilization of antibodies targeting ECs and EPCs are more ideal. EC and EPC related surface markers like CD 34, VEGFR-2 and CD 31 were applied to surfaces for more specific cell binding. For example, Tan et al showed that polyhedral oligomeric silsesquioxane poly(carbonate-urea) urethane modified with anti-CD34 antibodies successfully captured circulating EPC, which was absent on polymer without antibody modifications [100].

In vascular graft applications, growth factors like vascular endothelial growth factor (VEGF) [101] and basic fibroblast growth factor [102], are often used to enhance endothelialisation. For example, HUVEC cultured on a substrate with immobilised VEGF showed improvement in both proliferation and migration behaviour [103].

However, chemical or physical deposition of biomolecules is not a sustainable approach due to degradation or inactivation of the biomolecules. Thus, there is

a need to explore other methods, like surface topography, to improve endothelialisation or gene therapy for angiogenesis.

2.4.2.3 In situ endothelialisation via topography surface modification

Similar to biochemical cues surface topography can also modulate EC behaviours that are crucial in *in situ* endothelialisation. However, topographical cues haves an additional advantage of controlling cell alignment, which is important for creation of an atheroprotective environment. Cooke *et al.* observed that EC grown in straight region and aligned with the direction of laminar flow have an increased expression of nitric oxide synthase whereas randomly aligned EC found in the bifurcation with disturbed flow have decreased nitric oxide synthase expression [104]. One of the basic functions of nitric oxide synthase is the production of nitric oxide in the blood vessel, which can prevent platelet adhesion, aggregation and promote an atheroprotective environment [105]. In addition, gratings topography had also been shown to maintain the EC physiological phenotype by modulating the membrane mobility and activity of LOX-1 receptors that are related to uptake of lipids responsible for atherosclerosis [106].

Anisotropic topographies including grooves, trenches, ridges, and gratings are the commonly investigated topographies for EC behaviour. Regardless of the cell type and materials used, an overall improvement of EC alignment and elongation on anisotropic topographies were observed. Grooves ranging from 1 μm to 22 μm width on metal nitinol induced EC alignment and elongation that was not observed on the smooth surface control [107]. Similar results were observed on PDMS substrates with gratings topography cultured with bovine aortic EC [54].

Other than EC morphology, the formation of the EC layer is also important to preserve the atheroprotective phenotype. EC migration, adhesion and proliferation are the key cellular behaviours necessary EC monolayer formation. Similar to alignment, EC migration, adhesion and proliferation are also enhanced on gratings topography. It has been shown that migration rate increased by at least two fold on EC seeded on groove compared with the unpatterned control [107]. Furthermore, enhancement of EC proliferation and adhesion of rat aortic EC were observed with the use of surface topography [51].

Although most reports demonstrate that anisotropic topographical design is promising for endothelialisation, the optimal pattern density and grating width and height are still unknown. Some contradicting observation in EC proliferation were reported when similar topographies were used. For example, HUVEC proliferation decreased with nano-size gratings [7] while rat aortic EC proliferation increased with nano-size gratings [51]. In another study, proliferation of bovine aortic EC remained unchanged as compared to smooth PDMS surfaces or gratings (rough) PDMS surfaces [54].

In the search for a suitable design rule, the effects of anisotropic topographical design on endothelialisation are also important and valuable. For instance, Dickinson *et al.* reported enhanced elongation, alignment, adhesion and spreading on pillars of height lesser that 6µm [73].

Overall, topography can induce different cellular behaviours in ECs; however, the specific design rule in topography for endothelialisation is needed for scaffold design of vascular graft.

2.5 Endocytosis for drug and gene delivery application

2.5.1 Delivery systems for drugs and genes

Discoveries in genomics and pharmaceutical industries not only advances the field of medicine towards regenerative medicine and nanomedicine but also evolves the field of therapy. Traditional modes of drug delivery involving untargeted and burst release is unfavourable and could detrimental to the patient's health. As a result, there is increasing demand over the years for a new platform for an efficient, controllable and targeted delivery that address health and safety concerns of therapeutic agent delivery.

Two common systems for therapeutic agent delivery can be performed: injection of nanocarriers to targeted area; and a substrate-mediated delivery via scaffold implantation. There is an ongoing effort to modify nanoparticles to be responsive to *in vivo* environmental stimuli like pH and temperature as well as external stimuli like ultrasound, light, heat and magnetic field for a stimuli-triggered localised cargo release [108]. However, health safety issues on the usage of nanoparticles is still a concern [109]. In addition, delivering therapeutic agent as free nanoparticles intravenously often results in non-localised delivery due to the mobility of the nanoparticles.

Although substrate-mediated delivery is limited by the need for a scaffold, it is still a promising strategy that ensures localised and controlled delivery *in vivo*. Therapeutic agents are immobilised on a substrate in this mode of delivery, allowing control in the location of the delivery. This leads to more effective and targeted therapeutic treatment with lesser loading dosage. A common medical device that uses substrate delivery is drug and gene eluting stents [110]. These medical devices use stent to deliver and release therapeutic

agents in the blood vessel to prevent re-stenosis and maintain long term vessel patency.

2.5.2 Mechanisms of gene delivery

Gene delivery refers to the delivery of genetic materials like deoxyribonucleic acid (DNA) plasmid and small interfering ribonucleic acid (siRNA) into targeted cells. Successful cell transfection with genetic material allows the cells to produce desired proteins and biomolecules required for the therapeutic effect. This can be imagined as a self-sustaining mini-pharmacy that dispenses therapeutic agents to treat or prevent diseases and undesired cellular responses. Gene delivery mechanisms can be classified as either viral or non-viral delivery, depending on the vehicle. Viral gene delivery utilizes viruses for cell membrane penetration. Some examples of virus vehicles include lentivirus, adenovirus, retrovirus, and adeno-associated virus. Although this mode of delivery has a high transfection efficiency, there are concerns of immunogenic responses and uncontrolled gene expression to off-site targets, resulting in unwanted cellular responses [8]. Thus, the use of non-viral gene delivery is more favourable. The use of synthetic materials to encapsulate genetic materials for delivery allows predictable responses in the biological system. However, non-viral gene delivery suffers from poor efficiency, limiting desired therapeutic effect. Unlike viral vectors that are equipped with the capability to enter the cell and deliver the genetic material directly to the nucleus, non-viral vector has to overcome several barriers before transcription can occur. The 3 barriers of non-viral vectors are entry to the cells via the cell membrane, passage of the vehicle through the cytoplasm without degradation and entry into the cell nucleus through the nucleus membrane [111]. Without

reaching the cell nucleus, gene expression will not be possible. On average, only 0.01-1% of the genetic material arrive at the nucleus for transgene expression [112] thus limiting the transfection efficiency of non-viral gene delivery.

Overall, the efficiency and targeted drug and gene delivery needs to be addressed to advance the field of gene therapy for clinical applications.

2.5.3 Mechanism of endocytosis

One method to overcome the low transfection rate of non-viral gene delivery is to increase the cellular uptake of the vehicle. The vehicle gains entry into the cells via a process called endocytosis. Doherty *et al.* [113] analysed and explored the different type of endocytosis pathways and their mechanism. The different type of endocytosis pathways are illustrated in Figure 2.6.

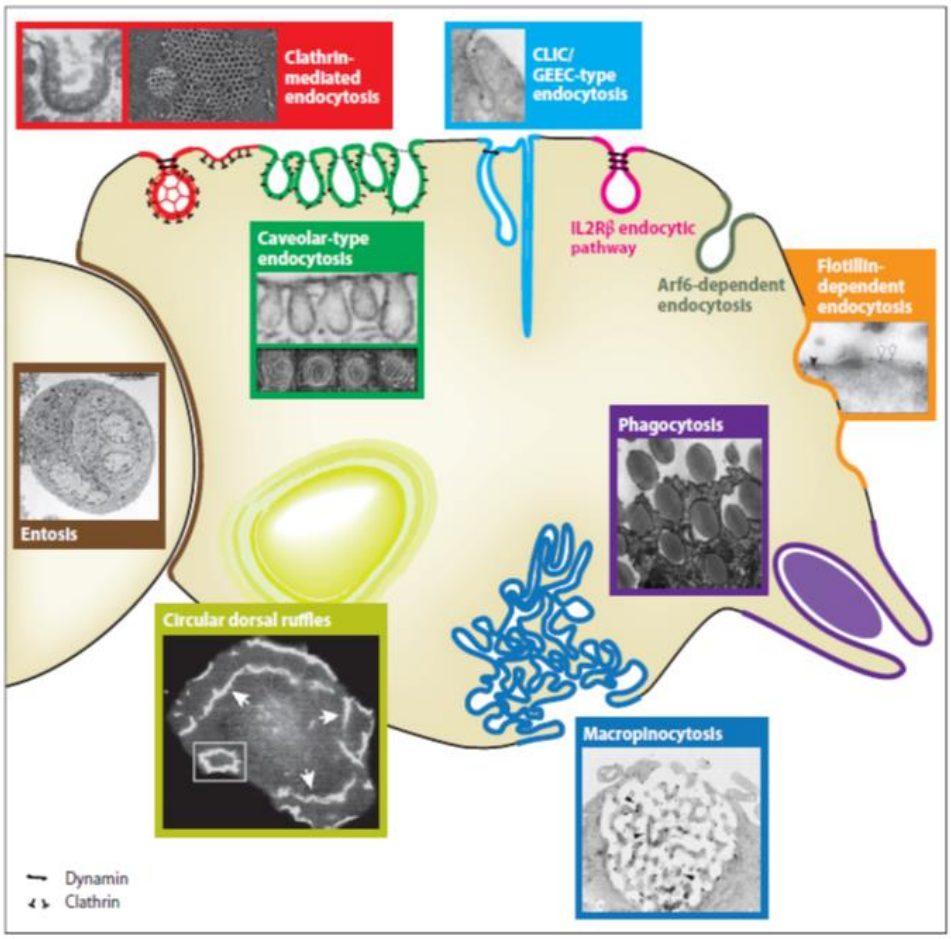

Figure 2.6: A summary of each endocytosis pathway with various imaging characterizations on structures known or thought to be involved in endocytic events adapted from reference [113].

The mechanism of each endocytic pathway is still not fully understood. Among these known pathway, macropinocytosis and receptor-mediated endocytosis, including clathrin-mediated and caveolae-mediated endocytosis, are the most widely studied and relevant to non-viral gene delivery.

Clathrin-mediated endocytosis refers to the uptake of cargo through internalization of clathrin ligand-bound receptors [114]. Some of the substances that are taken up via this type of endocytosis include low density lipoprotein, transferrin and epidermal growth factor [111]. Caveolae-mediated endocytosis is another type of a receptor mediated endocytosis involving

another cell membrane receptor, caveolins [115]. Cholera toxin [116] and simian virus (SV40) [117] were internalized via caveolae. Lipoplexes and polyplexes, two commonly used delivery vehicle in drug and gene delivery, utilizes these two endocytosis pathways. As reported by Rejman *et al.* [118], lipoplexes are internalized via clathrin-mediated endocytosis while polyplexes are internalized via caveolae and other clathrin-coated pits.

While clathrin-mediated and caveolae-mediated endocytosis take up cargo sized <100 nm and <60 nm, respectively [9, 119], larger sized particles enters the cells through non-receptor mediated pathways such as macropinocytosis. Macropinocytosis is known as fluid-phase endocytosis, where cells cargo with size of 1 – 5 μm through uptake of extracellular fluids and solutes. Fluid phase markers like fluorescein isothiocyanate (FITC)-dextran and positively charged complexes used in transfection [120] gain entry to the cells via macropinocytosis. With more understanding on the selected pathway of entry by the cargo, strategy can be apply to enhance that specific pathway leading to improved delivery efficiency.

2.5.4 Topographical cues on cellular endocytosis

There are 2 attributes where topography can modulate endocytosis: first, the size and shape of the delivery cargo; second, the topography of the underlying substrate that cells adhere to. In both cases, the cells can sense the topography or the shape of the particles and in turn modulate its endocytic behaviour.

2.5.4.1 Effect of particle shapes on cellular endocytosis

To improve the efficiency of non-viral gene delivery, different strategies and modification of the delivery vehicle such as particle chemistry [118], particle

size [119, 121], surface charges [122, 123] have been explored. In recent years, the effect of particle size on endocytosis was revealed with development of novel fabrication techniques to control the shape of delivery vehicle. Using particle replication in non-wetting templates, PRINT [124] and step and flash imprint lithography [125, 126] fabrication technique, particles of different shapes and sizes can be synthesised to study the effect of particle shape on endocytosis and the pathway of internalization. Gratton *et al.* [127] explored particles with cubes, cylinders and cylinder-rods shapes and varying size and aspect ratio on the internalization rate. Cylinder-rod shaped (aspect ratio: 3) particles displayed a higher percentage of internalization in the first 15 minutes of the experiment as compared to a cylinder shaped (aspect ratio: 1) despite having comparable absolute volume. In another study, Agarwal *et al.* [128] observed that HeLa cells, HEK 293 cells, and bone marrow-derived dendritic cells preferred to internalize PEG diacrylate hydrogel nanodisks over nanorods. However, HUVEC showed a different internalization prolife as compared to the other 3 cell types. Further analysis showed that clathrin-mediated pathway is used by HUVEC but not by HEK 293 cells, accounting for different internalization profiles [128]. This indicates that influence of shape in nanoparticle uptake is also dependent on the cell type. In addition to clathrin-mediated pathway, uptake of particles with different shapes were also observed through caveolae-mediated and macropinocytosis pathway [127]. Summarizing other related studies [129-132], it is evident that the shape of the particles play a major role in endocytosis. However, it is hard to differentiate between the effect of particle shape and particle size since both parameters were varied at the same time.

2.5.4.2 Effect of surface topography on cellular endocytosis

Strategies to improve the efficiency of non-viral gene delivery always focus on the design of the delivery vehicle. The effect of the substrate of topography of the underlying ECM on endocytosis is commonly overlooked. Although the effects of topography on other cellular behaviours are widely explored, little is known about its effects on cellular endocytosis.

The effect of topography on cell endocytosis was first reported by Dalby *et al.* [133] when fibroblast cells were cultured on 100 nm pillars topography. The cells attempted to endocytose the pillars, as observed from transmission electron microscopy. Adler et al [111] reported the use of substrate topography to improve endocytosis of green fluorescent protein (GFP) in human dermal fibroblasts. A 25% increase in GFP expressing population was observed when cells were cultured on 4 μm well topography. The effect of topography was also explored in siRNA transfection for gene silencing application. Solanki *et al.* [12] reported an increase of siRNA delivery in cells when cells were cultured on glass substrate pre-coated with silicon oxide nanoparticles of varying diameter as compared to the unpatterned control. Within the patterned substrate, the feature size of the topography also changed the percentage of gene silencing. The smallest particle size of 100 nm showed the highest GFP knockdown while the largest particle size of 700nm showed the lowest GFP knockdown. In another study, using nanofibers, lower siRNA internalization was observed as compared to the unpatterned control[13]. Yet unexpectedly, the cells on nanofibers gave a higher gene silencing effect. This implies that the effect of topography is not limited only enhance endocytosis but also gene expression or silencing processes.

Ultimately, more understanding on the mechanism of the modulation with topographical design is necessary to advance its application in drug and gene delivery.

Chapter 3 Patterning of PVA hydrogel to investigate the effect of topography on cell adhesion

3.1 Introduction

Physical cues are as important as biochemical cues in directing cell behaviours. Aside from acting as a reservoir for biomolecules, ECM also provides topographical cues to direct cell behaviours and responses, such as cell adhesion [72], elongation [54, 63], proliferation [51, 63], endocytosis [14, 134] and differentiation [56-58].

The effect of topography on cellular behaviours have been widely studied using materials like PDMS [54, 56, 72, 73], PA [62], PMMA [135], poly(lactic-co-glycolic acid) [136], polyurethane [7] and Si [71]. Another class of polymers that is less studied for topographical effect is hydrogel. Hydrogel is a hydrophilic material, synthesized by crosslinking hydrophilic polymers via physical or chemical methods. In recent years, it has gains popularity for application in soft tissue engineering and biomedical implants due to high water content and low elastic modulus, mimicking that of the native soft tissue. PVA is one such polymer that has been explored and used in biological application.

PVA is a synthetic polymer hydrogel with biocompatible property suitable for application in biomedical devices [137, 138]. Using different crosslinking methods, PVA hydrogel with tunable mechanical and chemical properties can be synthesized. Among all the different crosslinking method, the PVA synthesis by Chauat *et al.* [139] has the advantage of avoiding the use of toxic chemical crosslinker [140, 141]. Instead of aldehydes, sodium

trimetaphosphate (STMP) was used to crosslink PVA in alkaline and ambient condition. The synthesized PVA hydrogel possess tunable mechanical property suitable for vascular graft. However, bioactivity of PVA hydrogel need to be further improved to promote endothelialisation *in vivo*. Previous studies on PVA hydrogel showed poor cell adhesion *in vitro* [142, 143] and absence of endothelialisation of the PVA hydrogel vascular graft *in vivo* [139]. One possible solution is to take advantage of the effect of topography on material surface property and cellular behaviours to modify PVA surface, making it suitable for EC cell behaviour.

The patterning of PVA hydrogel has been demonstrated using photolithography [40] and soft lithography [41]. However, micron feature size limitation and the addition of chemical photoinitiator are not favourable for biological applications. Thus, it remains a challenge to fabricate PVA hydrogel with micro- and nano-scale features without the use of toxic chemicals.

This chapter will explore the 2D and 3D patterning on PVA hydrogel and to identify topography that improves its biological functionality, making it more favourable for cell adhesion for future vascular application.

3.2 Materials and methods

3.2.1 Preparation of crosslinking PVA hydrogel solution

PVA crosslinking solution was prepared similar to the previous report [139]. Twelve grams of 10 % aqueous solution of PVA (Sigma-Aldrich, 85-124kDa, 87-89 % hydrolysed) was crosslinked with 1 ml of 15 % (w/v) STMP (Sigma-Aldrich). After stirring for 5 minutes, ensuring that PVA and STMP were

homogenously mixed, 400 µl of 30% (w/v) sodium hydroxide (Sigma-Aldrich) was added dropwise into the mixture and stirred for another 10 minutes. Thereafter, the mixture was poured into a 50 ml centrifuge tube and centrifuged at the speed of 3000 rpm for 10 minutes to remove air bubbles. The clear mixture of PVA obtained was subsequently used for patterning of 2D and 3D PVA films using casting, NIL and dip-coating processes.

3.2.1.1 Patterning of 2D PVA films via casting method

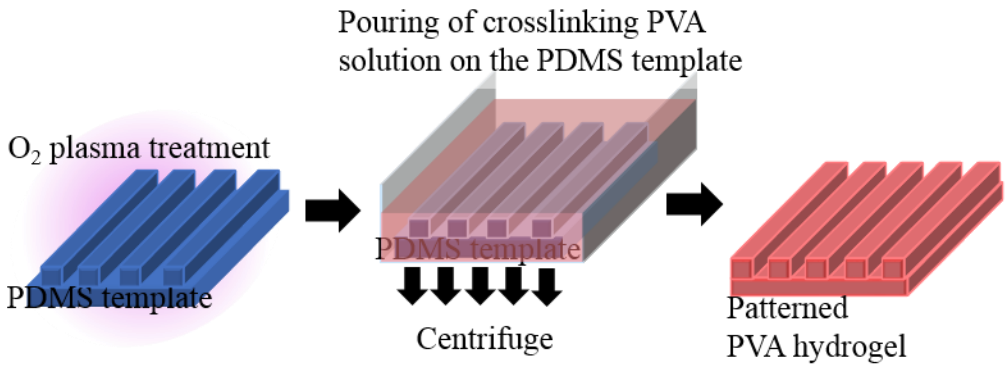

Figure 3.1: Illustration of patterning of PVA films via casting using PDMS mold.

Figure 3.1 showed the schematics of fabricating and patterning of PVA films via casting. Firstly, PDMS molds used for patterning of PVA films were fabricated from patterned Si molds using standard soft lithography process. Briefly, PDMS mixture was prepared at the ratio of 10:1 (elastomer base: crosslinker), desiccated under vacuum and cured at 70 °C overnight. Before casting, PDMS molds were oxygen plasma treated to improve wettability and fresh crosslinking PVA solution was poured on top of the PDMS mold. Next, the setup was centrifuged for 30 minutes at 1000 rpm before incubating in a controlled environment of 18 °C and 75-80 % humidity. After approximately 10-14 days, depending on the volume of PVA crosslinking solution, the

completely crosslinked PVA hydrogel was immersed in 1x phosphate buffer saline (PBS) and demolded from the PDMS mold. The patterned PVA hydrogel films was stored in 1x PBS before the experiment was carried out.

3.2.1.2 Patterning of 2D PVA films via NIL

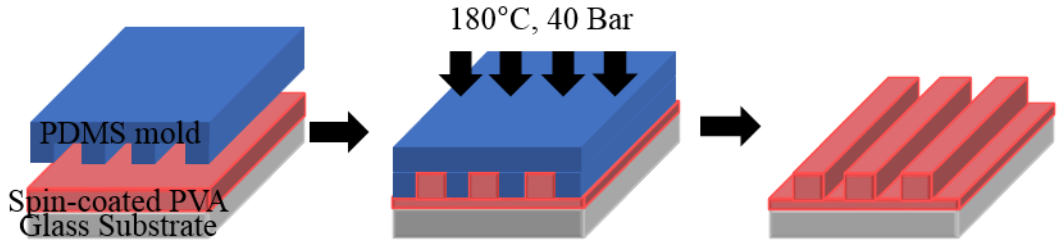

Figure 3.2: Illustration of patterning of PVA films via NIL

The process of using NIL for patterning of PVA is shown in Figure 3.2. First, a thin and partially cured PVA film was formed via spin-coating of crosslinking PVA solution at 800 rpm for 40 seconds on a clean glass coverslip. The thin film was dried at ambient condition for approximately 30 minutes, changing from a wet and transparent film to a semi-dry and opaque film. Next, a PDMS mold was placed on top of the PVA films and imprinted at 180 °C, 40 bars for 10 minutes using the Obducat system. The imprinted setup was released from the pressure after the system was cooled to 40 °C. Then, the crosslinked PVA films was demolded from the PDMS mold and rinsed with 1x PBS. The patterned PVA hydrogel film on glass coverslip was stored in dry condition before experiment was carried out.

3.2.1.3 3D patterning of PVA grafts via dip-coating process

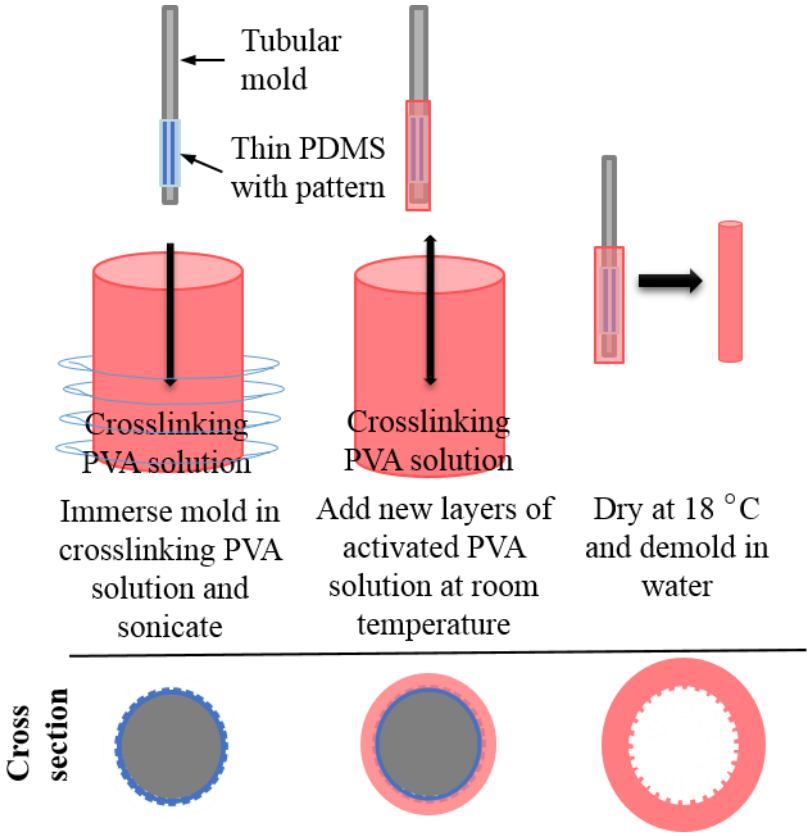

Figure 3.3: Three-dimensional (3D) patterning of PVA vascular grafts using dip-coating process. Schematic diagram of casting method for 3D patterning. Blue denotes PDMS which green denotes PVA.

A novel fabrication method of obtaining 3D patterning of PVA graft were developed as illustrated in Figure 3.3. Cylindrical mold was assembled by attaching a thin-film patterned PDMS on a rod with outer diameter of approximately 2 mm. The assembled cylindrical mold was oxygen plasma-treated and immersed in crosslinking PVA solution for sonication. After sonication, the cylindrical mold was repeatedly dip-casted in freshly-made crosslinking PVA solution. PVA tubes were dried at 18 °C and 75-80 % humidity environment. The crosslinked tube was then demolded in 10x PBS solution and subsequently stored in 1x PBS solution before usage.

3.2.2 Characterization of patterned PVA hydrogel using scanning electron microscope (SEM)

The topographies were verified by environmental scanning electron microscope (eSEM) and conventional SEM. For conventional SEM, PVA hydrogel film was air-dried overnight at ambient temperature and coated with 10 nm thickness of platinum (JEOL-JFC 1600 auto-fine coater). Thereafter, characterization was carried out using JEOL-JSM 6010 LV at high vacuum and accelerating voltage of 5-10 keV. In addition to conventional SEM, selected PVA hydrogel films were observed at its hydrated state using eSEM (Philips XL ESEM-FEG, INSERM, France) at accelerating voltage of 15 keV. SEM (n = 3) and eSEM images (n=1) were used to analyse the dimension of topographies (using Image J 1.26j) where at least 5 measurements were obtained for each sample.

3.2.3 Cell culture of cells on 2D patterned PVA hydrogel films

PVA films were placed in a 24-well plate and held down by silastic tubing (Dow Corning). Hydrated PVA films were rinsed with PBS, sterilized with UV light and immersed in 20 % penicillin-streptomycin (PAA) and 2% amphotericin-B solution (Sigma-Aldrich). The PVA films were repeatedly washed with PBS to remove the traces of the antimicrobials. On the other hand, the dried PVA films fabricated via NIL were sterilized with UV light. Next, PVA films were incubated overnight with fetal bovine serum (FBS) in 4 °C.

Human umbilical vein cell line EA.hy926 (ATCC) were seeded at a total of 20000 cells/cm^2 and cultured for 24 hours in Dulbecco's Modified Eagle's media (DMEM) high glucose (D7777, Sigma-Aldrich) with 1.5 g/L sodium bicarbonate, 10% FBS and 1% penicillin-streptomycin (PAA).

3.2.4 Fluorescence imaging of cells

EA.hy926 was rinsed with PBS before fixing in 4 % paraformaldehyde (PFA) for 15 minutes in 4 °C. The samples were then incubated with Alexa Fluor 488 Phalloidin (1:750) (Invitrogen) and 4',6-diamidino-2-phenylindole (DAPI) (1:2500) for 20 minutes before mounting in fluoromount (Sigma-Aldrich) for imaging. Samples were observed and imaged through epifluorescence microscopy (Leica DM IRB).

3.2.5 Quantitative analysis of cell adhesion on various PVA films

After 24 hours of incubation, the cells were rinsed with PBS before detaching from the substrate using trypsin-EDTA (Lonza). Trypsin neutralization solution (TNS, Lonza) was then added to neutralise the enzymatic detachment process. The collected cell suspension was centrifuged at 1000 rpm for 5 minutes and the cell pellet was snapped freeze using liquid nitrogen for 10-20 second and stored in -80 °C until analysis.

The cell number on patterned PVA films was measured and obtained using CyQUANT assay (LifeTechnologies). Before cell number determination, the CyQUANT GR dye/cell-lysis working solution was prepared following manufacturer protocol. For example, to prepare the working solution for 100 reaction, 20 ml of cell-lysis solution was diluted 20X by adding 1 ml of the cell-lysis buffer to 19 ml of nuclease-free distilled water. Next, the working solution was made by mixing 50 µl of CYQUANT GR dye stock solution homogenously with 20 ml of diluted cell-lysis solution. After the cell pellets was thawed at room temperature, it was re-suspended in 200 µl of the freshly prepared working solution and transferred to a microplate for fluorescent measurement using a microplate reader.

To quantify the cell number, a calibration curve was obtained by carrying out the CyQUANT assay using a cell pellet of known cell number. By matching the fluorescence to the calibration curve, the cell number for the individual samples was extrapolated.

3.2.6 In vivo implantation of 3D patterned PVA grafts in rat animal model

In vivo experiments were carried out by our collaborator in INSERM (Paris, France). Animal study was done in accordance with Principles of Laboratory Animal Care and with approval of the Animal Care and Use Committee of the Claude Bernard Institute (Paris, France). Adult male Wistar rats (450-600 g) were administered with sodium pentobarbital intraperitoneally (50 mg/kg). Under an operating stereomicroscope, the infrarenal aorta was exposed and ligated. A 1 cm segment of the infrarenal aorta was resected and replaced with the 2 mm internal diameter PVA tubular grafts, either unpatterned or patterned, using end-to-end anastomosis with Prolene sutures (10/0). No anticoagulants or antiplatelets were administered post-surgery. Upon explant, grafts were cryosectioned for standard hematoxylin and eosin (H&E) and immunofluorescence staining against nucleus (DAPI, Life Technologies) and RECA-1 antigen (Serotec).

3.2.7 Statistical analysis

One-way ANOVA with Fisher's LSD multiple comparison test were performed when comparing the cell density on different topographies. Two-way ANOVA with Sidak's multiple comparison test were performed when comparing the dimension of the feature topography between PDMS mold and patterned PVA films. Significant difference in the average value was considered when $P < 0.05$.

3.3 Results and discussion

3.3.1 Fabrication and patterning of 2D PVA hydrogel films via casting and NIL

Using STMP-crosslinked PVA, 2D patterning of PVA was achieved via the process of casting on PDMS mold as shown in Figure 3.1. PDMS is a crosslinked elastomer that is ideal for patterning of solvent-laden polymer such as PVA because of its ability to absorb residual solvent. This is useful to minimize the formation of bubbles in the patterned materials when the solvent has high affinity with the polymer. Plasma treatment also improved the wetting property of PDMS mold and centrifugation was performed to further improve the filling by removing the trapped air in the structures. With these modifications, the patterning of PVA hydrogel by casting on various PDMS molds were achieved for micron-size feature as shown in Figure 3.4.

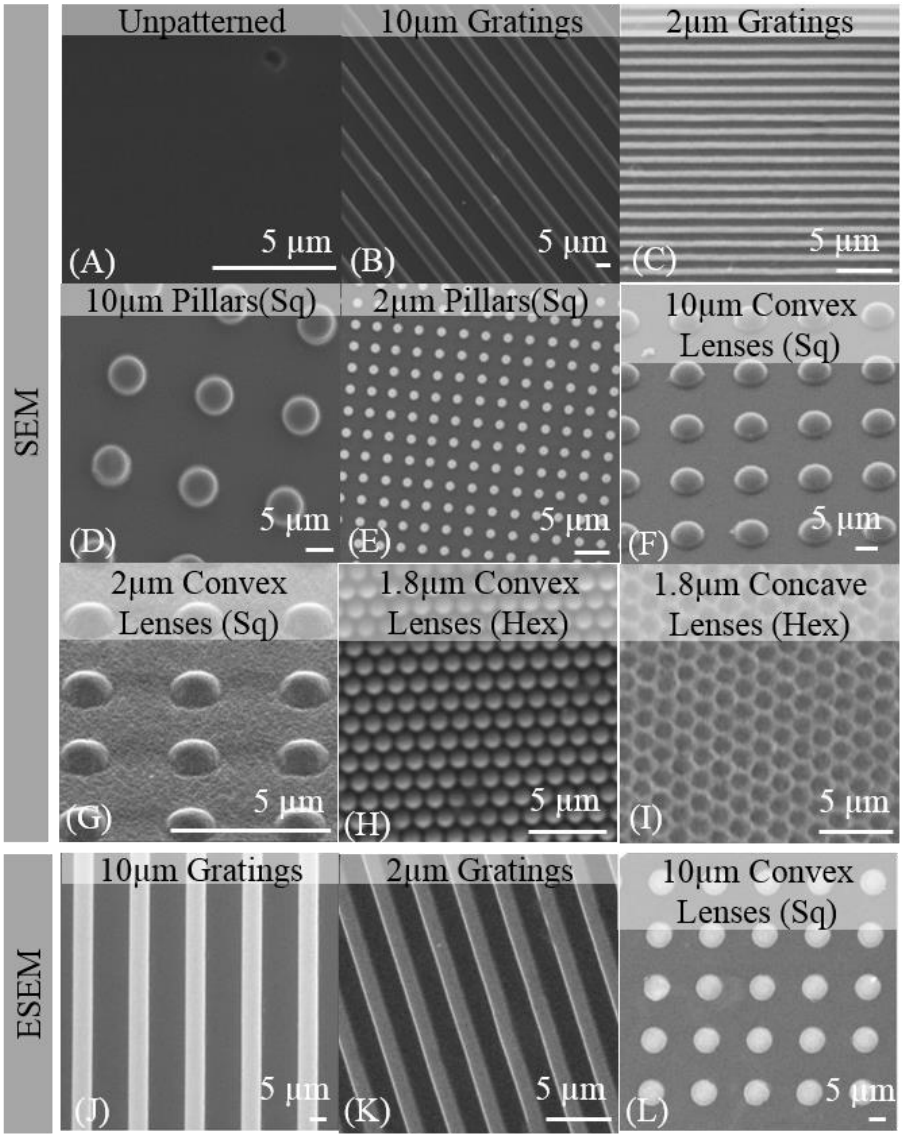

Figure 3.4: SEM and eSEM of PVA patterned films via casting process. SEM images of various topographies: (A) Unpatterned control, (B) 10 µm gratings, (C) 2 µm gratings, (D) 10 µm pillars in square array, (E) 2 µm pillars in square array, (F) 10 µm convex lenses in square array, (G) 2 µm convex lenses in square array, (H) 1.8 µm convex lenses in hexagonal array, and (I) 1.8 µm concave lenses in hexagonal array. eSEM images of 3 selected topographies: (J) 10 µm gratings (K) 2 µm gratings and 10 µm convex lenses in square array.

Table 3.1: Comparison of the topography dimension between actual dimensions from the PDMS mold replicated versus measured dimensions from SEM characterization of dried PVA films (n=3).

Topography on Si mold and PVA films	**Dimension on PDMS mold (obtained from vendor with +/- 5% variation)**	**Dimension measured from SEM images of PVA films**
10 µm Gratings	10.2 ± 0.6 µm (Width) 19.1 ± 0.4 µm (Pitch)	7.6 ± 0.3 µm (Width) 14.1 ± 0.3 µm (Pitch)
2 µm Gratings	2.0 ± 0.1 µm (Width) 2.9 ± 0.1 µm (Pitch)	1.4 ± 0.1 µm (Width) 2.8 ± 0.3 µm (Pitch)
10 µm Pillars (Square array)	10.3 ± 0.2 µm (Dia.) 19.2 ± 0.3 µm (Pitch)	6.0 ± 0.5 µm (Dia.) 17.0 ± 0.5 µm (Pitch)
2 µm Pillars (Square array)	1.5 ± 0.1 µm (Dia.) 4.0 ± 0.1 µm (Pitch)	1.3 ± 0.1 µm (Dia.) 3.2 ± 0.1 µm (Pitch)
10 µm Convex lenses (Square array)	10.5 ± 0.2 µm (Dia.) 19.7 ± 0.2 µm (Pitch)	7.6 ± 0.3 µm (Dia.) 15.1 ± 0.3 µm (Pitch)
2 µm Convex lenses (Square array)	1.8 ± 0.1 µm (Dia.) 3.9 ± 0.1 µm (Pitch)	1.4 ± 0.2 µm (Dia.) 3.4 ± 0.2 µm (Pitch)
1.8 µm Convex lenses (Hexagonal array)	1.6 ± 0.1 µm (Dia.) 2.0 ± 0.1 µm (Pitch)	1.2 ± 0.1 µm (Dia.) 1.5 ± 0.1 µm (Pitch)
1.8 µm Concave lenses (Hexagonal array)	1.4 ± 0.1 µm (Dia.) 2.0 ± 0.1 µm (Pitch)	1.1 ± 0.1 µm (Dia.) 1.4 ± 0.1 µm (Pitch)

Table 3.2: Comparison of topography dimension between measured dimensions from SEM characterization of PDMS mold versus measured dimensions from eSEM characterization of hydrated PVA films (n=1).

Topography on Si mold and PVA films	**Dimension measured from SEM images of PDMS molds**	**Dimension measured from eSEM images of PVA films**
10 µm Gratings	10.2 ± 0.6 µm (Width) 19.1 ± 0.4 µm (Pitch)	5.7 ± 0.5 µm (Width) 15.8 ± 1.2 µm (Pitch)
2 µm Gratings	2.0 ± 0.1 µm (Width) 2.9 ± 0.1 µm (Pitch)	1.2 ± 0.2 µm (Width) 3.0 ± 0.2 µm (Pitch)
10 µm Convex lenses (Sq)	10.5 ± 0.2 µm (Dia.) 19.7 ± 0.2 µm (Pitch)	7.2 ± 0.3 µm (Width) 15.0 ± 0.4 µm (Pitch)

SEM images verified 100% yield of the patterned area with topographies like gratings, pillars, and concave and convex lenses on PVA hydrogel (Figure 3.4 A-I). Topographies on PVA hydrogel displayed around 30-40% reduction in dimension, as compared with the respective PDMS templates (Table 3.1).

Two-way ANOVA analysis showed that most of the feature dimensions on patterned PVA films were significantly different from its respective PDMS mold except for 2 μm pillars and 1.8 μm concave lenses. Largest reduction was observed for topographies with the feature size of 10 μm. eSEM characterization was performed on the selected topographies (Figure 3.4 J-L) to verify topography dimensions in the hydrated state of the PVA hydrogel. Significant reduction in the dimension of the selected topographies were also observed (Table 3.2). This implies that regardless of the imaging techniques, the topography on PVA obtained through casting is consistently smaller than the topography on the PDMS mold. One possible reason for the reduction in feature could be due to the loss of water during crosslinking process. This could also explain why nano-size feature such as 250 nm gratings replicated using PDMS molds via casting showed shape distortion and poor yield. In addition, capillary forces increases on nano-size feature topography [144]. Thus higher resistance force experience by the PVA during filling leads to incomplete filling. Additional force might be required during patterning for nano-size feature topography. Nonetheless, the shape of the micron-size topography was still well replicated despite the smaller feature dimension measured.

To overcome the limitation of micron-size resolution, NIL patterning on PVA hydrogel was explored. NIL is a high-resolution patterning technique for topographies down to 5 nm in size [29]. Using NIL for PVA patterning reduced the time to obtain a stably patterned PVA hydrogel films and the introduction of pressure during the patterning process can also drive PVA patterning towards nano-size topographies. Figure 3.2 illustrated the patterning

of PVA hydrogel using NIL process. Since the crosslinking PVA solution has high water content, a pre-drying step was incorporated to remove excess water. PDMS mold was also used to assist the escape of residual water during imprinting. It was observed that imprinting on wet PVA solution leads to incomplete crosslinking, partial dissolution and poor patterning replication.

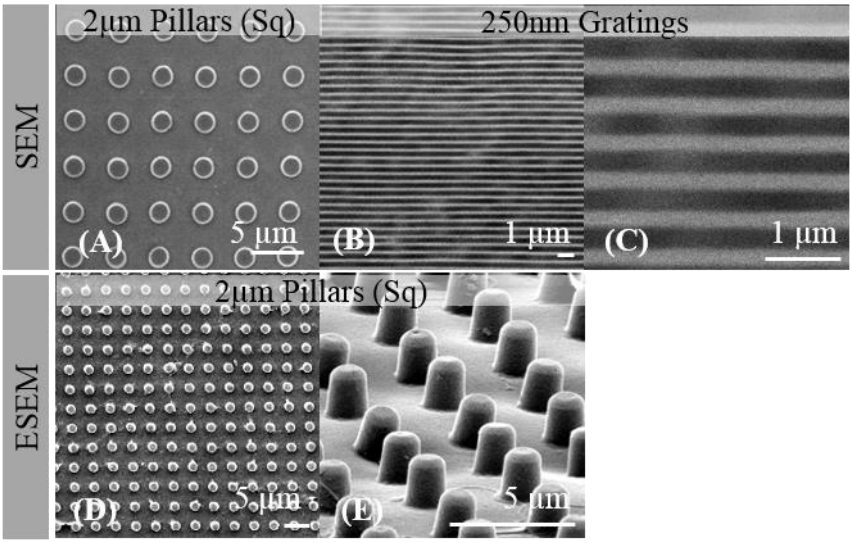

Figure 3.5: SEM of PVA patterned films via NIL (A) 2 μm pillars in square array (B,C) 250 nm gratings and eSEM of hydrated PVA films (D,E) 2 μm pillars in square array.

Successful patterning of 2 μm pillars on PVA hydrogel films was verified via SEM and eSEM (Figure 3.5 A, D-E). Compared with the diameter of 2 μm PVA pillars fabricated via casting (1.3±0.1 μm diameter), pillars fabricated using NIL achieved a diameter closer to 2 μm (1.9±0.1 μm), with no significant difference with dimension obtained from the PDMS mold. Next, patterning of 250 nm gratings topography was performed. PVA films with 250 nm gratings were successfully replicated with a grating width of 227.7±2.0 nm (Figure 3.5 B-C). As verified by the high fidelity of topography observed on PVA film patterned via NIL, the presence of pressure during patterning greatly improve the topography dimension as well as the patterning resolution of PVA

hydrogel. Using NIL patterning, topography with nano-size feature was achieved.

3.3.2 In vitro study on the effect of topography on EA.hy926 cell attachment on PVA hydrogel films

Studies had shown that mimicking the porous and fibrillar structures of the EC basement membrane resulted in increased EC adhesion [7, 54] showing that topography can modulate the EC behaviour. Thus, this part of the study examines the effect of topographical cues on PVA hydrogel on cell adhesion. Concurrently, topographical design for EC adhesion on soft materials will also be identified.

PVA 2D films with various topographies were fabricated and EA.hy926 cells were cultured on the PVA films for 24 hours before staining and quantifying the number of cells (Figure 3.6).

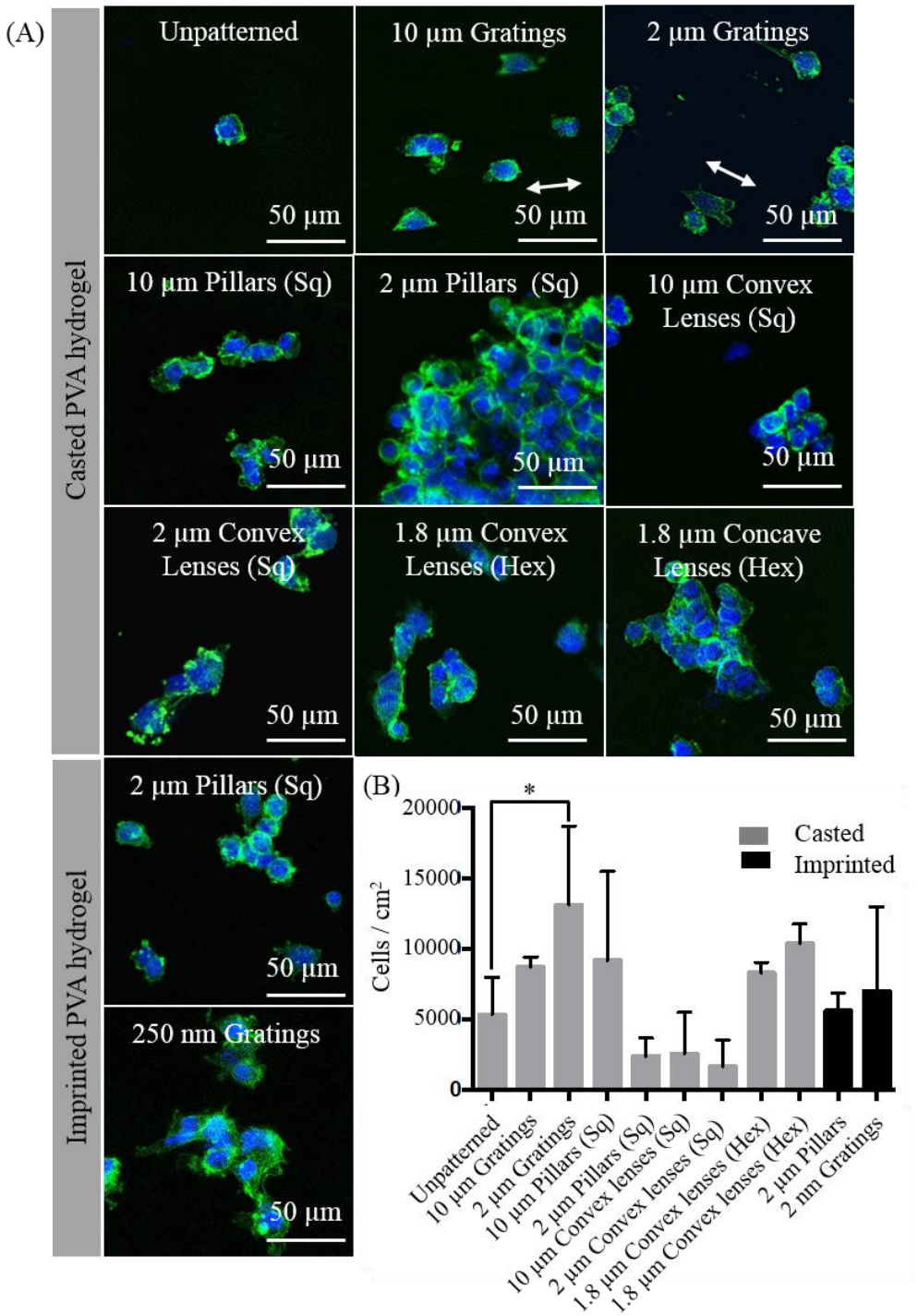

Figure 3.6: EA.hy926 adhesion on 2D patterned planar PVA films. (A) Images of fluorescent stained cells grown for 24 hours on patterned PVA films. Blue represents nucleus, green represents F-actin and white arrows denote gratings axis. (B) Cell density of cells attached to 2D patterned PVA films. Data is shown as average ± standard deviation. One-way ANOVA with Fisher's LSD post-hoc test was performed. * denotes statistical significance with $p < 0.05$.

The selection of topographies were identified based on the design parameters of topography orientation, geometry and feature size. These parameters are commonly varied and compared to determine their influence on cell behaviour. As observed in the experiment, EA.hy926 morphology and cell number changes when cultured on PVA films with different topography. While the unpatterned control showed low cell attachment with rounded morphology, patterned PVA films showed increase cell attachment with a more spread morphology after 24 hours. From the cell count, PVA films with 2 µm gratings showed significant increase in cell attachment as compared to the unpatterned control. Though no significant differences were observed, PVA films with 1.8 µm concave and convex lenses structures, 10 µm gratings and 10 µm pillars also showed notable increased in cell attachment (Figure 3.6 B). The observations are similar to previous studies where non-cell adhesive polyethylene glycol hydrogel with gratings and pillars of less than 10 µm enhanced fibroblast cell adhesion compared with the unpatterned control [145]. Beside feature size, this study also highlighted some potential design parameters like feature height and pattern density that could also affect cell adhesion. For instance, the main difference between 10 µm pillars and 10 µm convex lenses lies in their feature height. Comparing their cell count, a reduction of cell adhesion was observed on 10 µm lenses as compared to 10 µm pillars. Different cell number was also observed between 2 µm convex lenses and 1.8 µm convex lenses. Both topography have lenses structure of similar diameter but, their different pattern densities possibly caused the change in cell adhesion behaviour. However, studies on topography by varying these parameters will need to be conducted to verify this speculation.

Similarly, increased cell attachment was also observed on 2 µm pillars structures and 250 nm gratings PVA imprinted films. Yet comparing the cell count of the 2 µm pillars via imprinting and casting, imprinted PVA films have a higher cell attachment as compared to casted PVA films. This could be due to the cells ability to sense the rigidity of the glass substrate of the thin PVA films after imprinting. Secondly, the imprinting process is done at a rapid curing process that could affect the materials properties of the PVA hydrogel, resulting in better cell attachment. Thirdly, the diameter of 2 µm pillars via casting is smaller than imprinted 2 µm pillars. This dimension change could also have resulted in the chance in cell adhesion.

Overall, modification of 2D PVA hydrogel films with topography were demonstrated to have better capacity for cell adhesion *in vitro*. Since the potential application of PVA is in vascular graft, 3D patterning and *in situ* endothelialisation are also important and are investigated next.

3.3.3 Fabrication and patterning of 3D PVA hydrogel grafts via casting/ dip-coating

In situ endothelialisation is a widely explored strategy to improve long-term success and benefit of vascular grafts with small diameters (less than 6 mm) [146]. Despite its *in vitro* benefit in directing EC behaviour, topographical cues have yet to be explored for its translational application as a vascular graft. This is due to the challenges in non-planar patterning, especially in the lumen of a small tube with restricted working space. To bridge the gap in 3D patterning capability, a novel patterning technique was developed. Among the library of topography that was tested with cell adhesion on 2D patterned PVA, 10 µm gratings, 2 µm gratings, 1.8 µm convex lenses and 1.8 µm concave

lenses were used to demonstrate the novel 3D patterning due to higher cell adhesion on these patterns compared with the unpatterned control in the *in vitro* studies (Figure 3.6).

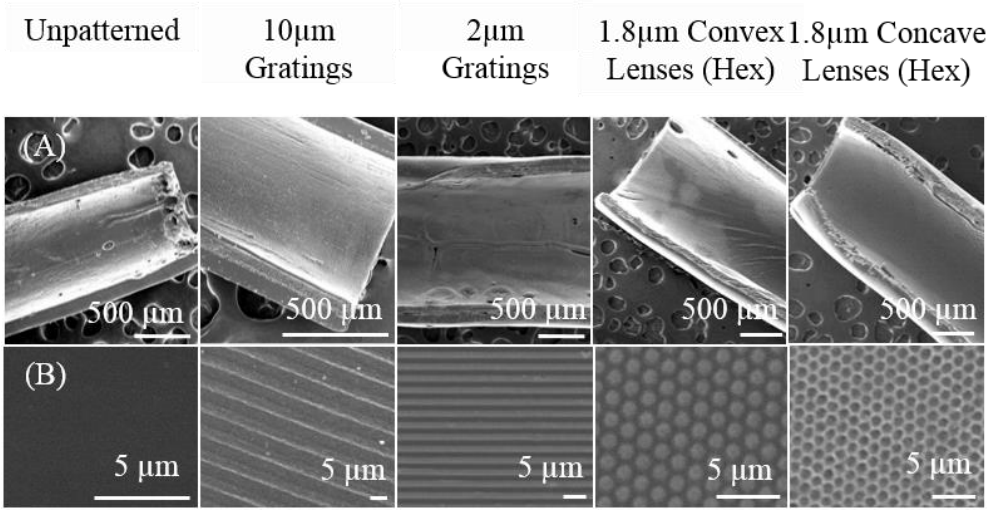

Figure 3.7: SEM characterization of the 3D PVA grafts. (A) The macroscopic view of the vascular graft and (B) the high magnification of the luminal topographies of the grafts.

As shown in Figure 3.7, 3D PVA hydrogel grafts were fabricated and SEM image of the lumen showed the presence of topography on its luminal surface. Notably, topographies were observed throughout the length of the 3D vascular graft. The topography shape was also observed to be well replicated from the SEM images.

To the best of our knowledge, this is the first demonstration of a 3D patterned vascular graft with different types of periodic topographies less than 10 µm in size to be present in the luminal surface.

3.3.4 In vivo study on the effect of topography on patency of PVA hydrogel vascular graft using rat animal model

To show the benefit of the 3D patterned PVA grafts, small diameter PVA grafts were implanted in a rat abdominal aorta as a proof-of-concept study.

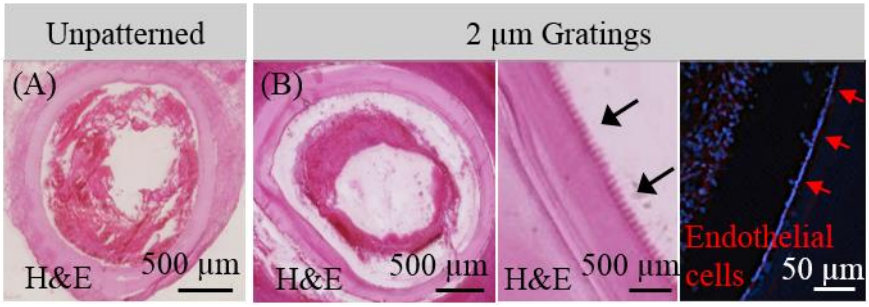

Figure 3.8: Histological analysis of PVA grafts implanted in rat abdominal aorta. After 20 days, (A) H&E showed the unpatterned PVA grafts (n=2) were occluded while (B) patterned PVA grafts with 2 µm gratings (n=2) remained patent. H&E showed 2 µm gratings on PVA graft retained after implantation, denoted by black arrows. Immunofluorescence stain showed RECA-1-positive EC (red) on the luminal surface of patterned PVA grafts with 2 µm gratings, as denoted by red arrows. Blue stain showed EC nuclei.

PVA vascular grafts without pattern (n=2) and with 2 µm gratings (n=2) were implanted (Figure 3.8). Outstandingly, patterned PVA grafts remained patent for 20 days without the anticoagulant or antiplatelet, while the unpatterned PVA grafts were completely thrombosed (Figure 3.8 A). Moreover, 2 µm gratings on PVA grafts were clearly visible on sections stained with H&E, thus affirming robust patterns that can withstand high shear stress in the aorta for 20 days (Figure 3.8 B). Most significantly, detection of EC by staining against RECA-1 antigen was observed on PVA grafts with 2 µm gratings. This has proven that the addition of topography helps EC attachment and further improves the performance of PVA hydrogel tubular graft.

3.4 Conclusion

In conclusion, 2D and 3D patterning of PVA hydrogel was successfully demonstrated with high yield and pattern integrity. Patterning of 2D PVA film was achieved using casting and NIL process and 3D PVA tubes was achieved using dip-coating process. The casting process presented for 2D PVA films is simple and does not require any specialized equipment, but the fabrication

process is limited to micron-size resolution. In contrast, patterning of 250 nm gratings was successfully demonstrated using NIL with high yield. The aid of pressure from the imprint process helped to overcome the capillary force in filling up nano-size structure. To aid the integration of topography into useful 3D platforms, a novel 3D patterning method was developed to achieve luminal patterning of tubular PVA graft. Micron-size patterning was achieved using this technique and to the best of our knowledge, this is the first demonstration of achieving patterns in the tube lumen.

Subsequently, using these patterned PVA films and grafts, PVA interaction with cells were improved and EC adhesion was enhanced. *In vitro* study showed enhancement of EC adhesion for PVA hydrogel with 10 and 2 µm gratings, 10 µm pillars and 1.8 µm concave and convex lenses with more spread EC morphology as compared to the unpatterned control. This indicates the importance of topography cue to modulate cell behaviour. *In vivo* study using PVA graft with 2 µm gratings also showed endothelialisation when implanted into a rat abdominal aorta, demonstrating for the first time the valuable effect of topography *in vivo*.

To sum up, both *in vitro* and *in vivo* experiments showed that the cell adhesion on PVA hydrogel were improved with topographical modification.

Chapter 4 Screening for topographical effects on endothelial cellular behaviours

4.1 Introduction

In the previous chapter, EC adhesion on PVA hydrogel was enhanced with topographical modification. However, due to the limited topographies tested in the previous chapter, the topographical design to modulate cellular behaviours cannot be affirm. Thus, there would be a need to conduct a screening experiment to identify the topographical design that will modulate EC cellular behaviours to promote endothelialisation. Nonetheless, the poor cell adhesion on PVA hydrogel can interfere with the comparison between the patterned and the unpatterned control, possibly masking the effect of topography on cellular behaviours. Hence, instead of using PVA hydrogel, PDMS is used as it is more favourable for cell attachment. In addition, PDMS is also widely used in the area of research that explore the effect of topography on cellular behaviours.

Each MARC chip contains 49 different topographies that equips the users with the flexibility in selecting a wide range of topographies for high-throughput screening application. Although there are similar technology platforms like BioSurface Structure Array (BSSA) [147] or ToPoChip [148] that also allow high-throughput screening of topographies, MARC chip offers a more versatile array of topographies in different dimension ranges. BioSurface Structure Array and ToPoChip platform are fabricated using photolithography techniques that limit the feature size to micron range and a long tedious process is necessary to obtain variations in feature height or depth on a single

chip. Whereas for MARC chip, each area is fabricated individually using the NIL process, thus, micron- and nano-size features with different height profiles can be assembled in one chip with ease and high pattern fidelity. This provides a wider selection of topographical design necessary for screening experiments.

MARC chip has been used in our group as a screening tool to investigate the effect of topography on cell differentiation [56-58]. For instance, 2 μm and 250 nm gratings were identified by the MARC chip screening to promote differentiation of primary murine neural progenitor cells to neurons [57]. This demonstrates the capability of MARC chip as a screening tool and its suitability as a platform for exploring various EC cellular behaviours especially adhesion and proliferation.

Endothelialisation can be promoted by increasing EC adhesion and proliferation. The use of topography to promote EC adhesion has been demonstrated in Chapter 3 using patterned PVA hydrogel. Similarly, others have demonstrated the topographical effect on EC proliferation [7, 55, 149]. In our group, we reported an increase in HUVEC proliferation when cultured on 70 nm TiO_2 gratings and 420 nm wells [55]. Other than the use of topography, the delivery of growth factors like VEGF or basic fibroblast growth factor (bFGF) or its respective DNA plasmid [102, 103] can also promote endothelialisation, as well as angiogenesis for the treatment of peripheral arterial disease [150]. The enhancement of endothelialisation through gene therapy depends on the overall transfection efficiency. Thus, the efficiency of HUVEC transfection would be another important cellular behaviour to study for enhancing endothelialisation.

In this chapter, MARC chip will be used as a platform to screen and identify topographical designs to modulate HUVEC adhesion, proliferation and transfection for future vascular application.

4.2 Materials and methods

4.2.1 Fabrication of MARC substrate

MARC chip was a 2.5 cm by 2.5 cm template that contains an array of different patterned areas of 2 mm by 2 mm. The patterned area was made up of polycarbonate (PC) films fabricated via NIL using different Si templates. The individually imprinted PC was diced to a size of 2 mm by 2 mm and assembled on a clean Si substrate using PDMS as an adhesive. This was subsequently used as a template for sample replication [57].

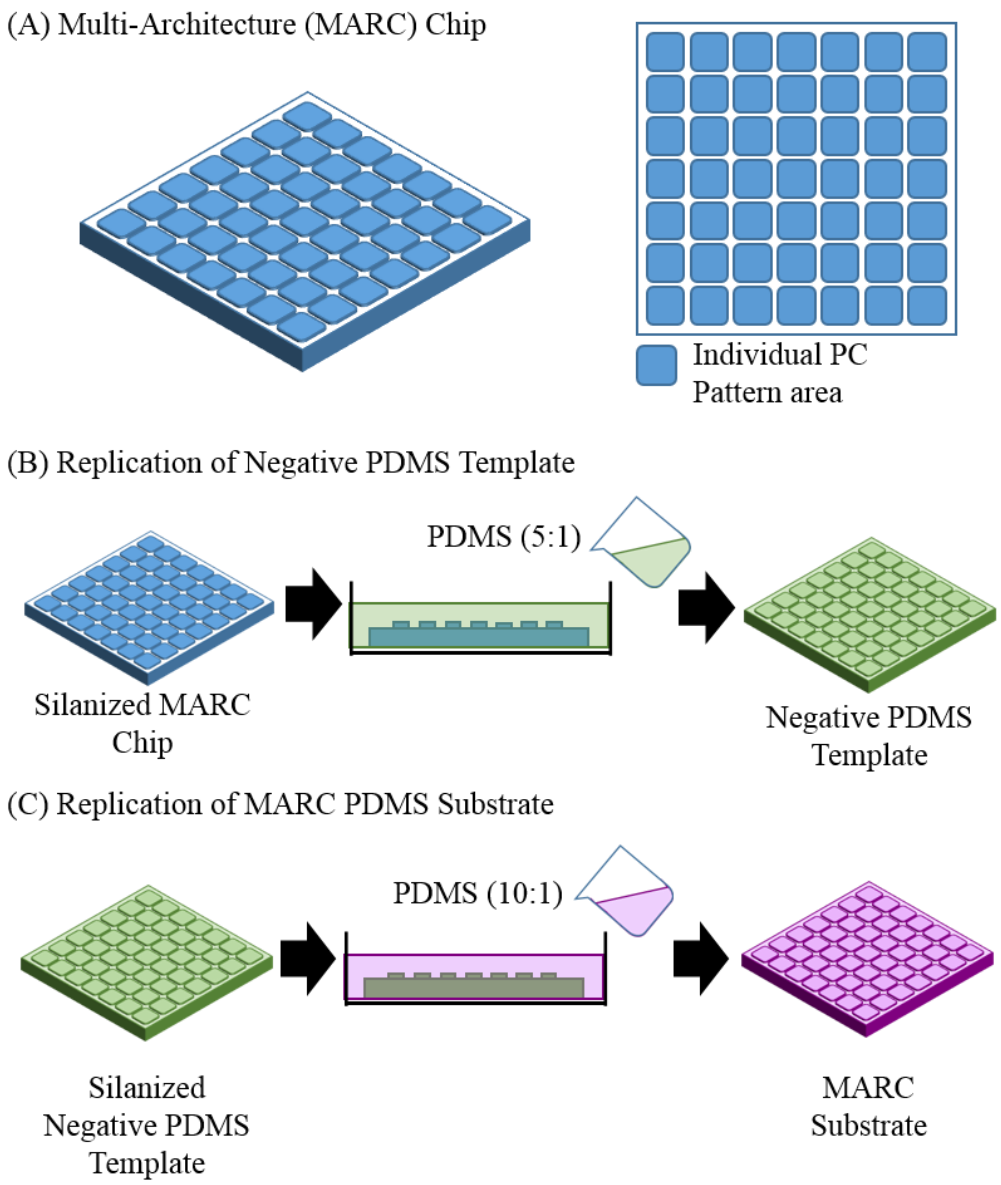

Figure 4.1: Fabrication of MARC substrate using soft lithography techniques. (A) Layout of MARC chip, consisting of an array of PC imprinted area (B) Replication of negative PDMS template using PDMS mixture of 5: 1 (elastomer base: curing agent) (C) Replication of MARC substrate using PDMS mixture of 10: 1 (elastomer base: curing agent)

Before PDMS replication was carried out using the MARC chip, the MARC chip was silanized with 1H,1H,2H,2H-Perfluorodecyltrichlorosilane (FDTS) (Alfa Aesar) overnight in a glass desiccator under vacuum. The hydrophobic coating allows ease of separation of the MARC chip from the PDMS polymer without damaging the patterned surface. Figure 4.1 illustrated the double

replication process performed on the silanized MARC chip to obtain PDMS substrates with topographies of the same pattern polarity. First, the negative PDMS template was fabricated by replicating the MARC template. Briefly, a PDMS mixture was prepared at the ratio of 5:1 (elastomer base: curing agent), desiccated under vacuum to remove air bubbles and poured over the MARC template in a petri-dish. The setup was cured overnight at 70 °C and the negative PDMS template was demolded from the silanized MARC chip. Next, the negative PDMS template was silanized with the same process used for MARC chip. A PDMS mixture was prepared at the ratio of 10:1 (elastomer base: curing agent), desiccated and casted over the silanized negative PDMS template. Similarly, the PDMS mixture was cured at 70 °C overnight. Finally, the MARC substrate was demolded from the negative PDMS template, ready to be used for the subsequent experiment.

4.2.2 Fabrication of topography for individual pattern substrate

A PDMS substrate of an individual pattern with an area larger than 1 cm^2 was fabricated by casting PDMS of ratio 10: 1 on an imprinted polycarbonate mold with the selected topography. The cured PDMS substrate was then demolded from the PC and used for subsequent experiment.

4.2.3 Characterization of topography by atomic force microscopy (AFM)

Atomic force microscopy (AFM) (Bruker, ICON) was used to verify the topography fabricated. The measurement was carried out using tapping mode and AFM data was post analysed using Gwyddion software [151] to obtain the surface profile of the topography.

4.2.4 Cell culture of HUVEC on various topographies

The PDMS substrates were treated with oxygen plasma for 1 min at 80 % power followed by decontamination with UV light for 20 minutes. HUVEC (Lonza) cultured to 80 % confluence level in endothelial growth medium, (EGM-2, Lonza) was rinsed with Hanks' balanced salt solution (HBSS, Sigma-Aldrich) containing 2 % of 4-(2-hydroxyethyl)-1-piperazineethane sulfonic acid (HEPES, Sigma-Aldrich) before trypsin-EDTA solution (Lonza) was used to detach the cells from the flask. TNS (Lonza) was then added to neutralise the enzymatic process after 3 minutes of incubation time. Finally, after centrifuging the cell suspension at 1300 rpm for 5 minutes, the obtained cell pellet was re-suspended in EGM-2 and seeded on the PDMS substrate. HUVEC of passage 4-5 was used for the experiment at a seeding density of 10,000 cells/cm^2 unless otherwise stated.

4.2.5 Adhesion assay of HUVEC on MARC chip

4.2.5.1 Cells cultured on MARC substrate

After 24 hours of incubation, the cells were fixed and fluorescently stained with DAPI and F-actin. Samples were observed and imaged using an epifluorescence microscopy (Leica DM IRB) for further analysis. The total cell number on each pattern of area 2 mm by 2 mm was obtained via image analysis using Image J software. For detailed analysis of the cell morphology, Metamorph software was used to quantify the cell area and circularity of single cells on the selected topography. Cell circularity is denoted by the shape factor, which equals to $4\pi Area/Perimeter^2$ where a value of 1 indicates a perfect circle. The measurement was obtained from an average of 50 single cells per selected topography.

4.2.5.2 Cells cultured on individual pattern substrate

After 24 hours, the cells were rinsed with HEPES-HBSS (Sigma-Aldrich) before being detached from the substrate using trypsin-EDTA (Lonza). TNS (Lonza) was then added to neutralise the enzymatic detachment process. The cell suspension was collected and centrifuged at 1300 rpm for 5 minutes. After aspirating the supernatant, the cell pellet obtained was quantified using the CyQUANT proliferation assay kit (Life Technologies.) as described in Chapter 3.2.5.

4.2.6 Proliferation assay of HUVEC on MARC chip

4.2.6.1 Cells cultured on the MARC substrate

The proliferation assay was carried out using the Click-iT® cell proliferation kit (Life Technologies).

EdU working solution of 10 µM solution was prepared from 10 mM EdU stock solution by diluting it with EGM-2. 20 hours after cell seeding on the substrate, half of the culturing media was replaced with fresh media containing EdU. The cells were incubated for another 4 hours before cell fixation with 4 % PFA and cell permeabilization with 0.5 % Triton-X were carried out.

The 500 µl of solution, containing 430 µl of 1X Click-it® reaction buffer, 20 µl of $CuSO_4$, 1.2 µl of Alexa Fluor® azide and 50 µl of EdU reaction buffer additive, was prepared and added to the samples for EdU detection. After 30 minutes of incubation at room temperature with protection from light, the samples were rinsed and stained for cell nuclei using DAPI following the protocol from Chapter 4.2.10. Epifluorescence images of the entire area of 2 by 2 mm for each pattern array were taken and analysed using Image J. The

proliferation rate was obtained from the ratio between the number of EdU positive cells and the total cell number obtained by quantifying the DAPI count.

4.2.7 Amplification and purification of DNA plasmid

P_{max} FP-Green-C vector (Lonza, 4.7 kb) which expresses maxFP-Green in mammalian cells were amplified in *Escherichia coli* DH5α and purified using an AxyPrep plasmid midiprep kit (Axygen Bioscience). The cultured bacteria containing the GFP plasmids were lysed, neutralised and collected in the filtering membrane. Different reagents were passed though the membrane to purify the DNA by removing the salt and endonucleases. The GFP plasmid was collected from the membrane using the elution buffer and DNA concentration was measured at the absorbance wavelength of 260nm (Nanodrop 2000, Thermo Scientific). The GFP plasmid was subsequently used for transfection experiment.

4.2.8 Transfection of HUVEC on PDMS MARC chip using Lipofectamine 2000

Transfection of the cells was carried out using lipofectamine 2000 (Invitrogen). 24 hours after cell seeding on a PDMS MARC substrate, the culturing media was replaced with Opti-MEM (Invitrogen) media containing lipofectamine 2000 reagent and GFP plasmid at a ratio of 1:1. GFP plasmid at the concentration of 250 ng/cm^2 was used with respect to culture area. After 3 hours of incubation, the media was replaced with fresh EGM-2 media and incubated for another 18 hours for GFP expression. The cells were fixed with 4 % PFA and stained for cell nuclei with DAPI.

4.2.9 Transfection of HUVEC on individual pattern substrate

HUVEC were cultured on selected individual pattern substrate and transfection was performed using lipofectamine 2000 similar to Chapter 4.2.8. After transfection, flow cytometry characterization was performed as described in Chapter 4.2.11.

4.2.10 Fluorescence imaging of cells on various topographies

HUVEC on various topographies were rinsed with HEPES-HBSS (Sigma-Aldrich) before fixing in 4% PFA for 15 minutes in 4 °C. The samples were then incubated with DAPI (1:3000) and/or Phalloidin (1:300) (Alexa Fluor, Invitrogen) for 20 minutes before mounting for imaging. Epifluorescence images were taken and analysed using Image J.

4.2.11 Flow cytometry analysis

Samples were rinsed with HEPES-HBSS saline (Sigma-Aldrich) solution and trypsin-EDTA (Lonza) was used to detach the cells from the substrate. TNS (Lonza) was then added to neutralise the enzymatic detachment process. The collected cell suspension was washed and re-suspended in phosphate buffered saline (PBS) before cells were fixed with 1 % (wt/vol) PFA for 15 minutes at 4 °C. The cells were centrifuged and rinsed with PBS before the solution was filtered through a 60 µm pore size nylon filter. The cells solution was then analysed using a flow cytometry (BD LSR Fortessa). Cells that were not transfected were used as the gating and negative controls. The percentage of fluorescent population was studied using the flow cytometry data analysis software, FlowJo.

4.2.12 Statistical analysis

For the experiment using the MARC substrate, a 2-tailed Mann-Whitney test was performed to compare between the unpatterned and patterned area on the array. From the Mann-Whitney test, the null hypothesis defines that the average cell number on the unpatterned area is the same as the average cell number on another patterned area unless $U_{Cal} < U_{Critical}$ [152]. Using the calculated U_{Cal} of < 18 (at 90 % C.I) and U_{Cal} of < 22 (at 85 % C.I), the topography with a significantly different value from the unpatterned control was identified.

For the individual pattern analysis for cell adhesion, one-way ANOVA was performed followed by Bonferroni's multiple comparison test, for the analysis of the cell behaviour between the different topographies and the unpatterned control. Analysis of p-value of at least <0.05 was considered as significantly different.

4.3 Results and discussion

4.3.1 Characterization of topographical structures fabricated via soft lithography

The MARC chip with 49 topographies were used in this study and its topographical geometry and dimensions were shown in Table 4.1

Table 4.1: List of 49 topographies and the dimension of their features in the MARC substrate used for the experiment, including the 5 unpatterned areas.

ID No	Topographical geometry	Dimensions [Diameter or Width x Pitch (centre to centre) x Height or Depth]
1	Unpatterned	-
2	Gratings	2 µm x 4 µm x 2 µm
3	Gratings	2 µm x 3 µm x 80 nm

4	Gratings	1 µm x 3 µm x 120 nm
5	Gratings	250 nm x 500 nm x 250 nm
6	Pillars (Square array)	10 µm x 20 µm x 10 µm
7	Pillars (Square array)	2 µm x 12 µm x 2 µm
8	Pillars (Square array)	2 µm x 4 µm x 2 µm
9	Pillars (Square array)	500 nm x 10 µm x 500 nm
10	Pillars (Square array)	250 nm x 500 nm x 250 nm
11	Holes (Square array)	1 µm x 7.5 µm x 1 um
12	Convex lenses (Hexagonal array)	1.8 µm x 2 µm x 700 nm
13	Unpatterned	-
14	Convex lenses (Square array)	800 nm x 1 µm x 300 nm
15	Pillars (Square array)	2 µm x 12 µm x 700 nm
16	Pillars (Square array)	2 µm x 12 µm x 500 nm
17	Pillars (Square array)	2 µm x 12 µm x 450 nm
18	Pillars (Square array)	2 µm x 12 µm x 350 nm
19	Pillars (Square array)	2 µm x 12 µm x 200 nm
20	Pillars (Square array)	500 nm x 10 µm x 300 nm
21	Pillars (Square array)	500 nm x 10 µm x 200 nm
22	Pillars (Square array)	500 nm x 10 µm x 100 nm
23	Pillars (Square array)	250 nm x 500 nm x 120 nm
24	Concave lenses (Hexagonal array)	1.8 µm x 2 µm x 700 nm
25	Unpatterned	-
26	Concave lenses (Square array)	800 nm x 1 µm x 300 nm
27	Hierarchical Micron gratings with perpendicaular nano gratings	(Pri) 2 µm x 4 µm x 2 µm (Sec) 250 nm x 500 nm x 150 nm
28	Hierarchical Micron gratings with parallel nano gratings	(Pri) 2 µm x 4 µm x 2 µm (Sec) 250 nm x 500 nm x 150 nm
29	Hierarchical Micron gratings w/ nano pillars	(Pri) 2 µm x 4 µm x 2 µm (Sec) 250 nm x 500 nm x 250 nm
30	Bumps	300 nm x 300 nm x 200 nm
31	Cones	270 nm x 300 nm x 350 nm
32	Inverse cones	270 nm x 300 nm x 350 nm
33	V-gratings	2 µm x 2µm x 1.5 µm
34	V-gratings	500 nm x 500 nm x 350 nm
35	U-gratings	2 µm x 2 µm x 700 nm
36	U-gratings	500 nm x 500 nm x 200 nm
37	Unpatterned	-
38	Gratings	10 µm x 20 µm x 10 µm
39	Hierarchical Micron gratings with perpendicular nano gratings	(Pri) 2 µm x 4 µm x 2 µm (Sec) 250 nm x 500 nm x 150 nm
40	Hierarchical Micron gratings with parallel nano gratings	(Pri) 2 µm x 4 µm x 2 µm (Sec) 250 nm x 500 nm x 150 nm
41	Hierarchical Micron gratings w/ nano pillars	(Pri) 2 µm x 4 µm x 2 µm (Sec) 250 nm x 500 nm x 250 nm
42	Convex lenses (Square array)	10 µm x 20 µm x 200 nm
43	Convex lenses (Square array)	10 µm x 20 µm x 2 µm
44	Convex lenses (Square array)	2 µm x 4 µm x 400 nm
45	Convex lenses (Square array)	2 µm x 4 µm x 800 nm
46	Convex hexagon lenses (Square array)	10 µm x 20 µm x 800 nm

47	Convex hexagon lenses (Square array)	10 µm x 20 µm x 2 µm
48	Unpatterned	-
49	Hexagonal donut	50 µm (outer), 10 µm (inner) x µm x 800 nm

The library of topographies selected for the MARC substrate for this study provided a good and balanced selection of design parameters. Topographies with different feature size (micron-size to nano-size) and orientations (anisotropic to isotropic) were selected. Topographies with similar features but different shape, pitch, height, cross-sectional and curvature profile were also included for more specific design parameter comparison.

Among the topographical design, design parameters such as the cross-sectional profile and curvature feature of the topography are sparely explored for their roles in modulating cellular behaviour. Gratings, U-gratings and V-gratings topographies are anisotropic topographies with different cross-sectional profile of square-shaped, V-shaped and U-shaped respectively (Figure 4.2 A). Topography with curvature was previously defined in Chapter 2.2.3 as topography with RC in z-direction such as lenses topographies and U-gratings. U-gratings is anisotropic topography with RC in z direction and lenses is isotropic topography with RC in z direction (Figure 4.2 B).

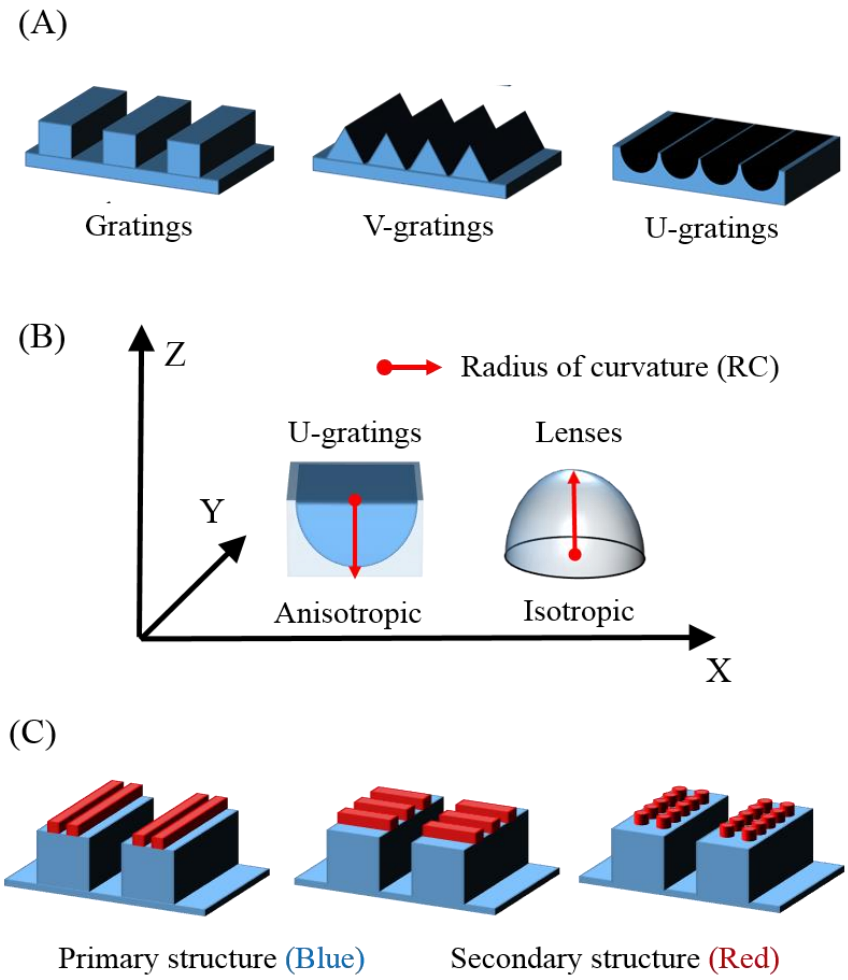

Figure 4.2: Illustration of topographies with the following design parameters: (A) Anisotropic topographies with different cross-sectional profile such as gratings, V-gratings and U-gratings with its cross-sectional profile in the shape of square, V and U respectively; (B) topographies with curvature such as U-gratings and lenses topographies with curvature in z direction (C) Hierarchical topography with gratings topography as the primary structure (Blue) and gratings or pillars as the secondary structures (Red) where the dimension of primary structures are always bigger than secondary structures.

In addition, a unique class of topography, hierarchical topography was also included in the MARC chip. Hierarchical topographies refer to structure with size, and shape variation in x, y and z- axis directions, additionally, the length scale of the structure is progressively smaller in the z-axis direction. In this thesis, the hierarchical topographies are 2-layer structure, generally with micrometer base layer (also referred to as the primary structure) and a sub-

micrometer structure in the second layer (also referred to as the secondary structure). A further variation in the hierarchical structure is the arrangement of the secondary structure. For example, the secondary structure may be present only on the top or embedded in the base structure. There are three hierarchical structures in the MARC chip as illustrated in Figure 4.2 C, where its secondary structures are located on the top of the base structures. Secondary structures such as nano-size gratings at 2 orientation; perpendicular or parallel to the primary structures and nano-size pillars were located on top of the primary structure, the micron-size gratings. Very often, the effect of the secondary features on the topography is ignored during the analysis of cellular behaviour on various topographies. The hierarchical topography in this thesis can investigate the effect of the secondary feature on cellular behaviour to bridge the knowledge in the design parameters on the secondary feature on the topography.

Replication of the topography in PDMS MARC via soft lithography was described in Chapter 4.2.1. AFM was used to characterize and verify the replicated MARC substrate (Figure 4.3). From the AFM characterization, the PDMS topographies were replicated with good fidelity such as the secondary structures on the hierarchical topographies (Figure 4.3 G and H). In addition, the 3D view of the V-gratings and U-gratings also showed that the shape of the gratings were well replicated with the distinct V-shaped and U-shaped cross sectional profile.

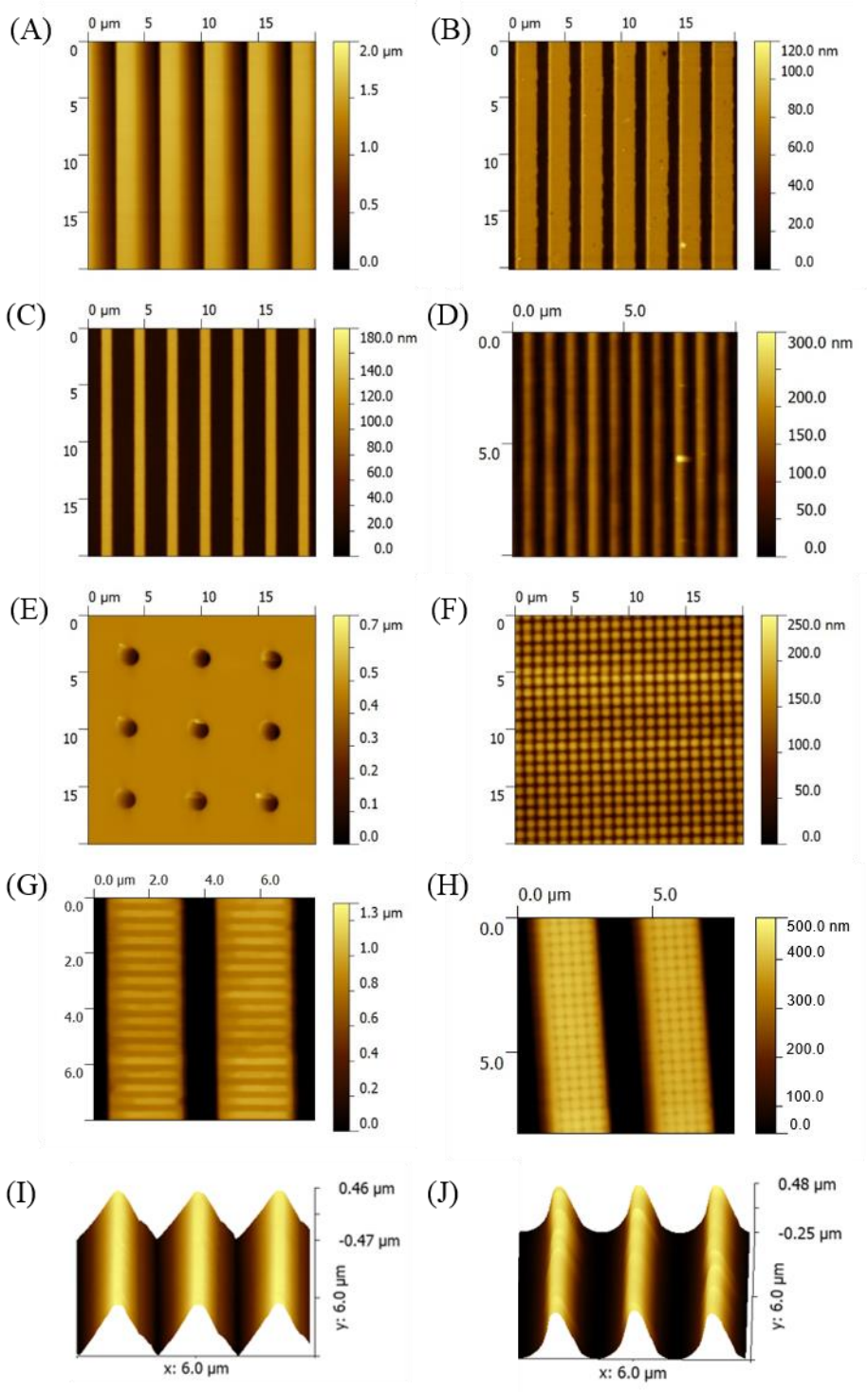

Figure 4.3: AFM of some representative topographies on MARC substrate. Top view of (A) 2 µm gratings (#02), (B) 2 µm gratings (#03), 1 µm gratings (#04), (D) 250 nm gratings (#5), (E) 1 µm holes (#11), (F) 800 nm concave lenses (#14), (G) hierarchical 2 µm gratings perpendicular with 250 nm gratings (#27) and (H) hierarchical 2 µm gratings with 250 nm pillars (#29) and 3D view of (I) 2 µm V-gratings (#33) and (J) 2 µm U-gratings (#35).

4.3.2 Screening of HUVEC adhesion using MARC chip

In this part of the thesis, primary cells HUVEC was used instead of the endothelial cell line EA.hy926. HUVEC is commonly used for physiological and pharmacological investigation thus making its cellular responses more applicable for the research community.

HUVEC were seeded at 10,000 cells/cm^2 on a PDMS MARC substrate. The cell number in 4 biological replica of the MARC substrate were quantified and analysed. Due to the small sample population (<20), the population was assumed to be non-parametric and the Mann-Whitney U-test was performed for statistical analysis [152]. Figure 4.4 A showed the calculated U_{cal} value arranged in the sequence of ascending U_{cal} value while Figure 4.4 B showed the cell count of different topographies and grouped by topographical design. In Figure 4.4 A, the red line denotes the $U_{Critical}$ value of 22 and the values, before the vertical black dashed line, corresponding to their respective topographies, were considered as being significantly different from the unpatterned control.

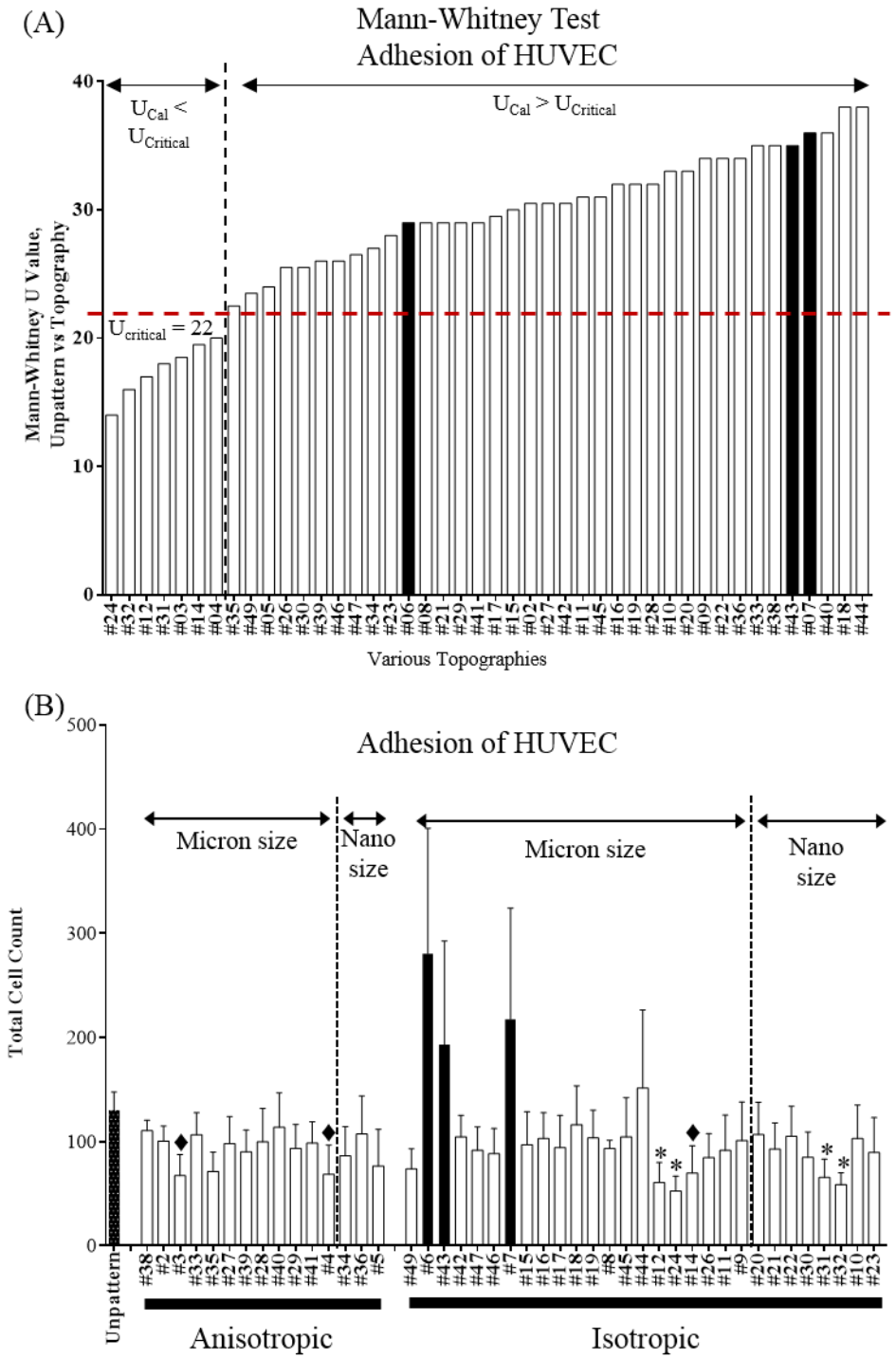

Figure 4.4: Cell adhesion of HUVEC on MARC substrate after 24 hours. Black bars denote the topographies that has a higher cell count than the unpatterned control and white bars denote the topographies that has a lower cell count than the unpatterned control. (A) Mann-Whitney test analysis ranking the U-value of the 44 topography with respect to the unpatterned control. Red line denotes the $U_{Critical}$ value of 22 at 85% C.I. (B) Overall HUVEC cell number on MARC substrate. * denotes the p-value < 0.1 (90% C.I) and ♦ denotes the p-value <0.15 (85% C.I) as compared to the unpatterned control. Error bars denotes the standard error of the mean (SE).

In general, the topographies studied had a negative influence on the HUVEC adhesion. The average cell count in Figure 4.4 B showed that cell number on topographies were generally lower as compared to the unpatterned control, and were denoted by the white coloured bars. All isotropic topographies showed a reduced cell density except the 10 µm pillars, 2 µm pillars and 10 µm convex lenses. Even though the cell number analysis did not show a significant increase, higher EC density was noted on 10 µm pillars topography on both PVA and PDMS polymer. The Mann-Whitney test at 85% C.I. level identified 7 topographies with significantly lower cell adhesion as compared to the unpatterned control (Table 4.2).

Table 4.2: Summary of average cell number from MARC substrate. (A) Various topographies selected based on Mann-Whitney statistical analysis. The order of topography is arranged in ascending cell count. (B) Various topographies that showed enhanced cell number.

	Pattern No	Topography dimension	Average cell number ± SE	U_{Cal} Value
(A)	**#24**	1.8 µm concave lenses	53 ± 12	14
	#32	Inverse cone, 270 nm pitch	59 ± 10	16
	#12	1.8 µm convex lenses	61 ± 17	17
	#31	Cone, 300 nm pitch	65 ± 15	18
	#03	1 µm gratings, 3 µm pitch	67 ± 17	18.5
	#04	2 µm grating, 3 µm pitch	69 ± 24	20
	#14	1 µm convex lenses	70 ± 23	19.5
	-	Unpatterned	130 ± 17	-
(B)	**#43**	10 µm convex lenses	193 ± 86	35
	#07	2 µm pillars, 12 µm pitch	217 ± 92	36
	#06	10 µm pillars, 20 µm pitch	280 ± 104	29

Significant cell density reduction were on isotropic topographies with RC in z direction such as 1.8 µm concave lenses, inverse cone, 1.8 µm convex lenses, cone and 1 µm convex lenses topographies. The cell number on these topographies reduced by 2-2.5 fold as compared to the unpatterned control. 1 µm concave lenses and bumps topography also contain all 3 topographical

designs. While the cell density on these topographies were not significant reduced, lower cell number were still observed (1 um concave lenses topography: 85 ± 22 cells, bumps: 85 ± 21 cells). Another topographical design with significantly reduced cell density were the micron-size gratings with low grating height. EC on micron-size gratings topography showed a 2 fold reduction in cell number as compared to the unpatterned control.

Cell adhesion is the process whereby the cells interact, adhere and spread on the surface via integrins binding [153, 154]. While cell density is a good parameter to interpret cell adhesion, information on the cells spreading is missing thus leading to incomplete analysis on the cell adhesion behaviour on various topographies. Hence, cell morphology study was done on topographies with reduced cell density for further cell adhesion analysis.

4.3.2.1 Effect of topography on HUVEC cell morphology

The cells cultured on these topographies were stained for cell nuclei and F-actin after 4 hours of adhesion to study the effect of topography on cell morphology (Figure 4.5).

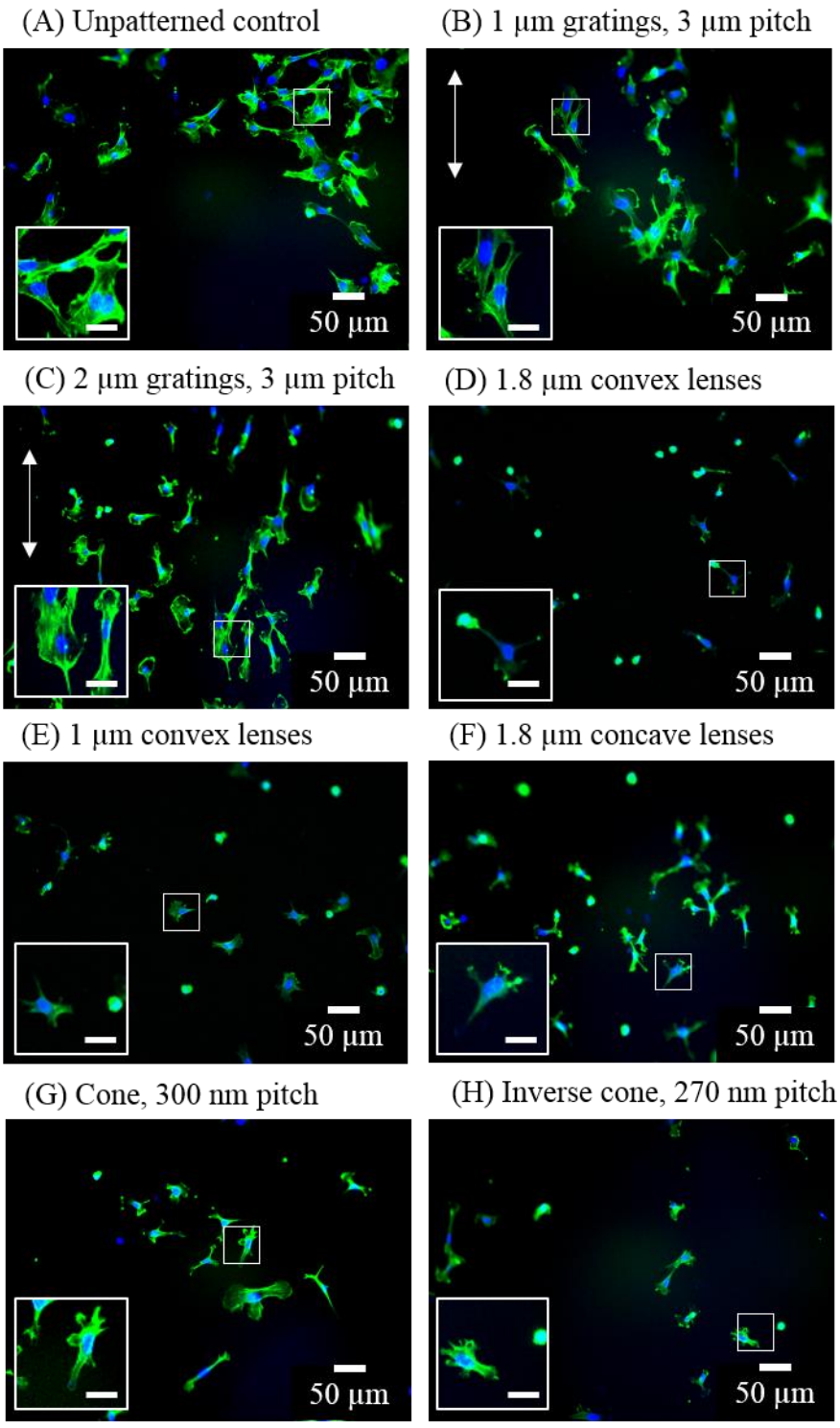

Figure 4.5: Fluorescence images of HUVEC stained for nucleus (DAPI, blue) and F-actin (Phalloidin, green) on various topographies. HUVEC were fixed and stained after 4 hours of culture. (A) Unpatterned control, (B) 1 µm gratings with 3 µm pitch, (C) 2 µm gratings with 3 µm pitch, (D) 1.8 µm convex lenses, (E) 1 µm convex lenses, (F) 1.8 µm concave lenses, (G) cone, with 300nm pitch, (H) inverse cone with 270 nm pitch. White arrow in (B-C) indicates the direction of gratings. Small insert represented a zoom-in image (x2) of the area denoted by the small white square and the scale bar = 25 µm.

HUVEC morphology on the unpatterned control and gratings topographies were different from the lenses and cone topographies. From the F-actin network, HUVEC on the unpatterned control and gratings were well spread and had a more "spindle"-shaped appearance. On the other hand, the morphology of HUVEC on the smaller diameter lenses and cone topographies appeared rounded and dendritic-like.

The appearance of dendritic-shape cells can imply a reduction in cell adhesion due to the disruption of non-muscle myosin-II activity. Non-muscle myosin-II is an actin-binding protein involved in integrin-mediated adhesion that participate in FA maturation [155]. Disruption in the activity in myosin-II was reflected in a change in the cell morphology. Cai *et al.* [156] reported that 15% of the cells population formed dendritic-like morphology when fibroblasts were treated with blebbistatin, an inhibitor of myosin-II activity. Without myosin-II, the downstream process of FA and polymerization will be affected, leading to poor cell adhesion on the topography. Thus, the appearance of dendritic-like cell morphology in this study could also indicate the change in FA responses, resulting in poor cell adhesion. Nevertheless, additional analysis on FA and myosin light-chain kinase expression will need to be studied to understand the change in FA on these topographies.

Other than dendritic morphology, rounded cell morphology was also observed on concave and convex lenses topographies. Detailed analysis on cell morphology was carried out on the selected group of topographies that displayed a significant reduction in cell density as compared to the unpatterned control. Cell circularity was quantified to identify the changes in

HUVEC cell morphology on the lenses topographies, especially with regard to the appearance of rounded cell morphology.

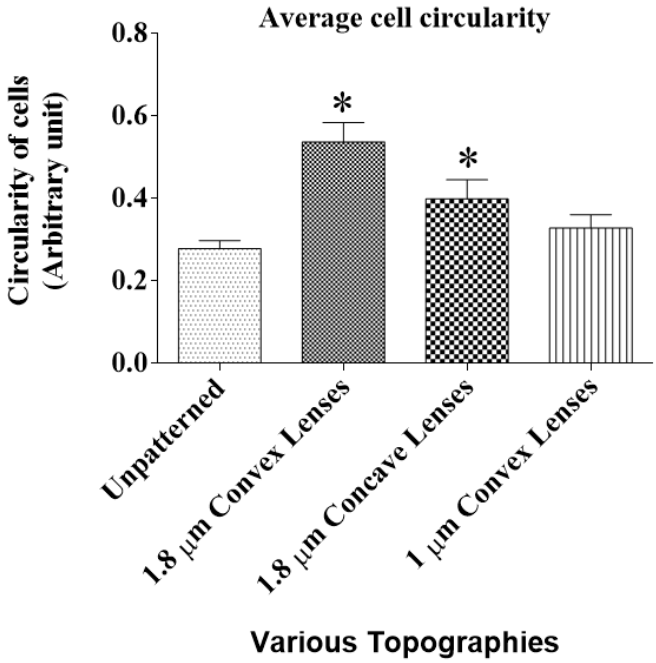

Figure 4.6: Average cell circularity of HUVEC on various topographies. The value of 1 indicates a perfect circle. * denotes statistical difference with p-value < 0.05 as compared to the unpatterned control. Error bars denote the SE.

Higher cell circularity, indicating a more rounded morphology, was observed for cells cultured on the selected topographies as compared to the unpatterned control. Specifically, cells on 1.8 μm convex and concave lenses showed significantly higher cell circularity as compared to the unpatterned control. Cell shapes and morphology are closely related to cell survival and a rounded cell morphology is often associated with an increase in cell apoptosis [157, 158]. Chen *et al.* [158] studied the effect of cell shape on cell apoptosis and growth using bovine capillary endothelial cells and human microvascular EC on ECM patterned substrate. EC cultured on small adhesive area appeared more rounded in shape, and an increase in apoptosis rate was observed. Similar observation was also reported by Watt *et al.* [157] using human

epidermal keratinocytes. With the appearance of more rounded cells, the increase in cell apoptosis rate might account for the poor cell number on lenses topographies.

Cell area is another parameter that can change with different cell morphology. For an adherent cell type like EC, sufficient cell spreading is required for cell survival and adhesion. Topography can also alter the cell area, affecting cell apoptosis and adhesion. Thus, the cell area of the selected topographies in Figure 4.6 was quantified as shown in Figure 4.7.

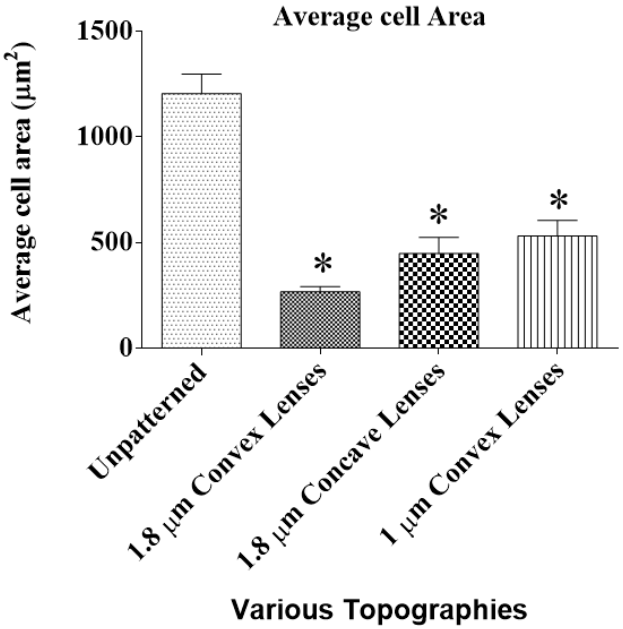

Figure 4.7: Average cell area of HUVEC on various topographies. * denotes statistical difference with p-value < 0.05 as compared to the unpatterned control. Error bars denotes the SE.

Significant reduction in cell area was observed on all the lenses topographies as compared to the unpatterned control. The cell area was most reduced on cells cultured on 1.8 μm convex lenses (267.3 ± 25.1 cm^2) with an approximately 4.5 fold reduction as compared to the unpatterned control (1205.7 ±.92.4 cm^2). A smaller cell adhesion area could possibly mean poor

cell interaction between the cells and the topography, leading to poor cell adhesion and increase in cell apoptosis rate. Compared with the results on cell circularity, cell area had an inverse relationship with cell circularity. 1.8 µm convex lenses had the highest cell circularity and the smallest cell area among the topographies. Both observations suggested a possible increase in cell apoptosis on these topographies that could cause excessive cell death, leading to poor cell density obtained.

4.3.2.2 Cell adhesion study in individual pattern PDMS substrate

A cell adhesion study was carried out on individually patterned PDMS substrate. 1.8 µm concave lenses, 1 µm gratings, 500 nm pillars and the unpatterned were selected for the individual pattern study to verify the screening results from the MARC chip. 1.8 µm concave lenses and 1 µm gratings topography were selected as they were significantly different from the unpatterned control. On the other hand, the 500 nm pillars topography was selected to represent topographies that did not modulate cell adhesion according to the MARC chip study.

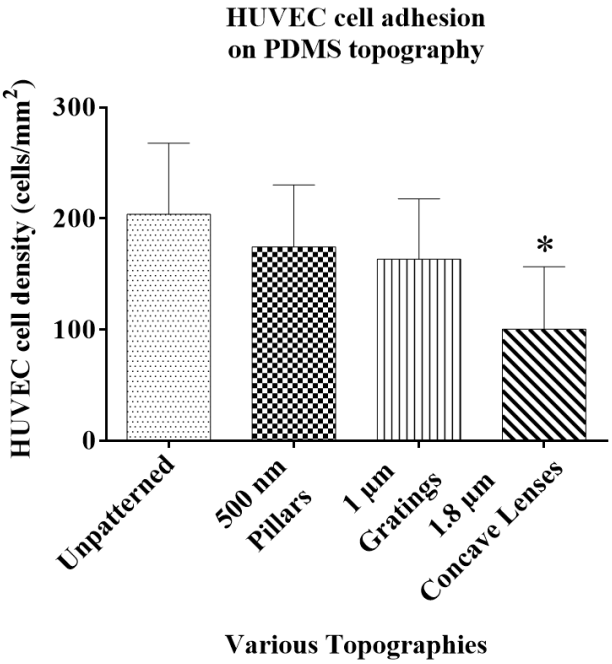

Figure 4.8: Cell density of HUVEC on different PDMS topography without coating after 24 hours. * denotes statistical significance with p-value < 0.05 as compared to the unpatterned control.

The cells density obtained from the individual studies showed that cell density on 500 nm pillars (175 ± 51 cells/ mm^2) was not statistically different from the unpatterned control (204 ± 58 cells/ mm^2). Similar results were obtained from the MARC chip study. In addition, the reduced cell attachment on 1.8 µm concave lenses was also validated. The individual pattern study showed that the cell density on the concave lenses was halved when compared to the cell density on the unpatterned control (101 ± 51 cells/ mm^2 vs 204 ± 58 cells/ mm^2). On the other hand, the cell density on 1 µm gratings did not match the observation in MARC chip screening. Although the cell density was lower (164 ± 49 cells/ mm^2), it was not significantly different from the unpatterned control. Unlike the MARC chip study, the individual pattern study did not have the complication of competitive adhesion from other surrounding topographies. Without interference from its environment, the effect of

topography on cell adhesion was more pronounced and accurately reflected the effect of topography on cellular behaviours. In addition, different methods were used for the cell density, manual cell counting for MARC chip analysis and CyQUANT proliferation assay kit for individual pattern analysis. CyQUANT assay is a more quantitative method for cell density quantification as compared to manual counting. The upscaling of area and cells analysed also reduced random error experienced in MARC chip experiment incurred by the usage of small area for analysis.

The screening experiment using the MARC chip opens up a new approach to investigate the effect of substrate topography on EC adhesion. Some of the results are non-intuitive and not readily interpretable.

4.3.2.3 Effect of materials influencing cells' responses on topography

Comparing the results obtained in Chapter 3 and 4, the effect of the same topography on EC were not consistent. In particular, 1.8 µm concave and convex lenses modulate EC adhesion differently. In Chapter 3.3.2, 1.8 µm concave and convex lenses showed to enhance EC adhesion but in Chapter 4.3.2, the same topographies showed to reduce EC adhesion. Apart from the differences in cell types and surface treatment, the most significant difference between the 2 studies is the material used. PVA hydrogel and PDMS were used in the study presented in Chapter 3 and 4 respectively. PVA hydrogel has a lower elastic modulus around the range of 0.35 MPa [159] as compared to the PDMS elastic modulus around the range of 3 MPa [160, 161]. Their vast differences between the elastic modulus may cause the difference in the cell responses on the same topography. Evidence from previous studies had shown that the elastic modulus of materials can direct different cell responses,

including cell adhesion. For example, increased macrophage attachment was observed on IPN surfaces with higher modulus. Changes in cell morphology was also observed as increased cell aggregation occurred on interpenetrating polymer network (IPN) with lower modulus [162]. In another study, formation of a stable cell network occurs on low modulus (140 Pa) functionalized polyacrylamide gels. Using high modulus (2500 Pa) gels, no networks were formed regardless of the presence of growth factors [163]. This further indicates the importance and influence of materials elastic modulus on cell-interface as well as cell-cell interaction. Thus, it is believed that the influence on cellular behaviours due to different elastic modulus of materials interfere with the observations when one studies topographical effect using different materials.

4.3.3 Screening of HUVEC proliferation using MARC chip

To probe the topographical design that affects cell proliferation, HUVEC was seeded at 10,000 cells/cm^2 density on the MARC substrate. Using an EdU proliferation kit, HUVEC cell proliferation after 20 hours of adhesion was investigated. Cell proliferation percentage was obtained by quantifying the DAPI and EdU nucleus count after an additional 4 hours incubation. Figure 4.9 showed the calculated U_{cal} value and the proliferation rate of different topographies arranged ascending U_{cal} value. From Figure 4.9 A, values of the topographies before the vertical black dashed line had a proliferation rate that was considered as significantly different from the unpatterned control.

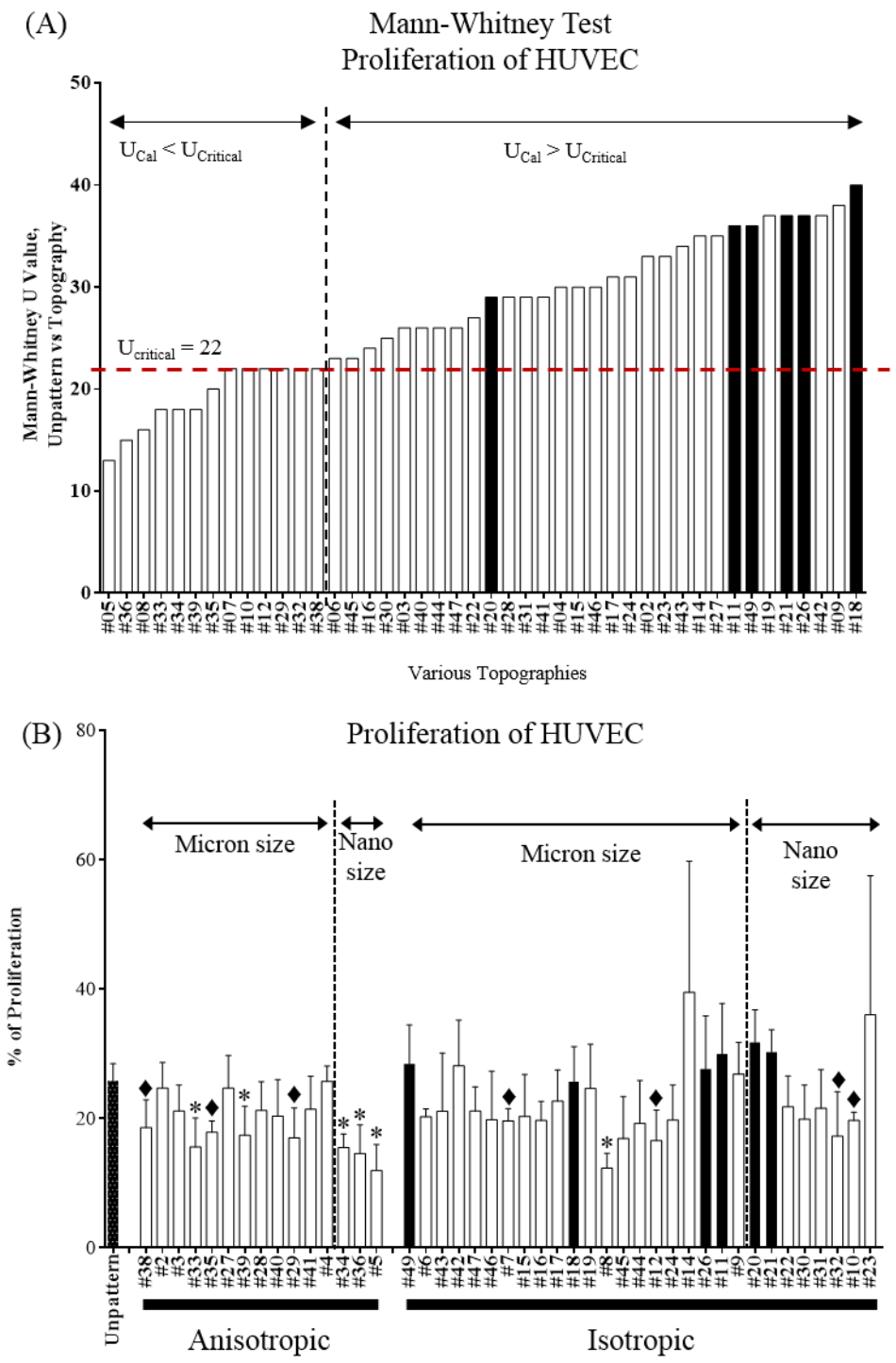

Figure 4.9: Cell proliferation of HUVEC on MARC substrate after 24 hours. Black bars denote the topographies that have a higher cell proliferation than the unpatterned control and white bars denote the topographies that have a lower cell proliferation than the unpatterned control. (A) Mann-Whitney test analysis ranking the U-value of the 44 topography with respect to the unpatterned control. Red line denotes the $U_{Critical}$ value of 22 at 85 % C.I. (B) Overall percentage of HUVEC proliferation on MARC substrate. * denotes the p-value < 0.1 (90 % C.I) and ♦ denotes the p-value <0.15 (85 % C.I) as compared to the unpatterned control. Error bars denote the SE.

There is a decrease in HUVEC for all the topographies belonging to anisotropic structure, on the other hand, the enhanced proliferation were detected on all the 6 isotropic topographies. In total, 13 topographies evaluated with the Mann-Whitney test analysis displayed proliferation rate that were statistically different from the unpatterned control, and are shown in Table 4.3 A.

Table 4.3: Summary of average proliferation rate from MARC substrate. (A) Various topographies selected based on Mann-Whitney statistical analysis. The order of topography was arranged in ascending proliferation rate. (B) Various topographies that showed enhanced cell proliferation.

(A)

Pattern No	Topography dimension	Average proliferation rate ± SE	U_{Cal} Value
#05	250 nm gratings	12.0 ± 3.5	13
#08	2 µm pillars, 4 µm pitch	12.3 ± 2.0	16
#36	500 nm U-gratings	14.6 ± 3.8	15
#34	500 nm V-gratings	15.5 ± 1.8	18
#33	2 µm V-gratings	15.6 ± 3.9	18
#12	1.8 µm convex lenses	16.6 ± 4.1	22
#29	2 µm gratings (btm) with 250 nm pillars (top)	17.0 ± 4.0	22
#32	Inverse cones, 270 nm pitch	17.2 ± 6.0	22
#39	2 µm gratings (btm) perpendicular 250 nm gratings (top)	17.4 ± 3.9	18
#35	2 µm U-gratings	17.8 ± 1.5	20
#38	10 µm gratings, 20 µm pitch	18.6 ± 3.7	22
#10	250 nm pillars, 500 nm pitch	19.7 ± 1.1	22
#07	2 µm pillars 12 µm pitch	19.7 ± 1.6	22
-	Unpatterned	25.8 ± 11	-

(B)

#18	2 µm pillars, 12 µm pitch, 350 nm height	25.7 ± 4.7	40
#26	1 µm concave lenses	27.6 ± 7.1	37
#49	50 µm hexagon donut	28.4 ± 5.2	36
#11	1 µm holes, 7.5 µm pitch	30.0 ± 6.8	36
#21	500 nm pillars, 10.5 µm pitch, 200 nm height	30.3 ± 3.0	37
#20	500 nm pillars, 10.5 µm pitch, 300 nm height	31.7 ± 4.4	29

There are some agreements between cell adhesion and proliferation in certain topographies. 1.8 μm convex lenses and inverse cone topography significant reduced cell adhesion and proliferation. The reduced cell adhesion may decrease the intercellular contacts between the cells, possibly leading to reduced HUVEC proliferation. For example, Heng *et al.* reported reduced cell proliferation using low HUVEC seeding density [164], indicating that cell density of the cells can influence cell proliferation where maximum cell proliferation was detected at an the initial seeding density of 1000 cells/cm^2.

Among the anisotropy structure, feature size appears to influence HUVEC cell proliferation. HUVEC proliferation rate on all nano-size gratings topographies were significantly decreased. HUVEC on 250 nm gratings (gratings with square cross-sectional profile) showed the lowest proliferation rate (12.0 ± 3.5 %), followed by 500 nm U-gratings (14.6 ± 3.8 %) and 500 nm V-gratings (15.5 ± 1.8 %). Compared to the unpatterned control, a 2 fold reduction in cell proliferation was observed on 250 nm gratings. This observation is in agreement with Liliensiek *et al.* [7], whose previous study was on HUVEC proliferation using gratings with square cross-sectional profile of different feature sizes. It was reported that HUVEC proliferation on 400 nm and 800 nm gratings were also reduced by 2 fold as compared to the unpatterned control and micron-size gratings. However, in their study, it was unclear if the cause of cell proliferation reduction was due to grating width or pitch reduction since both design parameters were changed concurrently. This uncertainty is avoided in the current study.

While maintaining the width of the gratings in the nano range, the pitch of the gratings were selected at 500 nm and 2 μm. The selected topographies include

500 nm U-gratings, 500 nm V-gratings, 2 µm U-gratings and 2 µm V-gratings. With similar nano-size grating width, cell proliferation on the 4 topographies were significantly lower as compared to the unpatterned control. This indicates that the change in grating pitch does not significantly modulate HUVEC proliferation. Instead, the grating width is believed to be the important design parameter that modulate HUVEC proliferation.

It is also interesting to note that the cross-sectional grating profile was also different in the 4 topography. However, changes in the HUVEC proliferation rate were not significant amongst them. Nevertheless, HUVEC proliferation rate was slightly higher on the 2 µm U-gratings (17.8 ± 1.5) as compared to the other 3 topographies. This implies that the cross-sectional profile of the topography potentially modulate cell proliferation and warrant a further investigation on these patterns.

4.3.4 Screening of HUVEC transfection using MARC chip

Using the MARC substrate as a screening tool, HUVEC transfection efficiency was investigated. The transfection experiment was carried out using lipofectamine 2000. The cells on the individual patterns were imaged and GFP positive cells were counted to obtain the efficiency of transfection. In order to identify the effect of specific topographies on the HUVEC transfection efficiency, the Mann-Whitney test was selected to analyse the results due to the small population number (Figure 4.10 A).

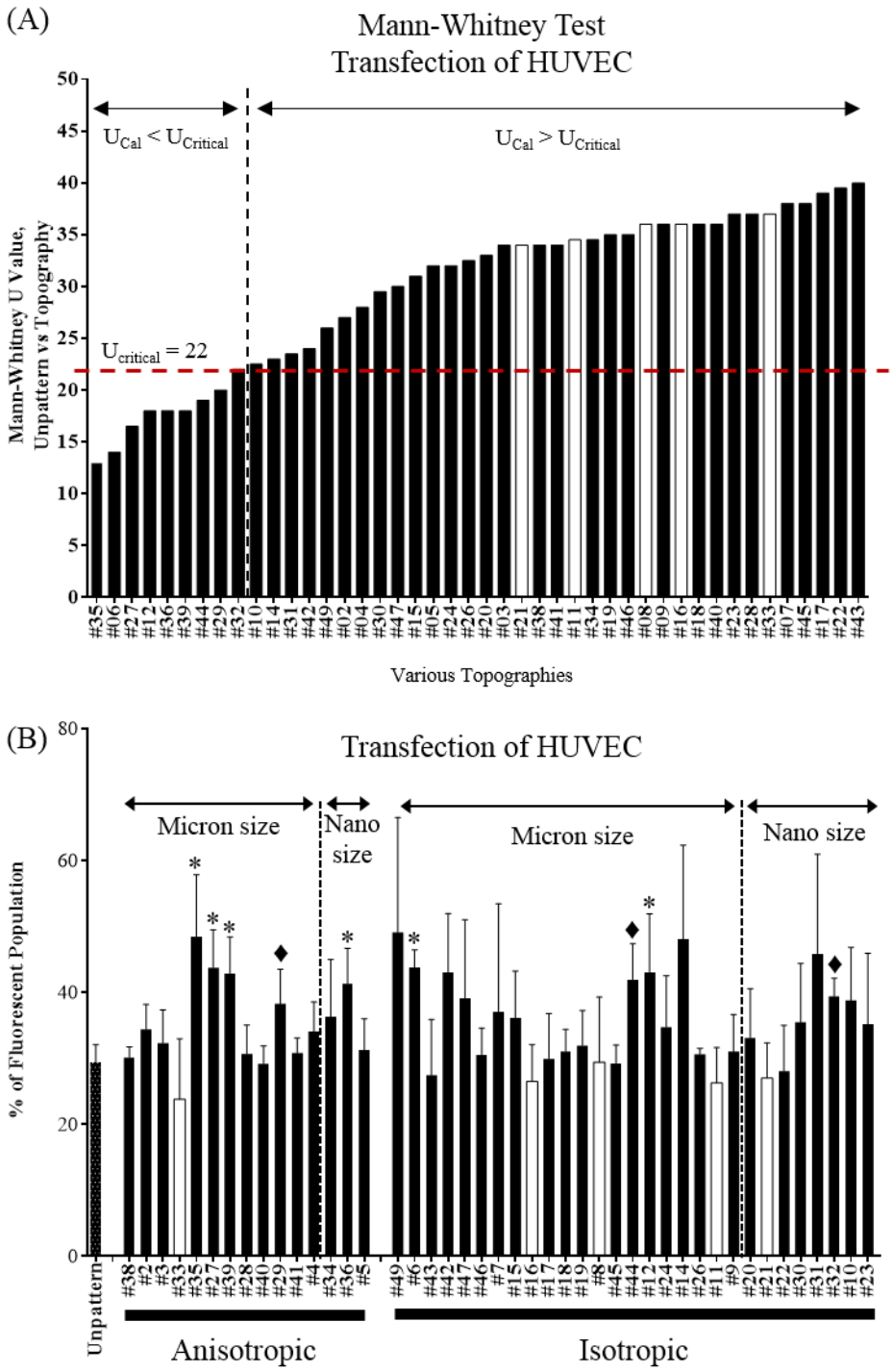

Figure 4.10: Transfection efficiency of HUVEC on MARC substrate after Lipofectamine-assisted GFP transfection. Black bars denote the topographies that has a higher fluorescent population and white bars denote the topographies that has a lower fluorescent population as compared to the unpatterned controls. (A) Mann-Whitney test analysis ranking the U-value of the 44 topographies with respect to the unpatterned control. Red line denotes the $U_{Critical}$ value of 22 at 85 % C.I. (B) Overall percentage of transfection efficiency based on the % of GFP positive HUVEC on MARC substrate. * denotes the p-value < 0.1 (90 % C.I) and ♦ denotes the p-value <0.15 (85% C.I)

as compared to the unpatterned control. Error bars denote the standard error on the mean (SE).

In general, the transfection of HUVEC was enhanced on almost all the topographies, except for 5 of them; 500 nm pillars , 1 µm holes , 2 µm pillars with 4 µm pitch , 2 µm pillars with 12 µm pitch and 2 µm V-gratings. However, they are not significantly different from the unpatterned control. On the other hand, 9 topographies were significantly different as compared to the unpatterned control with a C.I level of at least 85%. Their respective transfection values and topography dimension were shown in Table 4.4.

Table 4.4: Summary of average transfection efficiency rate from MARC substrate. (A) Various topographies selected based on Mann-Whitney statistical analysis. The order of topography was arranged in descending transfection efficiency. (B) Various topographies that showed decrease transfection efficiency

(A)

Pattern No	Topography dimensions	Average transfection efficiency ± SE	U_{Cal} Value
#35	2 µm U-gratings, 2 µm pitch	48.5 ± 8.1	13
#27	2 µm gratings perpendicular 250 nm gratings	43.8 ± 5.0	16.5
#06	10 µm pillars, 20 µm pitch, 10 µm ht	43.8 ± 2.3	14
#12	1.8 µm diameter convex lenses	43.1 ± 7.7	18
#39	2 µm gratings perpendicular 250 nm gratings	42.9 ± 4.8	18
#44	2 µm convex lenses, 4 µm pitch	42.0 ± 4.7	19
#36	500 nm U-gratings, 500 nm pitch	41.3 ± 4.7	19
#32	Inverse cones, 270 nm pitch	39.4 ± 2.4	22
#29	2 µm gratings with 250 nm pillars	38.2 ± 4.6	20
-	Unpatterned	29.4 ± 2.6	-

(B)

#08	2 µm pillars, 4 µm pitch	29.4 ± 8.5	36
#21	500 nm pillars, 10.5 µm pitch, 200 nm height	27.0 ± 4.6	34
#16	2 µm pillars, 12 µm pitch, 500 nm height	26.5 ± 4.8	36
#11	1 µm holes, 7.5 µm space	26.3 ± 4.6	36
#33	2 µm V-gratings	23.8 ± 7.9	37

The 2 µm and 500 nm U-gratings, 1.8 µm convex lenses, 2 µm convex lenses and inverse cones topographies showed enhanced transfection as compared to

unpatterned control. The increased in percentage of fluorescent population ranged between 34 – 65 % as compared to the unpatterned control. Notably, 1.8 µm convex lenses and inverse cones also modulate cell adhesion and proliferation as discussed earlier. The hierarchical topographies, 2 µm gratings perpendicular to 250 nm gratings and 2 µm gratings with 250 nm pillars, also enhance cell transfection with an increase of 47 % and 30 % respectively as compared to unpatterned control. However, no distinct feature size range were observed to modulate cell transfection. The topographies identified ranged from 10 µm pillars to 270 nm inverse cone topography. Similarly for orientation of the topographies, a mixture of isotropic and anisotropic topographies enhanced cell transfection.

To allow comparison of topography of specific topographical design, the topographies were grouped and further analysed. Topographical designs for further analysis were selected as followed: pillars topography with varying aspect ratio (Height/ Diameter, H/D) (Figure 4.11 A and B), pillars with varying diameter size (Figure 4.11 C), pillars with different shape (Figure 4.11 D), topographies with curvature (Figure 4.11 E) and the hierarchical topographies (Figure 4.11 F).

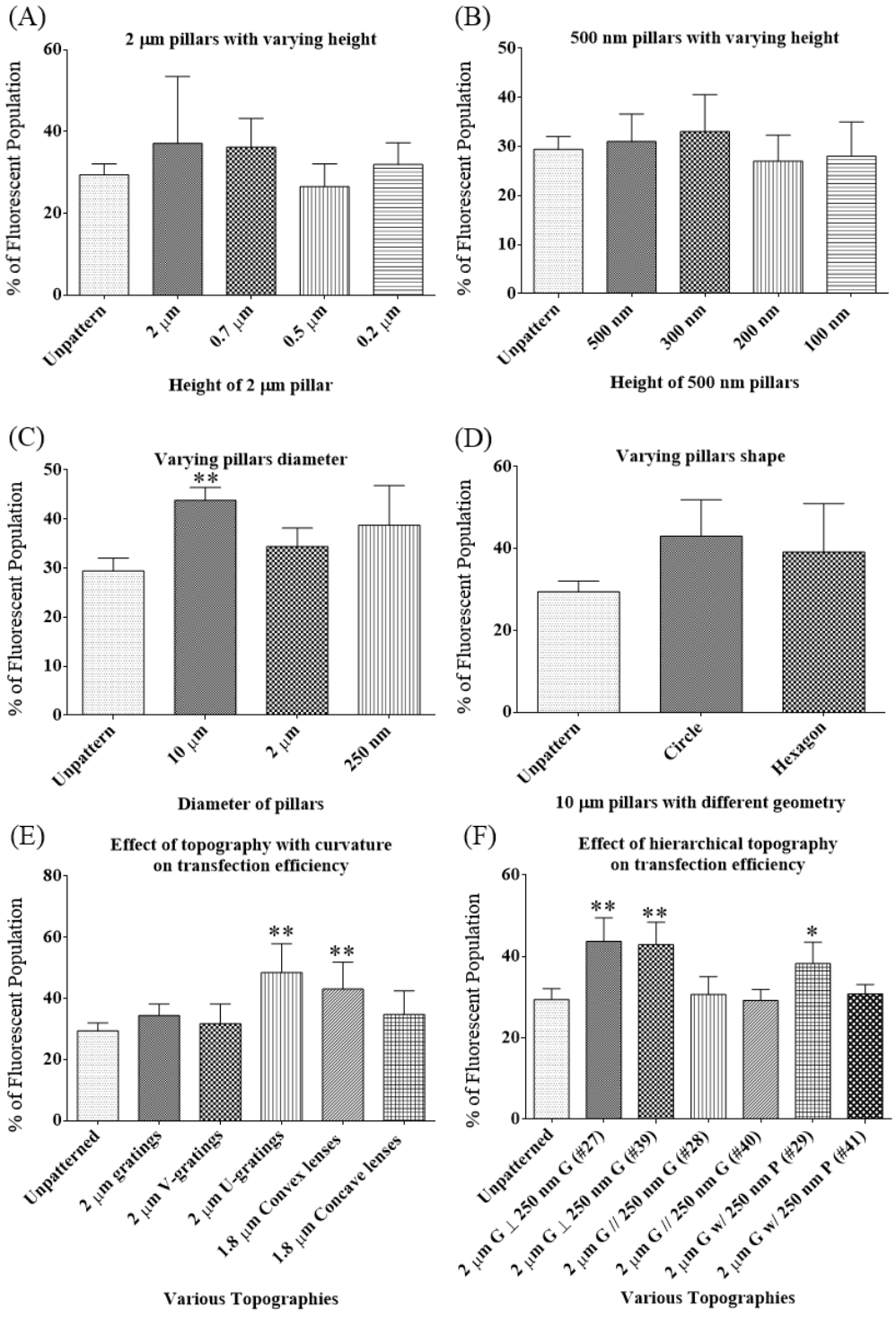

Figure 4.11: Sub-group analysis of transfection efficiency obtained from MARC substrate grouped based on the design parameters. (A) 2 μm pillars with decreasing height from 2 μm to 200 nm, (B) 500 nm pillars with decreasing height from 500 nm to 100 nm, (C) Circular pillars with decreasing pillar diameter but same packing ratio and aspect ratio of 1: 1: 1, (D) 10 μm pillars with circle- shape pillars or hexagon- shape pillars with 2 μm height, (E) topographies with x-y axis and z-axis curvature, (F) hierarchical topography.

** denotes the p-value < 0.1 (90 % C.I) and * denotes the p-value <0.15 (85 % C.I) as compared to the unpatterned control. Error bars denotes the SE.

The effect of aspect ratio (H/D) on transfection were analysis in pillars with different pillar diameter as shown in Figure 4.11 A and B. The variation of aspect ratio (H/D) of the 2 µm and 500 nm pillars topographies did not cause a significant change in the transfection behaviour. The change in the aspect ratio ranging from 1.0 to 0.1 on isotropic topographies did not induce any change to the transfection efficiency of the cells as compared to the unpatterned control.

In Figure 4.11 C, transfection efficiency on pillars topography with varying diameter size was studied. Transfection efficiency increased on all pillars topographies as compared to the unpatterned control although significant difference was only observed for 10 µm pillar. Despite the fact that no significant difference were observed between the pillars topographies, a slight dip in transfection efficiency was observed on the 2 µm pillars as compared to 10 µm and 250 nm pillars.

The effect of pillars geometry was analysed in Figure 4.11 D. No significant difference in transfection was observed between the pillars topographies with different pillar geometry while keeping the topography diameter size and aspect ratio (H/D) the same. The changed in edge roundness of the pillar shape did not change the transfection efficiency of the cells.

Topographies with and without curvature were compared in Figure 4.11 E while keeping their feature size to 2 µm. The topographies with curvature appeared more favourable for transfection. HUVEC transfection on topography with curvature such as 2 µm U-gratings, 1.8 µm convex lenses and 1.8 concave lenses were enhanced and no significant change was observed on

the topographies without curvature such as 2 µm gratings and 2 µm V-gratings as compared to the unpatterned control. Interestingly, in Table 4.4, the majority of the topographies with enhanced transfection were topographies with curvature. The results further indicated the positive influence of the curvature of the structures on transfection. A study by Solanki *et al.* [12] reported an increase in cell transfection with decreasing silicon dioxide particles size coated on a substrate. Apart from the change in features size of the particles, the intrinsic curved feature of spherical particles also indirectly introduced curvature in the topographical design. Though not discussed and evaluated by Solanki *et al.* [12], the transfection modulation observed in their study could also be the influence of the curvature present in the topography which is similar in our observation on cell transfection.

Transfection efficiency of various hierarchical topographies were plotted in Figure 4.11 F. The different secondary structure in various hierarchical topographies appears to modulate transfection differently. Transfection efficiency was enhanced on 2 of the hierarchical topographies, 2 µm gratings with perpendicular 250 nm gratings and 2 µm gratings with 250 nm pillars as compared to the unpatterned control. On the other hand, 2 µm gratings with parallel 250 nm gratings and 2 µm gratings (without additional secondary topography) did not significantly modulate cell transfection.

Among the sub-group analysis, the trend observed for topographies with curvature and hierarchical topography were more evident and significant, thus they were selected for further analysis. Individual pattern experiments were carried out using flow cytometry.

4.3.5 Investigate the design of topography on the HUVEC transfection in individual pattern study

4.3.5.1 The effect of topography with curvature on HUVEC transfection efficiency

The following topographies with curvatures were selected and fabricated to study the effect features curvature on HUVEC transfection; 1 µm gratings, 2 µm V-gratings, 2 µm U-gratings, 2 µm half cylinder, 1.8 µm concave lenses and 1.8 µm convex lenses. Firstly, the introduction of 1 µm gratings kept the pitch dimensions of all the topographies to 2 µm eliminate any influence the topographical design of different pitch size. Secondly, 2 µm half cylinder topography was used to allow studied between concave and convex structures for anisotropy topographies.

These topography were fabricated via soft lithography and AFM characterization was used as it provide quantitative profiling of the gratings topography with different cross-sectional profiles. AFM images in Figure 4.12 A – F showed that the topography were well replicated on PDMS. The cross-sectional profile of the gratings topography displayed in Figure 4.12 G – J further confirmed pattern fidelity of the gratings in the z-axis profile.

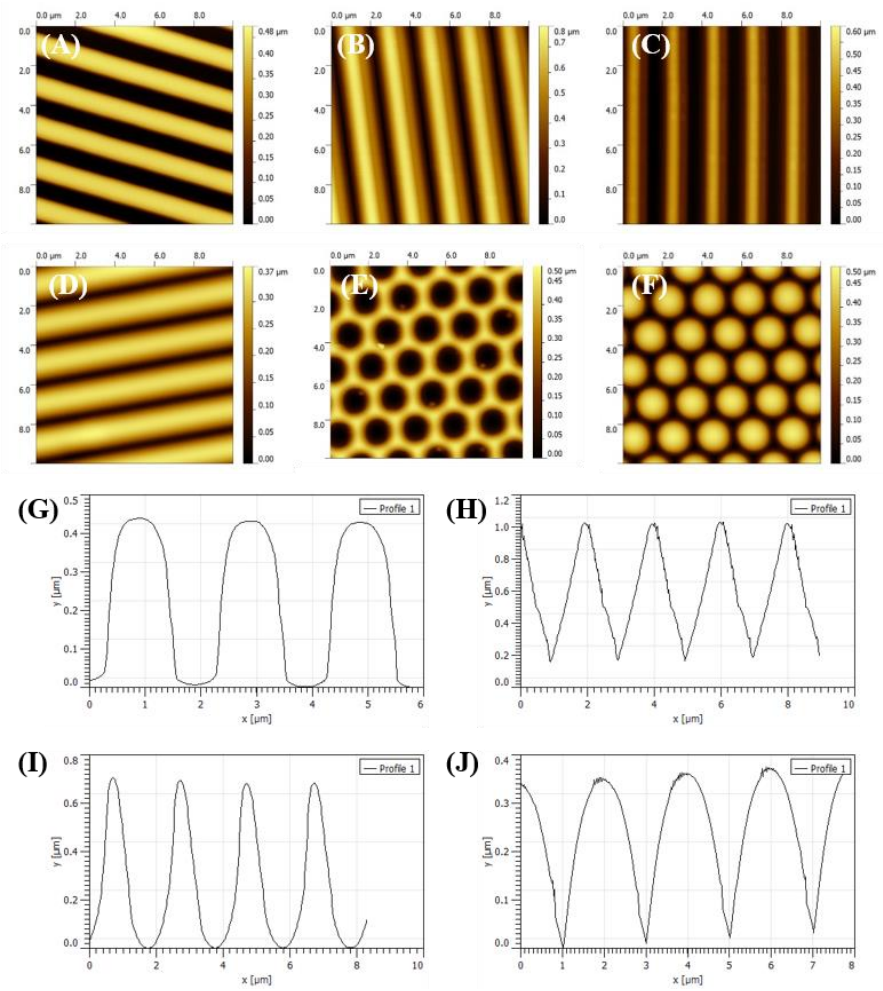

Figure 4.12: AFM images of various topographies using in the study. (A) 1 µm gratings, (B) 2 µm V-gratings, (C) 2 µm U-gratings, (D) 2 µm half cylinder, (E) 1.8 µm concave lenses, (F) 1.8 µm convex lenses. The cross-sectional profile of (G) 1 µm gratings, (H) 2 µm V-gratings, (I) 2 µm U-gratings, (J) 2 µm half cylinder.

GFP transfection was performed using lipofectamine 2000 and the percentage of transfection was obtained based on the percentage of GFP population from the flow cytometry analysis. Same initial seeding density of 10000 cells/cm^2 used in the MARC chip screening was used in the individual pattern study.

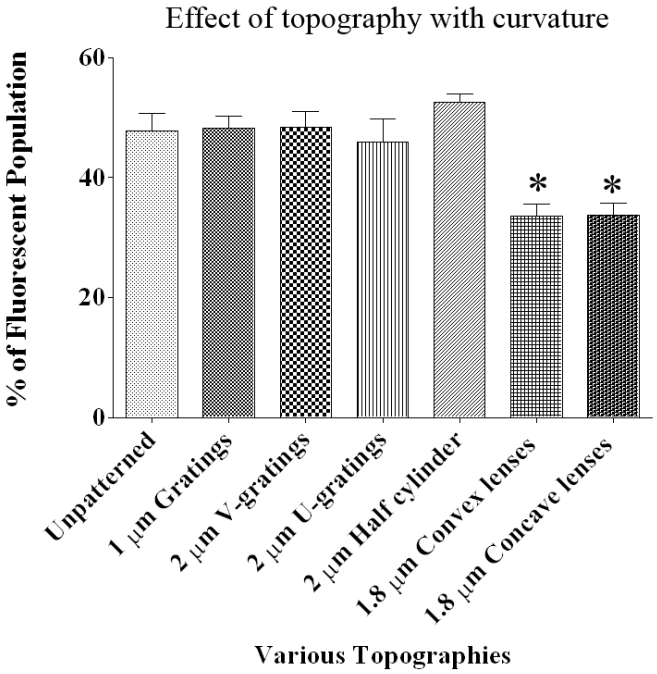

Figure 4.13: Flow cytometry analysis of GFP transfection using lipofectamine 2000 for 3 hour incubation time on HUVEC seeded on various topographies with curvature. * denotes p-value < 0.05 at 95% C.I as compared to the unpatterned control.

Flow cytometry analysis showed that HUVEC transfection efficiency decreased significantly on 1.8 µm convex and concave lenses topographies. This is indicated by the low percentage of fluorescent population detected as compared to the unpatterned control. The transfection efficiency of the other 4 topographies were comparable to that from the unpatterned control as the percentage of fluorescent population detected were not significantly different from one another. The effect of 2 µm V-gratings on HUVEC transfection was the same as that observed in the MARC chip (Chapter 4.2.8) and the individual pattern study. However, HUVEC transfection observation on 2 µm U-gratings, 1.8 µm convex lenses and 1.8 µm concave lenses topographies were different in the 2 studies. While transfection efficiency increased on 2 µm U-gratings and 1.8 µm convex lenses in the MARC chip study, the transfection efficiency of these topographies either remained the same or

decreased in the individual pattern study as compared to the unpatterned control respectively. Similarly for 1.8 μm concave lenses, transfection efficiency was comparable to the unpatterned control in the MARC chip study but the same topography had a lower efficiency in the individual pattern study. The discrepancy in findings from the 2 studies could be due to the quantification method used. Firstly, detection of fluorescent positive cells was more consistent and better controlled using flow cytometry since fluorescence intensity of the cells were obtained by the system detector. Secondly, the detaching of cells from substrate during the preparation in flow cytometry may results in more cell loss as compared to image analysis leading to inaccuracy of cell population analysed. Thirdly, insufficient cell analysed in MARC chip study can also lead to discrepancy in the results. A higher cell population number, 10000 events was analysed in flow cytometry as compared to that analysed in the imaging software (10000 cells versus 1000 cells).

Despite the discrepancy in the 2 studies, most importantly, the results showed that topography can modulate HUVEC transfection efficiency. The 1.8 μm convex and concave lenses significantly reduced HUVEC transfection as compared to the unpatterned control. These topographies were also previously reported in Chapter 4.2.5.2 and Chapter 4.2.6 to reduced HUVEC adhesion and proliferation respectively. The topographical effect of 1.8 μm convex and concave lenses on cell adhesion and proliferation could impact cell transfection, leading to reduced transfection efficiency. Firstly, variations in cell confluency at the time of transfection can affect transfection efficiency. Dalby *et al.* [165] studied β-galactosidase expression obtained by transfecting 293-H cells with different starting cell densities. Reduction in cell density

results in reduced β-galactosidase expression indicating the effect of cell confluency on transfection efficiency. In this study, the transfection on all topographies were carried out at the same time, regardless of the cell confluence on different topography. Hence, the reduction in transfection efficiency on 1.8 µm convex and concave lenses can be contributed by the low starting cell density resulted from the effect of topography on HUVEC adhesion. Secondly, cell proliferation can also affect cell transfection. Accessibility of the nucleus is easier during cell division thus, it is widely believed that dividing cells are more susceptible to non-viral transfection [111, 166]. For example, Fasbender *et al.* reported a proliferative cell, positively labelled with BrdU, were more likely to express the transgene than BrdU negative cells in cationic lipid-mediated transfection system [167]. In Chapter 4.3.3, HUVEC proliferation were reduced on 1.8 µm convex and concave lenses topographies. This cell response possibly reduced the probability of gene delivery directly to the nucleus, avoiding the conventional route through the cytoplasm to reach the nucleus for successful gene transfection. Thus, it is possible that the effect of 1.8 µm convex and concave lenses on cell adhesion and proliferation can impact overall cell transfection.

However, it is still possible that topography can influence the cell transfection process directly. The direct effect of topography on cell transfection is highly likely on the 2 µm U-gratings topography. Although HUVEC adhesion and proliferation was reduced on 2 µm U-gratings, HUVEC transfection efficiency was not significantly reduced in the same way as 1.8 µm concave and convex lenses topography. Thus, it is believed that 2 µm U-gratings topography enhanced HUVEC transfection efficiency to compensate for the effect of low

cell density and proliferation rate on overall transfection efficiency. On the other hand, the positive influence from the topography on transfection might be less significant on 2 µm V-gratings. Only cell proliferation on 2 µm V-gratings topography was significantly reduced, while cell adhesion on this topography was not affected. If the 2 µm V-gratings topography influenced the transfection efficiency at the same level as the 2 µm U-gratings topography, then a similar enhancement in transfection should be observed with the 2 µm V-gratings. However, studying the topography's design revealed that the difference between V-gratings and U-gratings topography lies in the topographies' curvature. Thus, it is possibly that the design of topography curvature can influence cell transfection. More investigation is required to understand the influence of topography curvature on cell transfection.

4.3.5.2 The effect of hierarchical topography on HUVEC transfection efficiency

Another set of topographies that was investigated was the hierarchical topography that consisted of 2 µm gratings as the primary structures with 250 nm gratings or 250 nm pillars as a secondary structure on the gratings ridges. Additionally, flatten 2 µm gratings fabricated by carrying out a secondary imprint using a blank Si, was added to the analysis to eliminate the effect of reduced spacing due to the secondary imprint process. The flatten 2 µm gratings acts as the primary structures control for the hierarchical topographies.

GFP transfection was carried out on various topographies and flow cytometry analysis on the GFP positive population was analysed. Similar to previous

sections, the same initial seeding density of 10000 cells/cm^2 used in the MARC chip screening was used in the individual pattern study.

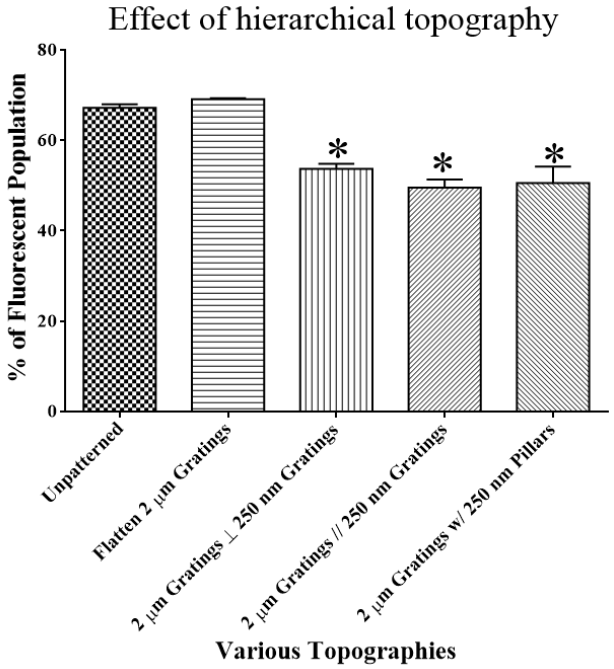

Figure 4.14: Flow cytometry analysis of GFP transfection using lipofectamine 2000 for 3 hour incubation time on HUVEC seeded on various topographies. * denotes p-value < 0.05 at 95% C.I as compared to the unpatterned control.

HUVEC transfection efficiency was significantly reduced on the 3 hierarchical topographies as compared to the unpatterned control. HUVEC transfection efficiency on flatten 2 µm gratings topography was not significantly different from the unpatterned control. The results obtained in individual pattern study were also different as compared to the MARC chip study. 2 µm gratings with perpendicular 250 nm gratings in the individual pattern study did not positively modulate HUVEC transfection efficiency as observed in the MARC chip study. In addition, the reduced HUVEC transfection efficiency on the remaining hierarchical topography was also not present in the MARC chip study. Similar to Chapter 4.3.5.1, this discrepancy in the findings is most

likely due to different quantification methods used and the difference in the number of cells analysed.

In the native environment that cells resides in, the basement membranes that cells interacts consists of multilayered of different topographies [43, 45-47]. While it is necessary to understand the effect and role of individual topographical design, the effect of multilayered structures is equally important to understand the cell interaction with its native basement membranes topographies. Hence, hierarchical topography, a topography with multilayered structures is suitable for exploratory studies to systematically investigate the effect of multilayered topographies on cell behaviours. In this thesis, the hierarchical topography is a 2-layers topography designed to study the effect of the secondary structures on cell behaviours.

Modulation of transfection was observed on all three hierarchical topographies as compared its primary structures control topography, flatten 2 μm gratings topography. The presence of secondary structures affected the cell transfection and resulted in the significant decrease in transfection observed. However, the topographical design in the secondary topographies in modulating transfection could not be determined. Although no statistical difference were observed between the hierarchical topography in the individual topography study, the analysis in the MARC substrate showed different transfection efficiency on 250 nm pillars and perpendicular 250 nm gratings secondary structures as compared to parallel 250 nm grating secondary structures. Nevertheless, the preliminary study on hierarchical topography open up new research direction to study the effect of multilayered topographies on different cellular behaviours.

4.4 Conclusion

In this chapter, the MARC substrate was used as a screening tool to study HUVEC adhesion, proliferation and transfection efficiency. The high-throughput platform allows screening of 49 different topographies in a single chip. In addition, a novel fabrication process allows incorporation of all different design parameters, overcoming the patterning limitation from using the photolithography process. From the MARC chip screening, HUVEC adhesion, proliferation and transfection were established to be affected by different topographies.

Various topographies with curvature were identified to modulate HUVEC adhesion and proliferation. Although the topography identified for the cell behaviour is not always the same, all these topographies had curved features with its RC in the z-direction. Some of the identified topographies include 1.8 µm concave lenses, 1.8 µm convex lenses, and 1 µm convex lenses topography with RC in z direction. Significant reduction in cell density and the appearance of dendritic-like and rounded cells morphology of HUVEC were observed on the lenses topographies. The appearance of these cell morphology could indicate the increased in cell apoptosis and the decreased in the activity of myosin II leading to poor cell adhesion. In addition, decreased in proliferation was also showed on 1.8 µm convex lenses topography in the MARC chip screening. Other than cell adhesion and proliferation, topographies with curvature also modulate transfection efficiency. The 1.8 µm concave lenses and the 1.8 µm convex lenses were observed to significantly reduced cell transfection in the individual patterned study. The modulation of

cell transfection can be indirectly caused by the effect of topography on cell adhesion and proliferation as observed on 1.8 µm concave and convex lenses.

Nano-sized anisotropic topography showed a significant reduction in cell proliferation. Compared to their corresponding micron-size topographies, micron-size gratings demonstrated a higher proliferation rate with the exception of 2 µm U-gratings and 2 µm V-gratings topography. Unlike gratings, the width of 2 µm U-gratings and 2 µm V-gratings remains in the nano range despite the increase in pitch size. The increase in pitch size did not increase the cell proliferation thus indicating that the size of the grating width is more crucial in modulating cell proliferation as compared to the pitch size.

Unlike other topographies used in the thesis, the hierarchical topographies are 2-layers topographies used to study the effect of secondary structures on cell behaviours. Preliminary results showed that all 3 hierarchical topographies significantly reduction in cell transfection efficiency as compared to unpatterned control or its primary structures control, the flatten 2 µm gratings topography. Hence, demonstrating that the effect of secondary features could modulating cell transfection.

In summary, topography with curvature, anisotropy topography with nano-sized width and hierarchical topography were some of the distinct and unique topographical designs identified to modulated HUVEC adhesion, proliferation and transfection.

Chapter 5 Effect of micro and nano-topography on cell endocytosis in drug and non-viral gene delivery system

5.1 Introduction

Low transfection efficiency of non-viral gene delivery limits the application of gene therapy treatment to patients thus, different strategies were studied to enhance the transfection efficiency. In Chapter 4.3.5.1, HUVEC transfection was modulated by topography with curvature such as 1.8 μm concave lenses, 1.8 μm convex lenses and 2 μm U-gratings. There are two design parameters in these topographies, the curvature in z direction and the spatial orientation such as micron size isotropic and nano size anisotropic structures that could modulate the transfection. Thus, in this chapter, to simplify the study, one parameter, the spatial orientation, was selected for further investigation. In this chapter, basic topographies like 2 μm pillars, 200 nm and 250 nm gratings were used to investigate topographical design role of feature size or anisotropicity on endocytosis and transfection.

Since this study is targeted towards gene therapy treatment, stem cells and cancer cells are more relevant models for this study. The challenge of transfecting stems cells and the targeted delivery of therapeutic agents to cancer cells motivate the use of these cells in the study. In addition, fibroblast cell serve as a good model for basic cellular study.

Endocytosis is a process used by eukaryotic cells to internalized compounds and substance from their surrounding environment. During drug and gene delivery, vehicles gain entry into the cells via endocytosis especially in gene delivery. Studies have shown that enhancement in the endocytosis process

have been reported to improve the transfection efficiency [9, 166]. Thus, the effect of topography on endocytosis are closely related to the enhanced transfection observed in our previous study.

This chapter aims to understand the effect of the feature size and anisotropicity on endocytic activity and transfection efficiency of the cells.

5.2 Materials and methods

5.2.1 Fabrication of various topographies via NIL

Patterned topographies used were fabricated using NIL with additional post-imprint process to obtain 3 different categories of topography. They are upright, residual free and collapsed structure.

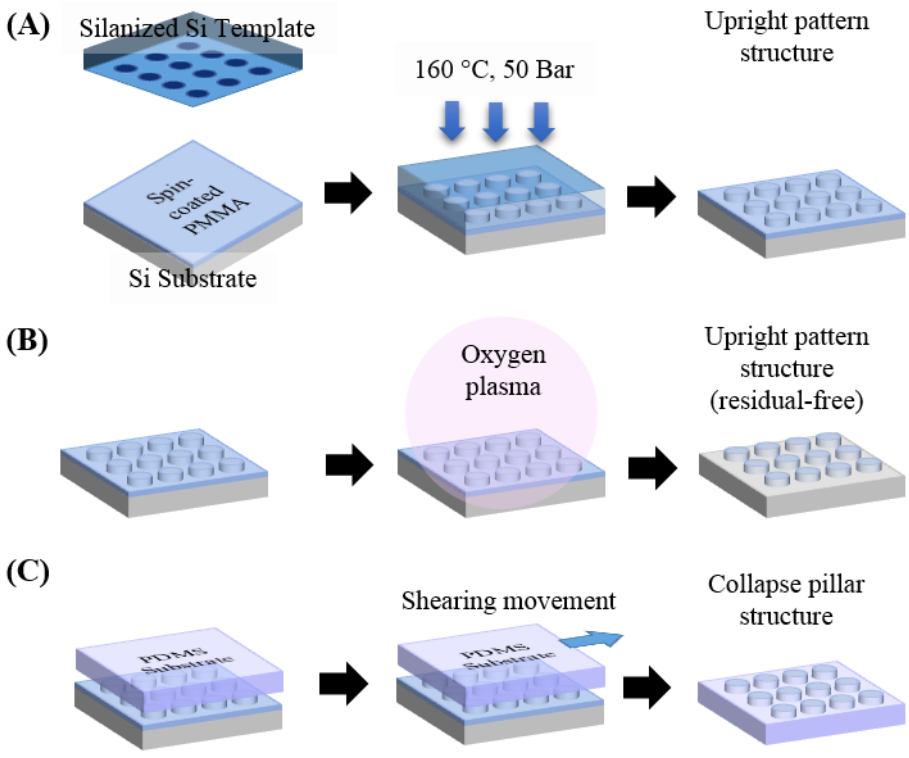

Figure 5.1: Fabrication and patterning of various topographies using NIL. (A) PMMA upright-patterned structure on Si substrate (B) PMMA with Rhodamine B residual free pillars structure on Si substrate (C) Polystyrene (PS) with Rhodamine B collapsed pillars structure on PDMS substrate.

5.2.1.1 Fabrication of upright microstructure

Patterning of upright PMMA microstructure was carried out using NIL as illustrated in Figure 5.1 (A). Prior to imprinting, the Si template was silanized with FDTS (Alfa Aesar, 96% purity) overnight in a glass desiccator. The hydrophobic fluorinated coating reduced the surface energy to allow ease of demolding between the Si template and the imprinted material without damaging the patterned surface. A thin PMMA (Microresist technology, MW 35000 g/mol) layer was deposited on a clean Si substrate via spin-coating. Next, the silanized Si template was placed on top of the spin-coated surface and imprinting was carried out at 160 °C under a pressure of 50 bar for 10 minutes. Upon cooling to 40 °C, the Si template was manually demolded from the imprinted PMMA layer.

5.2.1.2 Fabrication of residual free microstructure

Rhodamine B (5 mg, Sigma-Aldrich) was added to 30 ml of PMMA prior to the patterning process described for the upright-pattern topography (Chapter 5.2.1.1). Addition of rhodamine B allowed visualization of the pillars after it was internalized by the cells. Oxygen plasma treatment was applied on the imprinted topography using a reactive ion etching machine (Plasmalab 80plus, Oxford) to obtain the residual free pillars.

5.2.1.3 Fabrication of collapsed pillars topography

Rhodamine B (5 mg, Sigma-Aldrich) was added to 30ml of 23 wt/vol % of polystyrene (PS) in toluene (Sigma-Aldrich). With similar setup used for PMMA patterning process (Chapter 5.2.1.1), imprinting process of PS was carried out at 180 °C at 60 bars for 10 minutes. Next, PDMS substrate (Dow corning) was fabricated. First, PDMS elastomer-base was mixed with its

curing agent at a ratio of 10: 1 until homogenous. Using a vacuum desiccator, first round of desiccation was carried out to remove the air bubbles that were introduced during the mixing process. The degassed PDMS mixture was then poured into a petri-dish and a second round of desiccation was carried out until no bubbles were seen in the mixture. PDMS was cured at 70 °C for at least 18 hours and was used to shear and collapse the PS pillars [168]. The cured PDMS substrate was brought into contact with the top surface of the imprinted PS pillars. A lateral force was applied to the PDMS substrate resulting in a horizontal displacement, overcoming the cohesive force between the PS pillars and the imprinted layer. During the process of shearing, collapsed PS pillars were also transferred onto the PDMS substrate, creating a regular array of collapsed pillars.

5.2.2 Characterization of the imprinted topographies by SEM

SEM (JEOL, JSM-6700F) was used to verify the imprinted structures fabricated. Samples were coated with a gold film thickness of approximately 10 nm using a gold coating machine (JOEL, JFC-1200). This was necessary for non-conducting samples to reduce the charging effect during characterization. The characterization was carried out using an accelerating voltage of 5 keV, at a working distance of 6 mm. The dimensions of the topography were obtained from at least 15 measures.

5.2.3 Cell culture on various topographies

Bone marrow human mesenchymal stem cells (hMSCs) (CD105+, CD166+, CD29+, CD44+, C14-, CD34-, CD45-, Lonza) were cultured and expanded in serum containing mesenchymal stem cell growth media (MSCGM, Lonza) according to manufacturer's protocol. Human MSCs of passages number 5-7

were used for the experiments. Breast cancer cells, MCF 7 (ATCC) were cultured in Eagle Minimum Essential Media (Sigma) containing 10% FBS (Gibco, Invitrogen), 1 % penicillin-streptomycin (Gibco, Invitrogen) and 0.01 mg/ml bovine insulin (Sigma). COS 7 fibroblast (ATCC) were cultured in DMEM (Gibco, Invitrogen), 10 % FBS (Gibco, Invitrogen) and 1 % penicillin-streptomycin (Gibco, Invitrogen).

Substrates with nanoimprinted structures were placed in a 6-well tissue culture plate and sterilized with UV light for 20 minutes. Cells were seeded at a density of 10,000 cells/cm^2 except for the PS collapsed pillars on PDMS substrate where a seeding density of 5000 cells/cm^2 was used.

5.2.4 Internalization of FITC-dextran

Respective cells were cultured on various nanoimprinted substrates as described in Chapter 5.2.3. After 24 hours, FITC-dextran molecule (Sigma-Aldrich, MW 40000 g/mol) of concentration of 1 mg/ml was added to all the samples except for the positive control where a higher concentration (2 mg/ml) was added to the cells cultured on the unpatterned PMMA substrates. At the specific time points of interest, the cells were detached for flow cytometry analysis. For the comparison study of internalization of two different molecular weight FITC-dextran molecule, the experiment was carried out with another FITC-dextran molecule of higher molecular weight (Sigma-Aldrich, MW 500000 g/mol) using COS 7 cells.

5.2.5 Transfection of bone marrow hMSCs on various topographies using lipofectamine 2000

GFP plasmid amplification and purification were done similar as Chapter 4.2.7 and transfection was similar to Chapter 4.2.8 with the following changes. Human MSCs was cultured in MSCGM media and incubate for 3 and 6 hours in Opti-MEM containing lipofectamine 2000 reagent (µl) and GFP plasmid (µg) at a ratio of 1: 2.5. GFP plasmid of concentration of 250 ng/cm^3 were used.

5.2.6 Flow cytometry analysis

For FITC-dextran internalization studies, patterned substrate containing the cells were rinsed with phosphate buffered saline (PBS) solution. Trypsin-EDTA was used to detach COS 7 and MCF 7 cells from the substrate while accutase (Stem Cell Technologies) was used for hMSCs. The appropriate medium was then added to neutralise the enzymatic detachment process. The collected cell suspension was fixed and filtered following Chapter 4.2.11 protocol. The cells solution was then analysed using a flow cytometry analyser (Dako Cytomation Cyan LX). Cells cultured in the absence of FITC-dextran were used as the gating and negative controls where a minimum of 10000 events were recorded for each of the triplicate samples.

Similar process was applied for the transfection efficiency studies using hMSCs whereby non-transfected cells were used as the gating and negative controls.

For both experiment, the percentage of fluorescence population and mean fluorescence intensity were studied using FlowJo.

5.2.7 Internalization of residual free and collapsed pillars

Various type of cells were cultured on rhodamine labelled residual free and collapsed pillars for 24 hours with the culture condition mentioned in Chapter 4.2.3. Next, the cells were fixed in 4 % PFA and stained for F-actin and nucleus using Oregon Green 488 Phalloidin and DAPI respectively. For visualization of the fluorescently labelled pillars, laser scanning confocal microscope (Olympus FluoView FV1000) was used. Z-sections of the cells on residual free and collapsed pillars substrate were taken at 0.1 µm and 0.3 µm internal respectively.

5.2.8 Fluorescence imaging of cells

Cells fixation was carried out in 4% PFA for 15 minutes in 4 °C before permeabilization using 0.1% Triton-X-100 in PBS for 15 minutes in room temperature. The samples were then incubated with Alexa Fluor 546 Phalloidin (1:750) (Invitrogen) and DAPI (1:2500) for 20 minutes before mounting for imaging. Samples were observed and imaged using an epifluorescence microscopy (Leica DM IRB).

5.2.9 SEM of cells on pillars topography

Samples with cells seeded were fixed in 4 % PFA, washed in 0.1 M sodium cacodylate, and post-fixed in 2 % OsO_4 in 0.1 M sodium cacodylate of pH 7.2. Next, the samples were dehydrated by soaking in the sequence of 50 %, 70 %, 80 %, 90 % and 100 % absolute ethanol solution. After dying by evaporation of hexamethyldisilazane (HMDS), the samples were coated with a thin gold layer and characterized using SEM (Quanta FEG 200) at high vacuum mode with an accelerating voltage of 10 to 15 kV.

5.2.10 Statistical analysis

One-way ANOVA analysis was performed before Bonferroni's multiple comparison post hoc test to analyse the internalization or transfection efficiency between the different topographies and the control. P-value of at least <0.05 were considered as significantly different.

5.3 Results and discussion

5.3.1 Characterization of nanoimprinted topographical structures

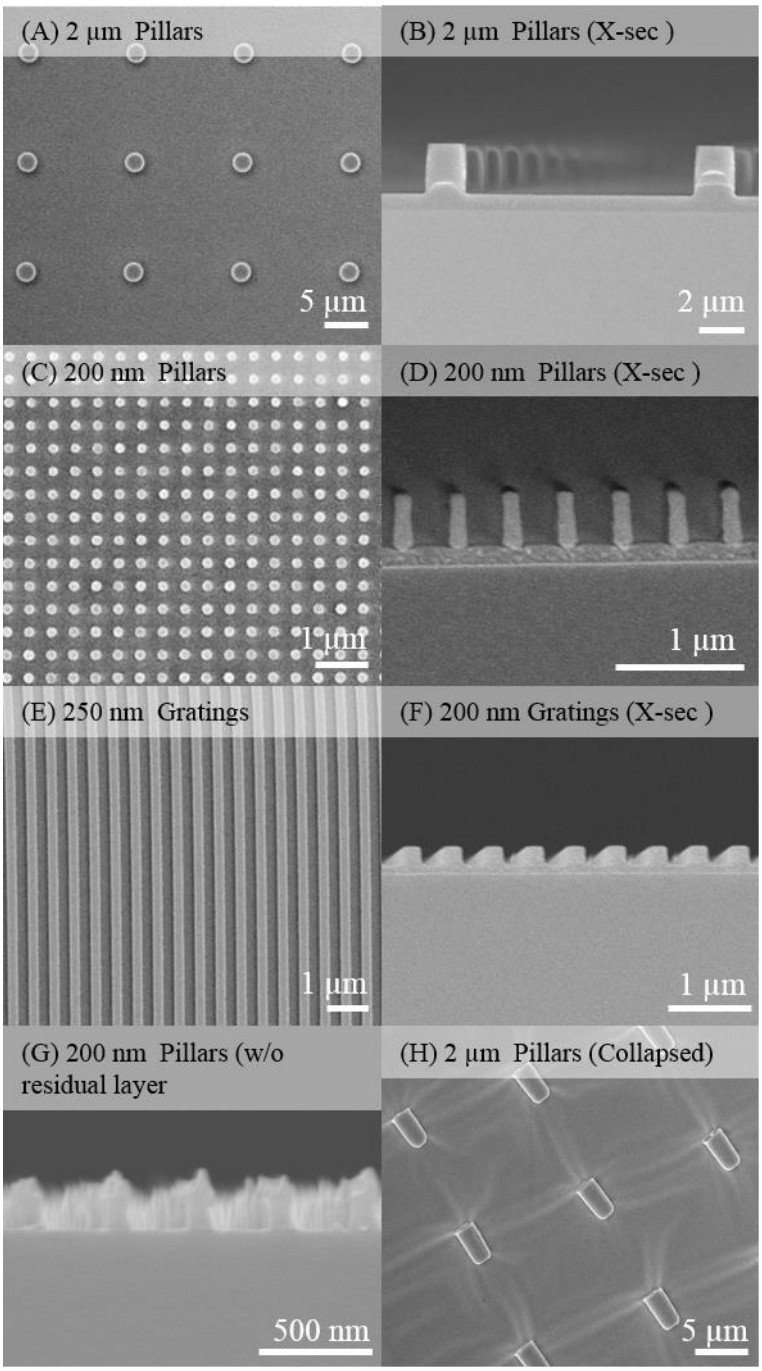

Figure 5.2: SEM of topographies fabricated via NIL and its respective post-processes. (A) Top and (B) cross-sectional view of 2 µm diameter PMMA pillars with 2 µm height and 10 µm space, (C) top and (D) cross-sectional view 200 nm diameter PMMA pillars with 400 nm height and 200 nm space, (E) top and (F) 250 nm PMMA gratings with 250 nm height and 250 nm space, (G) cross-sectional view of 200 nm rhodamine-PMMA pillars and (H) 2 µm rhodamine-PS collapsed pillars on PDMS substrate (top view).

Three different topographies were selected for this study: 2 µm diameter pillars (1: 1 aspect ratio, 12 µm pitch), 200 nm diameter pillars (1:2 aspect ratio, 400 nm pitch) and 250 nm width gratings (1:1 aspect ratio, 500 nm). The selected topography gave a good representative of topography of micron- and nano-size as well as anisotropy (pillars) and isotropy (gratings) type of structure. Figure 5.2 A-F showed the top view and cross-sectional view of PMMA upright topography. For the studies on baso-lateral uptake, SEM images of 200 nm diameter rhodamine-PMMA upright pillars without residual layer and 2 µm diameter rhodamine-PS collapsed pillars were shown in Figure 5.2 G-H. All the SEM images showed that the nanoimprinted structures achieved high pattern fidelity with dimension within 80 % of the dimension to the Si template used for patterning as shown in Table 5.1.

Table 5.1: Dimension of diameter, width, space and height of nanoimprinted PMMA topographies with their original Si molds dimension. (Diameter/width x pitch x height) as: 2 µm pillars (2 µm x 12 µm x 2 µm) , 200 nm pillars (200 nm x 400 nm x 400 nm) and 250 nm gratings (250 nm x 500 nm x 250 nm). (n=3)

Topography	Diameter/ Width	Pitch (center to center)	Height
2 µm pillars	2.0 ± 0.1 µm	12.4 ± 0.1 µm	2.1 ± 0.1 µm
200 nm pillars	182.7 ± 11.9 nm	409 ± 82.7 nm	408.8 ± 15.7 nm
250 nm gratings	210 ± 10.7 nm	528.1 ± 12.4 nm	243.5 ± 12.5 nm

5.3.2 Effect of topography on endocytosis on the apical surface of cell membrane

In general, cell endocytosis can be divided into four different pathways, namely clathrin-mediated, caveolae, macropinocytosis and phagocytosis has been comprehensively reviewed [112, 113, 169, 170]. From existing studies, it was is known that FITC-dextran internalization and gene transfection

processes result from macropinocytosis [113, 169] and clathrin-mediated endocytosis [118, 171] respectively. Thus, studying FITC-dextran internalization and GFP transfection of different cell types and topographies could indicate the effect of topography on different cell endocytosis pathway.

5.3.2.1 Effect of topography on FITC-dextran internalization on different cell type

The internalization efficiency of FITC-dextran by hMSCs seeded on different topographies were studied to detect the effect of topography on modulating cell endocytosis, in particular to macropinocytosis. However, long incubation time could result in saturation of cell internalization of FITC-dextran, masking the effect of topography on the cellular internalization. Thus, different incubation timings of hMSCs with FITC-dextran molecules were studied.

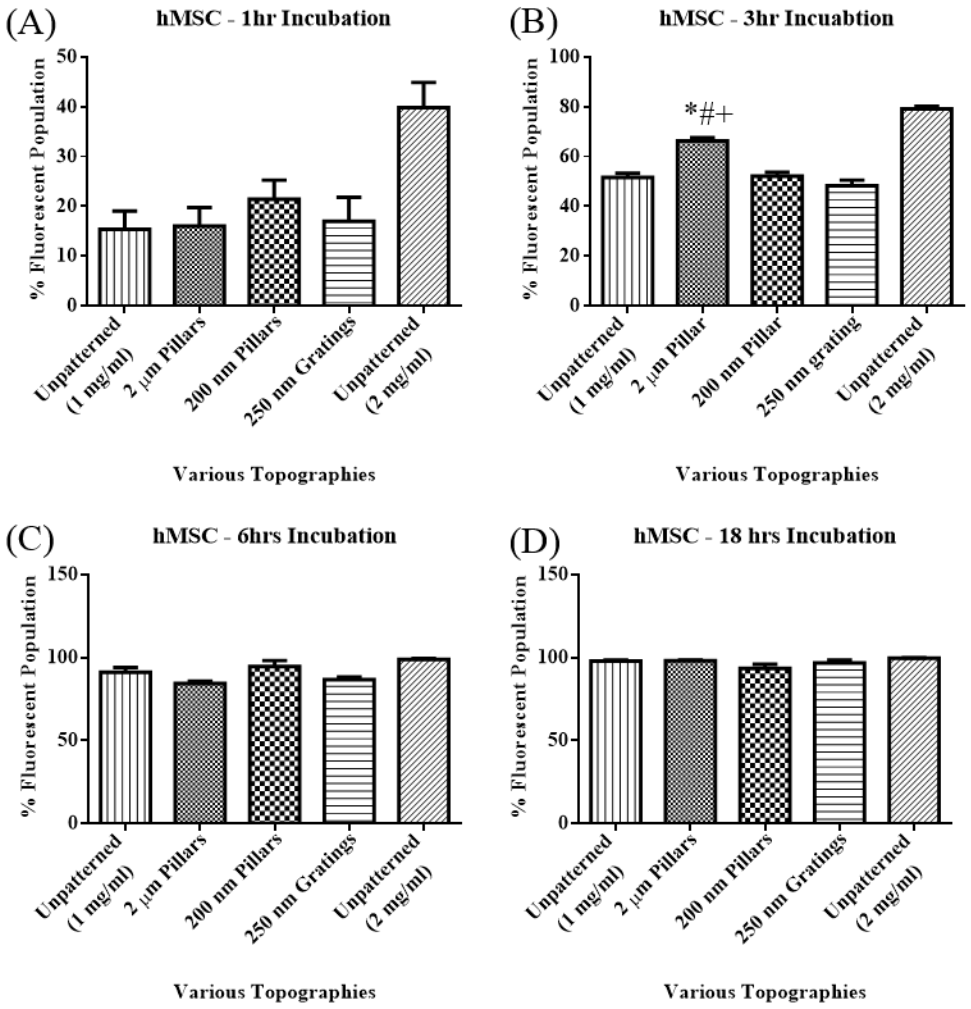

Figure 5.3: Flow cytometry analysis of FITC-dextran internalization on hMSCs on various topographies at different time point. Overall percentage of fluorescent population of hMSCs on the unpatterned control (1 mg/ml and 2 mg/ml FITC-dextran concentration), 2 μm pillars, 200 nm pillars and 250 nm gratings (1 mg/ml FITC-dextran concentration) at (A) 1 hours, (B) 3 hours, (C) 6 hours, and (D) 18 hours incubation time. P (<0.01 * - vs the unpatterned control (1mg/ml), # - vs 250 nm gratings, + - vs 200 nm pillars, n=3)

As shown in Figures 4.3 (C) and (D), the percentage of fluorescent population indicated the saturation of FITC-dextran in hMSCs in all topography including the unpatterned control. At 18 hour, hMSCs on 2 μm pillars gave a 98.0 ± 1.4% of fluorescent population. Similar values were obtained for hMSCs on 200 nm pillars (93.5 ± 5.7%), 250 nm gratings (96.6 ± 3.6%) and the unpatterned control (1 mg/ml) (97.9 ± 1.4%). Similarly, at 6 hour incubation time, hMSCs

on 2 µm pillars, 200 nm pillars, 250nm gratings and the unpatterned control (1 mg/ml) displayed comparable fluorescent population percentage (2 µm pillars: 84.4 ± 1.8 %, 200 nm pillars: 94.5\6 ± 6.3 %, 250 nm gratings: 86.7 ± 2.0 %, unpatterned control (1 mg/ml): 91.1 ± 5.8%). The above measured values showed that at 18 and 6 hour incubation time, the uptake of FITC-dextran by hMSCs was saturated and thus masking differences in uptake between different topographies.

On the other hand, at 3 and 1 hour incubation time, saturation of the uptake of FITC-dextran by hMSCs was not observed. At 3 hour incubation time, hMSCs on 2 µm pillars showed a significantly higher percentage of fluorescent population as compared to cells on the unpatterned control (1 mg/ml) (66.3 ± 2.4 % versus 51.7 ± 2.8 %). Lastly, at 1 hour time point, it was observed that hMSCs on patterned topography displayed a higher percentage of fluorescence population (2 µm pillars: 16.0 ± 8.4 %; 200 nm pillars: 21.4 ± 9.4 %; 250 nm gratings: 17.0 ± 10.9 %) as compared to the unpatterned control (1 mg/ml) (15.4 ± 8.2 %). However, these differences were not statistically significant. Results from the incubation time study suggested that topography effects could only be observed at earlier time points (1 and 3 hours) before saturation of internalization was reached (6 and 18 hours). In addition, it was also evident that internalization of FITC-dextran by hMSCs was affected by different topographies, especially the 2 µm pillars topography.

Next, similar experiments were carried on 2 other different cell types, COS 7 and MCF 7 to determine if the effect of topography on internalization was cell type dependent. COS 7 is an example of a fibroblast cell type whereas MCF 7 is a cancer cell line.

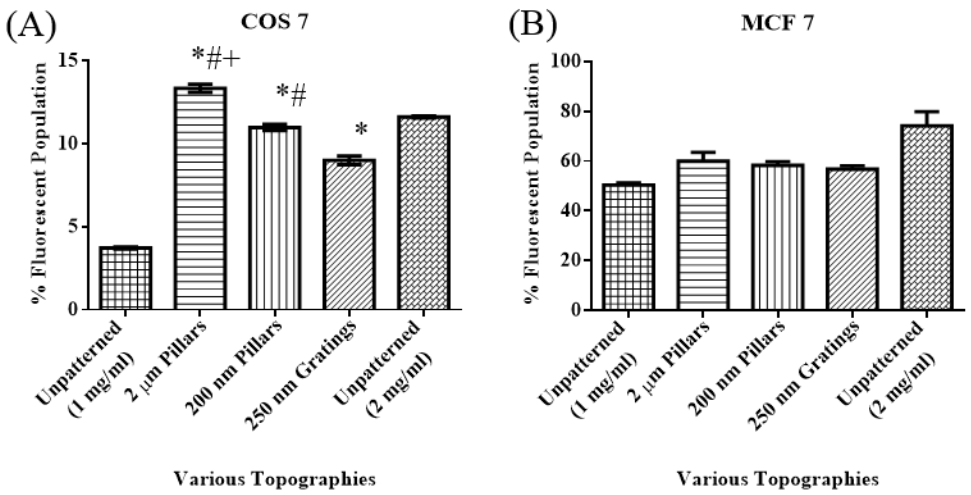

Figure 5.4: Flow cytometry analysis of FITC-dextran internalization on COS 7 and MCF 7 on various topographies after 24 hours incubation time. (A) Overall percentage of fluorescent population of COS 7 on the unpatterned control (1 mg/ml and 2 mg/ml FITC-dextran concentration), 2 μm pillars, 200 nm pillars and 250 nm gratings (1 mg/ml FITC-dextran concentration), (B) Overall percentage of fluorescent population of MCF 7 on the unpatterned PMMA (1 mg/ml and 2 mg/ml FITC-dextran concentration), 2 μm pillars, 200 nm pillars and 250 nm gratings (1 mg/ml FITC-dextran concentration). P <0.01 * - vs unpatterned control (1 mg/ml), # - vs 250 nm gratings, + - vs 200 nm pillars, n=3

After 24 hours FITC-dextran incubation time, no saturation of FITC-dextran uptake was observed. In Figure 5.4 A, COS 7 seeded on various topographies (2 μm pillars: 13.4 ± 0.4 %; 200 nm pillars: 11.0 ± 0.3%; 250 nm gratings: 9.0 ± 0.4 %) had a significantly larger fluorescent population as compared to the unpatterned control (1 mg/ml) (3.7 ± 0.1 %); this result was similar to the trend observed for hMSCs at 3 hours incubation time. In addition, significant differences of FITC-dextran uptake on topographies were observed with COS 7 seeded on 2 μm pillars with the highest enhancement and 250 nm gratings showed the least enhancement. However, the significant enhancement of FITC-dextran uptake observed in both hMSCs and COS 7 on various topographies were not observed in MCF 7.

Although a higher percentage of fluorescent population were obtained on MCF 7 cultured on topography as compared to the unpatterned control (2 µm pillars: 60.0 ± 8.0 %; 200 nm pillars: 58.3 ± 4.0 %; 250 nm gratings: 56.8 ± 3.1 % versus the unpatterned control (1 mg/ml) : 50.4 ± 1.7 %), no significant differences were detected between all topographies (Figure 5.4 B).

The increased in percentage of FITC-dextran positive population in hMSCs and COS 7 cultured on 2 µm pillars indicated that a specific pathway for FITC-dextran internalization might be enhanced on the micron-size. Since FITC-dextran molecules have been previously reported to be internalized through macropinocytosis, it is speculated that this pathway could be highly activate using micron-size pillars topography. Conversely, no significant difference was observed in the FITC-dextran internalization by MCF 7 cells cultured on all the tested topographies.

The effect of topography on endocytosis is different between hMSCs and COS 7. On 2 µm pillars topography, COS 7 cells demonstrated a stronger influence than hMSCs cells. The COS 7 cells display a 2 fold increase while only a 0.3 fold increase was observed for hMSCs cells. Different cell types have different basal rates of endocytosis, which is often implicated in various different cellular functions. However it was unclear if the effect of topography on similar endocytosis pathway could give similar enhancement rate in different cell type. To the best of our knowledge this is the first report to show the effect of substrate topography on endocytosis is cell type dependent.

5.3.2.2 Effect of FITC-dextran molecular weight (MW) on COS 7 internalization rate via topographical cues.

For application in drug and non-viral gene delivery, the efficiency of endocytosis is directly affected by the varying sizes of drug or gene molecules. In this study, the effects of different molecular weight (MW) of FITC-dextran molecules were investigated with respect to substrate topography variation. In the COS 7 FITC-dextran experiment, a higher MW FITC-dextran of 500000 g/mol, instead of 40000 g/mol used in the previous experiment (Figure 5.5).

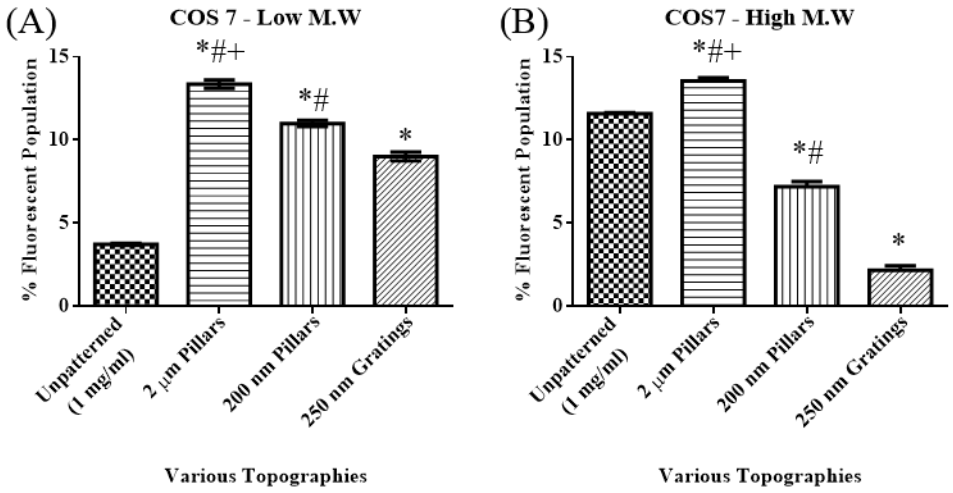

Figure 5.5: Flow cytometry analysis of FITC-dextran internalization in COS 7 using two FITC-dextran of different MW, 40000 g/mol versus 500000 g/mol (A) Overall percentage of fluorescent population of COS 7 using FITC-dextran of 40000 g/mol on various topographies, (B) Overall percentage of fluorescent population of COS 7 using FITC-dextran of 500000 g/mol on various topographies. (P <0.01 * - vs unpatterned control (1mg/ml), # - vs 250 nm gratings, + - vs 200 nm pillars, n=3)

Using a higher MW FITC-dextran resulted in a decrease in fluorescent population across all the patterned substrate except for the 2 μm pillars (13.6 ± 0.3 % versus 13.4 ± 0.4 %) for high and low MW FITC-dextran respectively. All other topographies showed a decrease in fluorescent population, 200 nm pillars (7.2 ± 0.4 % versus 11.0 ± 0.3 %) and 250 nm gratings (2.2 ± 0.4 % versus 9.0 ± 0.5 %). Yet, the ranking of percentage of fluorescent population

within the topography samples still remains the same. Pillars with 2 μm diameter still induced the highest amount of FITC-dextran internalization and 250 nm gratings showed the least internalization rate. However, the degree of decrease across the topography become more pronounced with higher MW FITC-dextran. Higher percentage of fluorescent cells was also observed on the higher MW FITC-dextran as compared to low MW FITC-dextran. The change in MW may be caused by a change in molecule chain length which could affect the rate of endocytosis as reported by Cai at el. [172]. As the molecule chain length increases, both endocytosis and cell apoptosis increases suggesting that the effect of topography on endocytosis were partly dependent on the nature of the cargo.

5.3.2.3 Effect on various topographies on cell morphology

Macropinocytosis is initiated from actin-rich regions of the plasma membrane called ruffles that are closely coordinated by actin and Rho GTPases (Rho, Cdc 42, Rac) [173]. As shown in previous chapter and also by other research groups, topography can alter cell morphology. These morphological changes are closely linked to FA that have interconnected regulation with actin cytoskeleton. To understand the possible reason of the increase FITC-dextran uptake by cells on different topography, the effect of topography on the cell morphology was further investigated via F-actin staining as shown in Figure 5.6 and Figure 5.7.

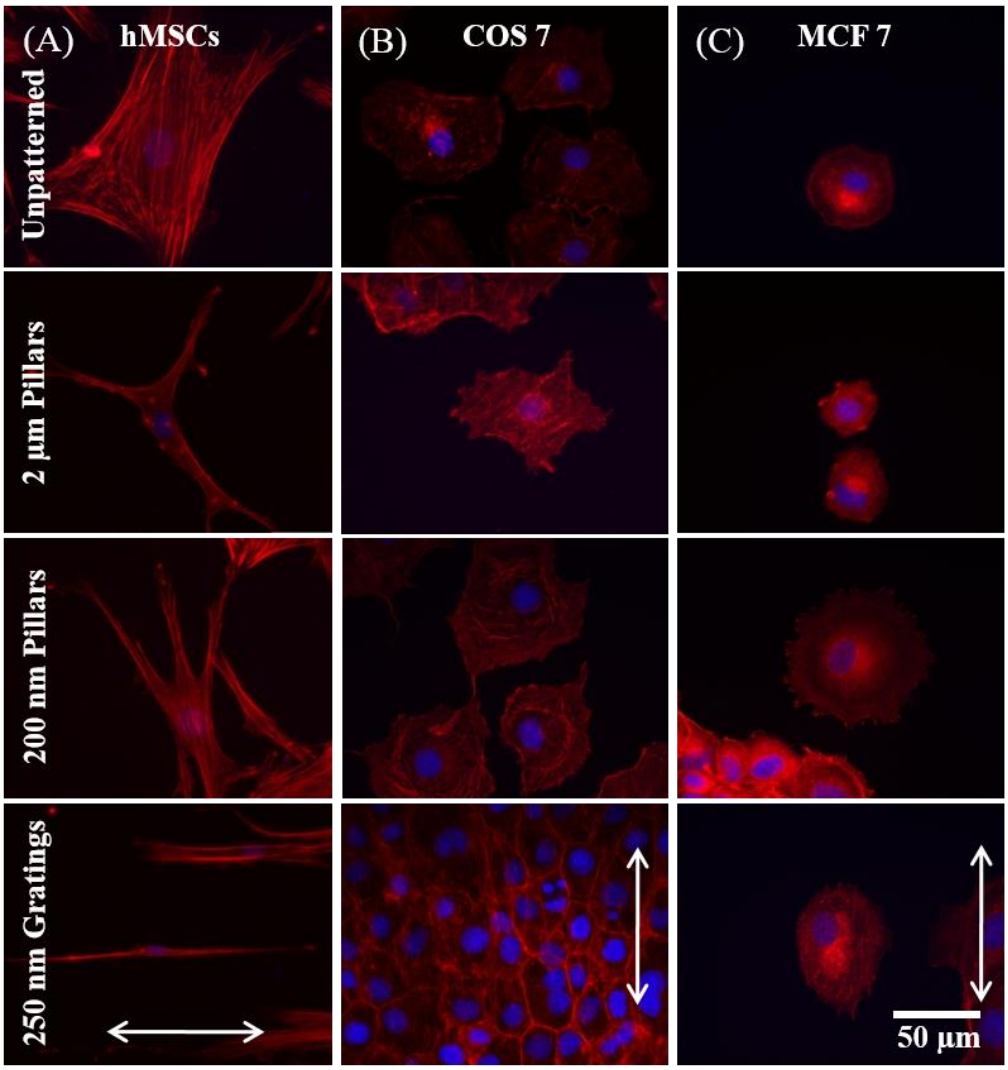

Figure 5.6: Fluorescence images of different cells on various topographies. Cells on the unpatterned control, 2 µm pillars, 200 nm pillars and 250 nm gratings stained for F-actin (red) and nucleus (blue). Column (A) showed hMSCs cultured on various topographies, column (B) showed COS 7 cultured on various topographies, column (C) showed MCF 7 cultured on various topographies. Grating axis was indicated by the double ended arrows.

Characteristic morphologies were observed in fluorescently labelled hMSCs, COS 7 and MCF 7 cells after 24 hours of culture on the various topographies. In general, cells were more spread out on the unpatterned control and pillars topography as compared to gratings topography where they exhibited an elongated morphology. Particular to hMSCs, the cells adopted varying morphologies with different surface areas, the largest area being on the

unpatterned control. A larger cell surface area gives a larger contact area for the cells to interact with its surrounding. This should lead to an increase in internalization. However, this was not observed as the cells with the largest surface areas did not exhibited the highest internalization. Thus, these results suggested that the effect of topography on macropinocytosis was independent of the surface area of contact with FITC-dextran molecules.

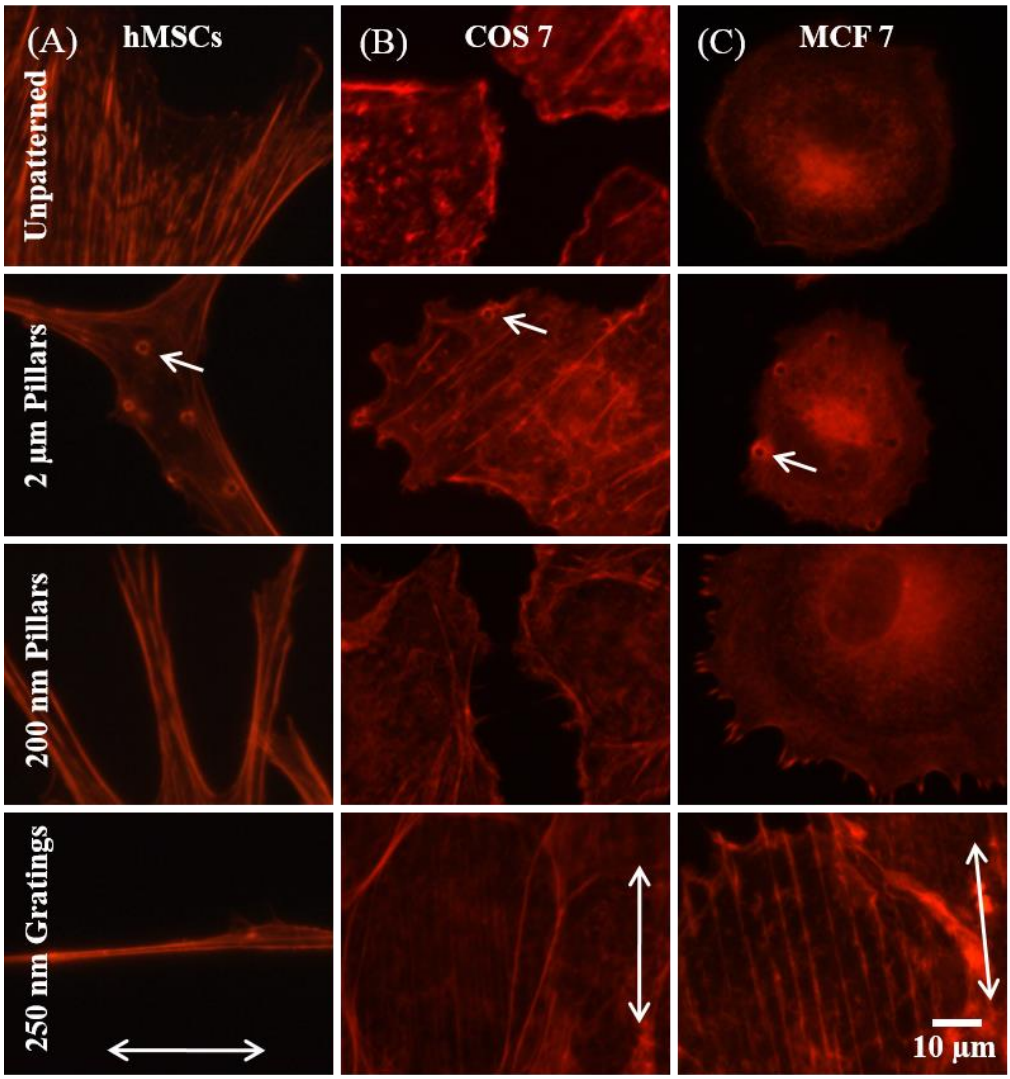

Figure 5.7: Magnified images of fluorescently stained cells on various topographies. F-actin (red) of different cells on the unpatterned control, 2 µm pillars, 200 nm pillars and 250 nm. Column (A) showed hMSCs cultured on various topographies, column (B) showed COS 7 cultured on various topography, column (C) showed MCF 7 cultured on various topographies. Actin-dense ring regions were observed to coincide with the underlying pillars topography on the micron-size structure as indicated by the white arrows. F-

actin in 250 nm gratings were aligned and elongated to the grating axis as indicated by the double ended arrows.

The distribution of actin cytoskeleton after culture on these topographies were different as shown by their F-actin stress fibers (Figure 5.7). In particular, when cells are cultured on 2 μm pillars, intracellular actin-rich rings were observed regardless of the cell type. These actin-rich rings outlined the top surface of the upright pillars topography where the cells were in contact. Higher intensity actin-rich regions were observed in the 2 μm pillars compared to the 200 nm pillars while no such regions were seen on the gratings topography. These actin-rich regions were connected together into a web shape by stress fibers of the cells. Meanwhile, cells cultured on the 250 nm gratings substrate showed a distribution of stress fibers that were aligned to the grating axis. The increase in actin dense regions observed in cells on the micron-size pillars could change the intercellular contractility, which up regulate Rho GTPases to enhance ruffling and macropinocytosis as seen in hMSCs and COS 7 on 2 μm pillars topography. Whereas in MCF 7, less actin-rich regions were observed, corresponding to an insignificant difference in FITC-dextran internalization when cultured on different topographies. Comparing to hMSCs and COS 7, MCF 7 which is a cancer cells type that exhibits increased motility, leading to increase in ruffling in MCF 7 metastatic cells. This could be used to explain why insignificant difference was observed in the internalization experiment using MCF 7 cells [174, 175].

Topography, like growth factors, can stimulate cellular migration [135, 176, 177]. The effect of topography on cell migration could be another reason for the increased cell internalization. Different expression of integrin subunits were observed when hMSCs were cultured on different topographies [178].

This suggests that integrin trafficking rates are different in hMSCs on different topographies. During cell migration, integrins are reallocated from disassembling FA to new assembling FA at the leading edges. Clathrin-mediated endocytosis of β-1 integrins were shown to be involved in the initial step of integrin redistribution [179]. However, a recent study demonstrated that cell stimulation using platelet-derived growth factor for cell migration causes a rapid redistribution of integrins to the dorsal circular ruffles before being internalized through macropinocytosis [180]. Thus, the increased rate of macropinocytosis observed can be a synchronized result of increased integrin transport on micron-size topography. Comparing different topographies, cellular migration is generally lower on gratings compared to pillars substrates. In addition, the pattern density of nano-sized pillars is much higher than micron-size pillars topography. Thus, cells have difficulty finding a suitable path for attachment and migration, hence exhibit slow motility in nano-sized pillars topography [181]. However, the link between topography and integrin transport will require further investigation.

Thus far, topographical cues have been successfully demonstrated to enhance cellular internalization, mainly via the macropinocytosis pathway. This further developed the usage of surface topography in the field of drug delivery application.

5.3.2.4 Effect of topography on non-viral GFP transfection of hMSCs

Next, to understand the effect on topography on different endocytic pathway and its application in non-viral gene delivery application, hMSCs cultured on different topographies were transfected with GFP plasmid via lipofectamine 2000 reagent.

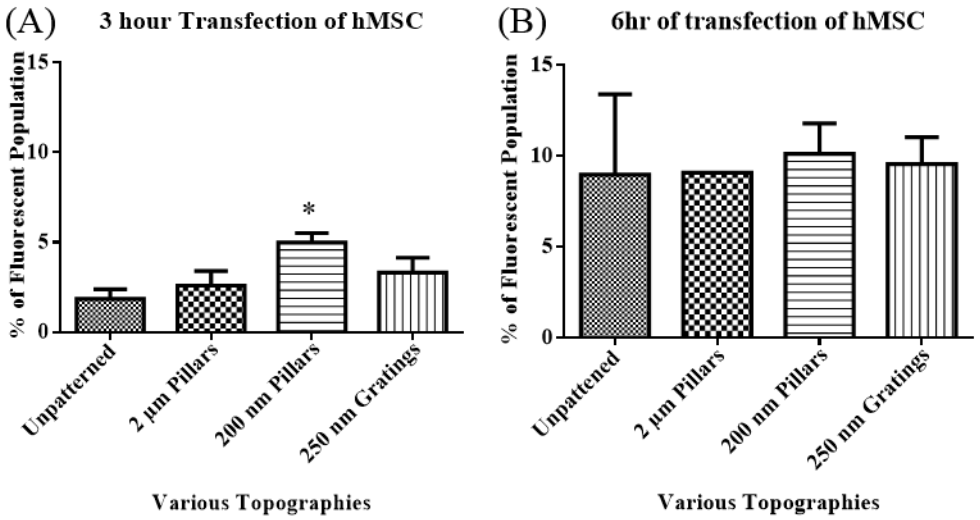

Figure 5.8: Flow cytometry analysis of GFP transfection using lipofectamine 2000 on hMSCs seeded on various topographies. (A) Overall percentage of GFP positive population for 3 hours transfection incubation time, (B) Overall percentage of GFP positive population for 6 hours transfection incubation time. P <0.01 * - vs unpatterned control.

An increase in the fluorescent population was observed 3 hours after hMSCs were transfected while adhering to various topographies (Figure 5.8 A). The hMSCs cultured on 200 nm pillars displayed a mean fluorescent population of 5.0 ± 1.2 %, a significant 2.5 fold increase in fluorescent population as compared to the unpatterned control (1.8 ± 1.2 %). For 2 µm pillars and 250 nm gratings, a higher mean fluorescent population (2 µm pillars: 2.6 ± 1.5 % and 250 nm gratings: 3.3 ± 1.8%) than the unpatterned control was also obtained but the increase was not statistically significant. On the other hand, at the 6 hour transfection time point, no difference could be observed on the various topographies (Figure 5.8 B). The percentage of fluorescent hMSCs transfected on the unpatterned control and patterned PMMA remained the same. This further supported the point that the effect of topography on endocytosis occurs at earlier time point before saturation was achieved.

Human MSCs are known to be highly sensitive and difficult to transfect, requiring electroporation for enhanced transfection efficiency. This is often performed with the risk of increased cell death [182]. Unlike the FITC-dextran internalization, hMSCs cultured on 200 nm pillars showed mean fluorescent population and higher transfection efficiency compared to 2 μm pillars. FITC-dextran internalization reportedly require macropinocytosis pathway whereas cellular uptake of lipofectamine-mediated GFP plasmid occurs mainly by clathrin-mediated endocytosis [118, 171]. This reiterates the point that topographies can enhance different endocytosis pathway.

The amount of protein binding onto surfaces depends on the surface energy and exposed surface area [183]. The amount of adsorbed proteins increased significantly with nanoscale topography. Substrate topography provides an enhanced surface area for the adsorption of proteins, where nanoscale topography further increases surface area. By calculating the surface area on the three different topographies used, 200 nm pillars (369.9 μm^2) gave the highest increment while 2 μm pillars (156.6 μm^2) gave the least increment in total exposed area, comparing to the unpatterned control (144.0 μm^2). The differences in protein adsorption on the topographies can affect cells as they are equipped with intrinsic ability to sense minute-scale physical differences in the extracellular matrices.

Other than protein adsorption, nanoscale topography is also able to influence the deposition of polyplexes compound on the surface. This could increase the effective concentration of the delivery vehicle on the surface and cell surface that in turn increases the transfection of the cells. With 200 nm pillars showing a higher surface area as compared to the rest, the deposition of the polyplexes

overtime can increase the local concentration that the cells are subjected to and increase transfection efficiency. Studies had shown that increased DNA complex attached at the cell surface eventually increased transfection efficiency [184].

Another possible reason for the increase in endocytosis is the modulation of FA turnover on topography, resulting in different intracellular contractility of the cells. Adherent cells interact with their surrounding microenvironment through the modelling of FA. FA are used in cellular motility and can be modulated using substrate topography. FA size reflects the state of the intracellular actin-contractility of the cells. hMSCs that were cultured on nanogratings showed reduced vinculin expression compared to the unpatterned control, implying a decreased actin cytoskeletal contractility on nanogratings topography [178]. Endocytosis related proteins like integrins, clathrin and caveolin-1 are shown to be regulated by actin cytoskeletal tension [185-187]. For example, monkey kidney epithelial cells cultured on fibronectin patterns showed spatial heterogeneity in the clathrin coated pit lifetime the non-adherent regions showed a longer clathrin coated pit lifetime and resulted in changes to the global cellular endocytosis rates [188]. The topographies used in the studies were similar to the micron-size topography with negligible height used in this study. This indicates that the use of topography may have similar effect on modulating the cytoskeletal arrangement within the cells that consequently regulate the plasma membrane tension and endocytosis rate. From our results, it appears that hMSCs on nano-size structures had a higher correlation with receptor-mediated endocytosis.

5.3.3 Effect of topography on endocytosis on the baso-lateral membrane of the cell

FITC-dextran internalization studies have demonstrated that topography can be used to modulate cell endocytosis through the apical surface of the cell. Thus, it is interesting to determine if topography has a similar effect on the baso-lateral membrane. In the field of drug and gene delivery, nanoparticles are often use as a vehicle to deliver the substance of interest into the cells. Gratton et al reported that rod-shape like particles are preferentially internalized by HeLa, indicating that the shape of the nanoparticles matters [127]. However, internalization of nanoparticles on adherent cells using the apical surface of the membrane is common and not much is explored regarding endocytosis through the baso-lateral side of the cells. To further understand the effect of topography on endocytosis, 2 different topographies were devised to fabricate a substrate with detachable topography that functioned as a topographical cues and vehicle.

From the previous study of cells cultured on the micron- and nano-size pillars, no breakage and detachment of the pillars were observed. With the presence of residual layer, it was not favourable for the cells to break, detach and internalize the pillars topography. Thus, two different types of topographies, 200 nm pillars without residual layer and 2 µm pillars collapsed on PDMS substrate were used in the next part of the study.

5.3.3.1 Internalization of 200 nm residual free upright pillars

First, the 200 nm PMMA pillars containing rhodamine was plasma etched using oxygen plasma to remove the underlying residual layer. This aided in reducing the force required for the cells to detach the pillars and subsequently

internalized the cargo. Human MSCs were then cultured onto the substrate and the internalization of the rhodamine-PMMA pillars were visualized using confocal microscopy as shown in Figure 5.9.

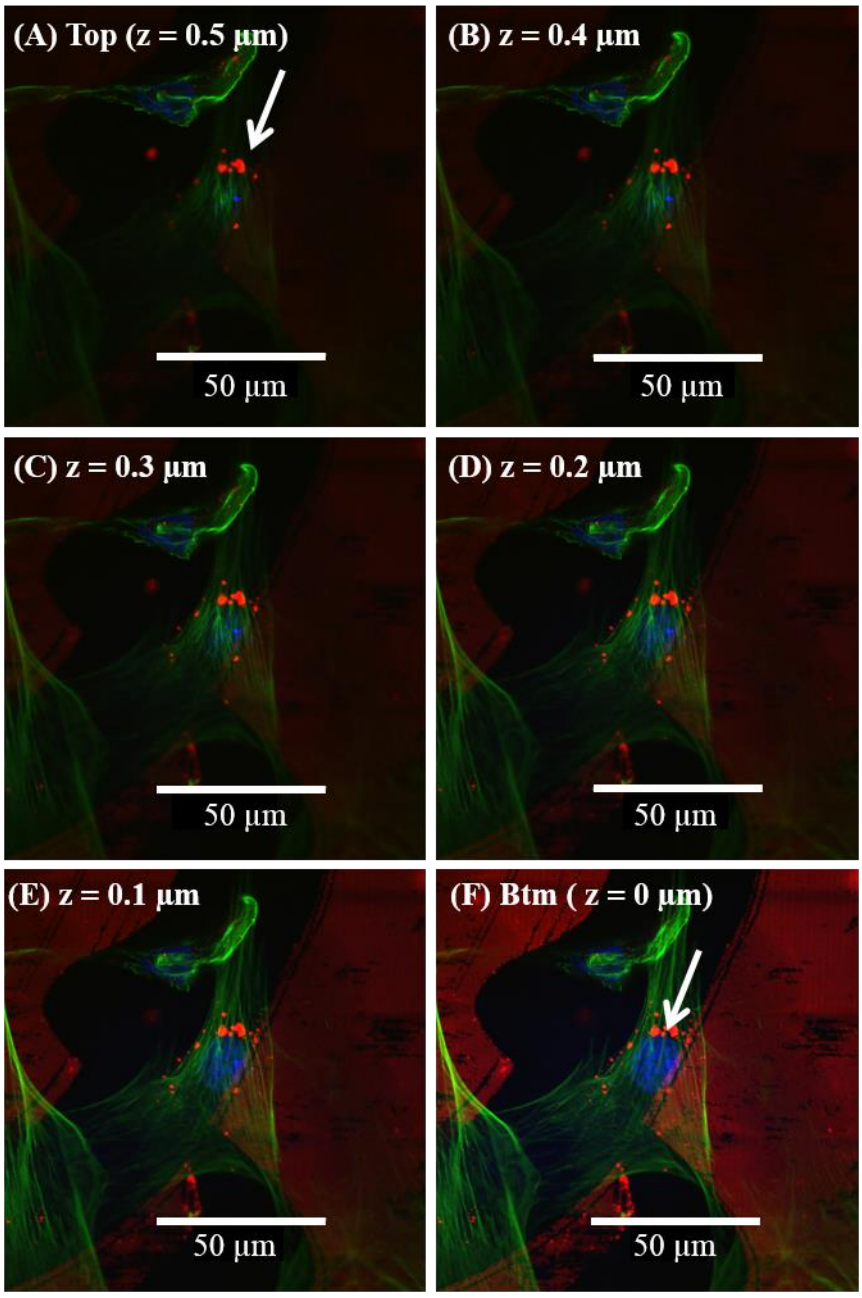

Figure 5.9: Confocal z-stack fluorescent images of hMSCs cultured on 200 nm upright pillars without residual layer after 24 hours. Each successive image represent 0.1 µm z-step from the apical surface to the baso-lateral surface of the cells. Arrows indicate possible internalized 200 nm pillars.

Figure 5.9 A-F showed confocal images of fluorescently stained hMSCs with z-section in 0.1 µm successive steps. Upright pillars without residual layer were incorporated with rhodamine (red) for visualization and differentiation from other cellular organelles and intracellular structure. As the focal plane moved from the basal surface to the apical surface of the cells, the signal intensity of the pillars decreased and the focus of the pillars become blurred. A few pillars (denoted by arrows in Figure 5.9 A-F) appeared to remain in focus. These pillars appeared to have been internalized by the hMSCs. To understand how cells interact with its topography, cells cultured on topography were fixed and characterized using SEM.

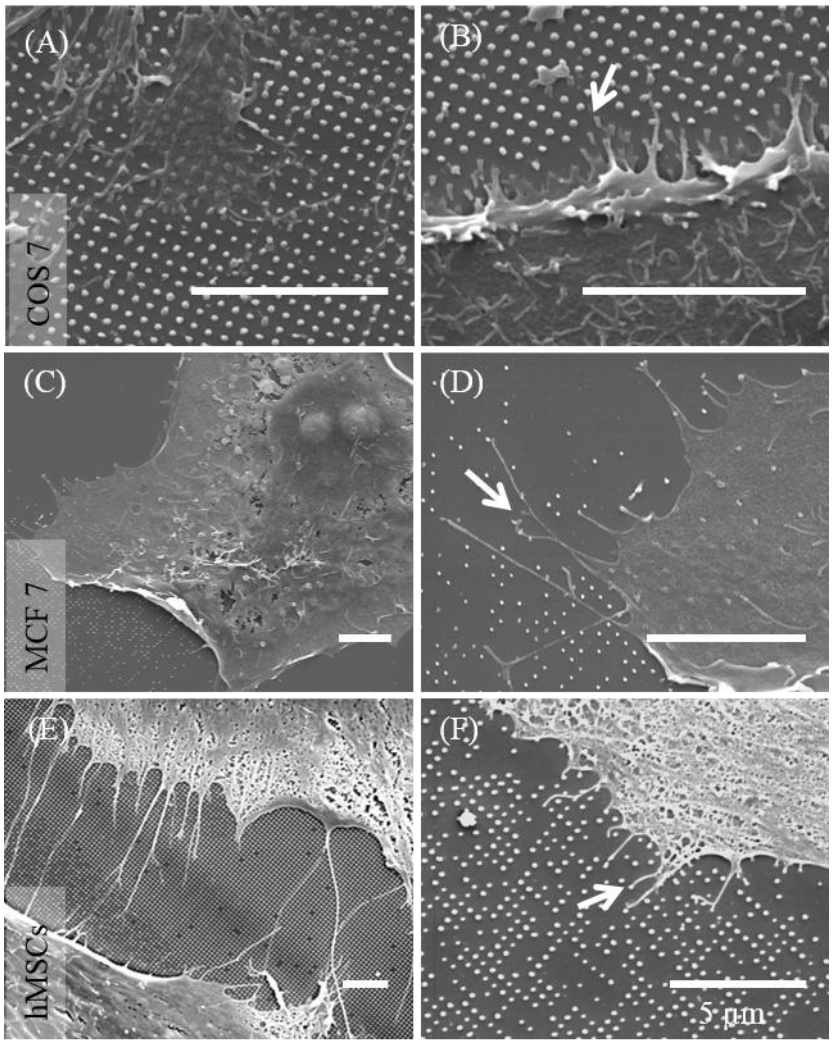

Figure 5.10: SEM images of (A-B) COS 7, (C-D) MCF 7 and (E-F) hMSCs on 200 nm pillars. All cell types showed increased filopodia extension directed towards the nanopillars and appear to "grab" the pillars towards themselves, detaching the pillars from the substrate as indicated by arrows seen in (B, D and F).

Figure 5.10 showed COS 7, MCF 7 and hMSCs residing on these residual free nanopillars showed presence of long and extensive filopodia projections. These observation were consistent with other studies, where cells were reported to have extended their long filopodia extension to reach out to the nano-size structures [133]. Filopodia are thin membrane protrusions [189, 190] found at the migrating front end of the cells that act to probe the extracellular environment. SEM observation showed that the cells were able to specifically target their filopodia onto these nano-size pillars and affixed themselves onto these structures to exert a pulling force onto these structures for cellular locomotion. The missing pillars near the cells were suspected to be pillars broken by the cells during its interaction with the substrate. In an earlier study, 1 µm cylindrical PRINT particles were shown to be internalized mainly via clathrin-mediated endocytotic pathway as well as micropinocytosis [127]. However, the system in this study uses nanopillars adhered to the surface. Due to the proximity of the nanopillars on the baso-lateral surface of the cells, uptake of these structures by the apical surface of the cells were unlikely. This could possibly mean that the internalization of these particles are not restricted to clathrin-mediated endocytosis or macropinocytosis.

5.3.3.2 Internalization of 2 µm collapsed rhodamine-PS pillars

Another structure to study the effect of baso-lateral membrane endocytosis was the 2 µm rhodamine-embedded polystyrene pillars. COS 7, MCF 7 and

hMSCs were cultured for 24 hours on this topography and confocal imaging characterization were carried out.

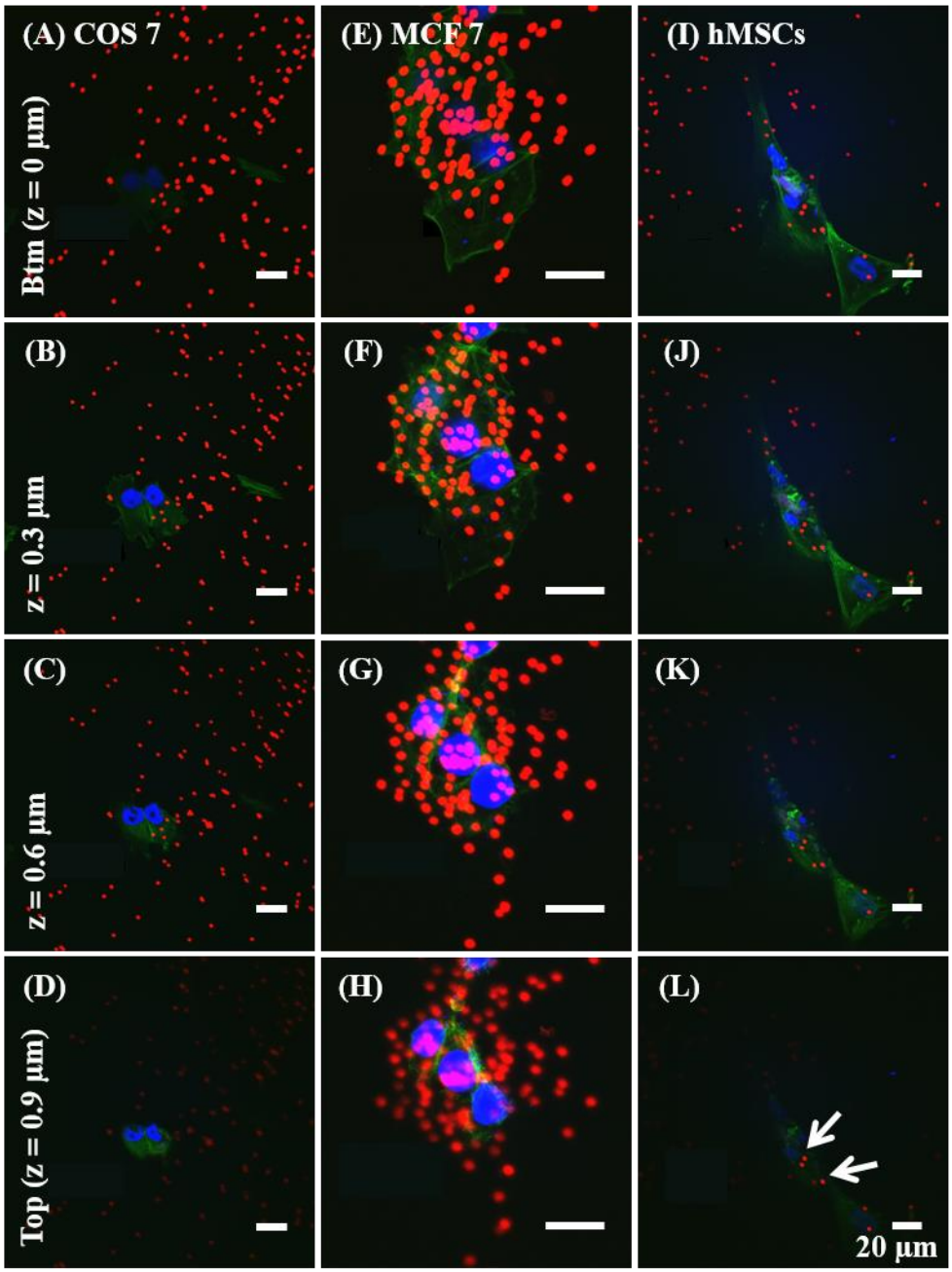

Figure 5.11: Confocal z-stack fluorescent images of COS 7, MCF 7 and hMSCs on 2 µm collapsed rhodamine-PS pillars. Each successive image represent 0.3 µm z-step from the baso-lateral surface to the apical surface of the cells. Arrows indicate possible internalized 2 µm collapsed pillars.

Figure 5.11 showed the successive z-section confocal images of COS 7, MCF 7 and hMSCs stained for F-actin and nucleus on the topography. Among the three cells types, internalization of the 2 μm pillars was only observed for hMSCs cells. This indicates that topography-mediated baso-lateral membrane endocytosis was cell type dependent and similar to apical membrane endocytosis. However, it was interesting to note that a large number of pillars (as indicated by the red fluorescence) appear to reside in the baso-lateral surface of the MCF 7 cells, even though they were not possibly not internalized. This suggested that MCF 7 cell attempted endocytosis of these structures but were be hindered due to the large size of the pillars. For hMSCs, it was observed that most of the internalized particles reside within the peri-nuclear region of as indicated by the white arrow in Figure 5.11 L. This preferential internalization by hMSCs might be due to the larger intracellular contractility present in hMSCs compared to other cells types that were significantly smaller in size. Compared to the residual-free pillars in this design of topography, cells need to exert lesser force to access the self-detached pillars as the adhesion forces between the structures and the underlying substrates were much reduced. However, to fully understand and control this mode of internalization, more detailed investigation is required to develop its application into drug and gene delivery system.

5.4 Conclusion

In this chapter, the effect of topography feature size and spatial orientation on endocytosis and transfection were conducted.

PMMA imprinted topographies of 2 μm pillars, 200 nm pillars and 250 nm gratings were fabricated with high yield and fidelity. These topographies were

used to investigate the effect of substrate topography on COS 7, hMSCs and MCF 7 endocytosis and transfection efficiency. FITC-dextran internalization experiment on these cells revealed the effect of topography on endocytosis to be cell type dependent. The FITC-dextran internalization of COS 7 and hMSCs varied on different topography. No differences were observed in the internalization efficiency of FITC-dextran by MCF 7 on all pattern and the unpatterned control. Topographical design to modulate cell endocytosis was identified from the FITC-dextran internalization of COS 7 and hMSCs. Cells cultured on 2 µm pillars showed higher internalization as compared to 200 nm pillars and 250 nm gratings. However, a different topographical design was identified in hMSCs transfection using lipofectamine. Instead of 2 µm pillars topography, hMSCs transfections efficiency was higher on 200 nm pillars topography. Nevertheless, isotropic topography enhanced endocytosis and transfection more as compared to anisotropic topography. We speculate that the different topography rule for the 2 process are due to the different pathway through which FITC-dextran molecules and DNA-lipoplexes were endocytosed. It is widely reported that FITC-dextran molecules enter the cells via macropinocytosis while DNA-lipoplexes are endocytosed mainly by clathrin-mediated endocytosis. This study demonstrated the potential to use topography to select a more efficient endocytosis pathway for drug and gene delivery. Overall, this observation also proved our hypothesis that topography feature size can modulate cell internalization and transfection, possibly by activating different endocytosis pathway. In addition, isotropy topography better enhance endocytosis and transfection as compared to anisotropy topography.

The effect of topography also modulated the internalization of cells through the baso-lateral membrane. To mimic the scenario of using the topography as delivery vehicle while playing its role in modulating cell endocytosis, 200 nm residual free pillars and 2 µm collapsed pillars topography were developed. Results from these studies showed that hMSCs were able to internalize both the pillars. Thus the results validated the proof-of-concept to use topography as both the modulator and vehicle for drug and gene delivery.

Chapter 6 **Conclusion**

Understanding and selecting the suitable topography to modulate specific cellular behaviours is important for the incorporation of topography in biomedical applications. Despite increasing evidence that topography can affect cellular behaviours, a systematic study to understand topographical design to modulate and control cellular behaviours is missing.

In this thesis, patterning of biomaterials such as PVA hydrogels, PDMS and PVA were performed and the effect of topographical design on cell adhesion, proliferation, endocytosis and transfection were studied. Through this thesis, various topographies have been identified to modulate the cellular behaviours of ECs (EAhy926, HUVEC), fibroblast cells (COS 7) and human adult stem cells (hMSCs).

1. Cell adhesion

   The EC cell adhesion on PVA hydrogels was enhanced by topographical modification. From the *in vitro* PVA study, it has been demonstrated that the cell density of EAhy.926 cells was significantly increased on 2 μm gratings topography as compared to the unpatterned PVA control. In addition, the effect of topography on enhanced EC adhesion was also shown *in vivo*. ECs were detected in the luminal surface of the PVA graft with 2 μm gratings after 20 days of graft implantation into a rat aorta. These results showed that topography improved the cell response on PVA hydrogels to enhance EC adhesion on the materials. While enhancement of EC adhesion was demonstrated on patterned PVA hydrogels, reduction of EC adhesion was observed on patterned PDMS. Significant reduction in

HUVEC density has been observed on 1.8 μm concave lenses topography in the MARC chip screening and individual pattern study as compared to the unpatterned PDMS control. Other topographies such as 1.8 μm convex lenses, inverse cones, cones, and 1 μm convex lenses were also identified in the MARC chip screening for significantly decreased cell adhesion on PDMS.

2. Cell proliferation

HUVEC cell proliferation was also modulated on various PDMS topographies. The MARC chip screening of HUVEC proliferation showed that the HUVEC proliferation was significantly reduced on various topographies such as 250 nm gratings, 2 μm and 500 nm V-gratings, 2 μm and 500 nm U-gratings, 1.8 μm convex lenses topography, 2 μm gratings with 250 nm pillars and 2 μm gratings with perpendicular 250 nm gratings as compared to the unpatterned PDMS control. However, cell density can also influence cell proliferation responses. For example, reduced cell density on 1.8 μm convex lenses also reduced the intracellular contact between the cells and eventually leads to the reduction of cell proliferation.

3. Cell endocytosis

The effect of topography on cell endocytosis was studied via the FITC-dextran internalization by the cells cultured on various PMMA topographies. Significant enhancement of FITC-dextran internalization by COS 7 were detected when cells were cultured on 2 μm pillars, 200 nm pillars and 250 nm gratings topography as compared to the unpatterned PMMA control. On the other hand, significant increase in internalization

was only observed for hMSCs cultured on 2 µm pillars topography. Hence, various topographies can enhance cell endocytosis and the modulation is cell type dependent.

4. Cell transfection

   Cell transfection of HUVEC and hMSCs can also be modulated by various topographies on PDMS and PMMA respectively. From MARC chip screening, enhanced HUVEC transfection efficiency has been showed on various topographies such as 2 µm U-gratings, 1.8 µm convex lenses, 2 µm gratings with 200 nm pillars and 2 µm gratings with perpendicular 250 nm gratings. However, a decreased in HUVEC transfection efficiency on some of these topographies were observed in the individual pattern study conducted. Significant decrease in transfection was observed on 1.8 µm convex lenses, 2 µm gratings with secondary structures such as 200 nm pillars and perpendicular 250 nm gratings. The difference in the observation might be due to the different quantification method and total number of cells used and analysed in the 2 experiment. In this thesis, enhanced cell transfection was also demonstrated using a different cell type, hMSCs. When cultured on 200 nm pillars topography, significant increase in the percentage of GPF fluorescent positive hMSCs was detected as compared to the unpatterned PMMA control.

In addition, the thesis also sought to identify the role of specific topographical design in modulating cellular behaviours. Examining the topographies that modulate various cellular behaviours, the following topographical designs were identified.

1. Topography with RC in z direction

   Among the topographies identified, lenses topographies such as 1.8 μm concave lenses and 1.8 μm convex lenses, exhibit significant influence on the 3 cellular behaviours as compared to the unpatterned PDMS control. These lenses topographies have common topographical designs of isotropic features with RC in z direction. From our studies, reduction in HUVEC cell adhesion, proliferation and transfection have been shown on 1.8 μm concave and convex lenses topography. These topographies could increase cell apoptosis and disrupt non-muscle myosin-II activities leading to modulation on HUVEC adhesion, proliferation and transfection.

   In addition, anisotropic topography with RC in z direction such as 2 μm U-gratings is believed to enhance HUVEC transfection. From the study of HUVEC on 2 μm U-gratings, while reduction in cell adhesion and proliferation were observed, the transfection efficiency of HUVEC was comparable to the unpatterned PDMS control. This indicates that HUVEC transfection efficiency on the 2 μm U-gratings may have increased in order to compensate for the unfavourable condition for cell transfection due to low cell density from poor cell adhesion and proliferation.

2. Feature size (nano-size vs micro-size)

   The difference in features size also modulate the proliferation rate of HUVEC. Gratings topography with nano-size width reduced HUVEC proliferation. From the MARC chip screening, topographies such as 250 nm gratings, 500 nm V-gratings, 500 nm U-gratings, 2 μm V-gratings and 2 μm U-gratings showed significant reduction in cell proliferation as

compared to the unpatterned PDMS control. Notably, the grating width of these topographies are in the nano-size with varying pitch size. Hence, as compared to grating pitch, grating width in nano size can modulate HUVEC proliferation.

In addition, feature size also modulate different cell behaviour in hMSCs. Micron-size features enhanced cell endocytosis while nano size features enhanced cell transfection. From our studies, 2 μm pillars induced higher FITC-dextran internalization while 200 nm pillars induced higher transfection efficiency. In addition, enhanced in transfection also indicated that feature size can modulate different endocytosis pathway where micron size enhanced macropinocytosis while nano size enhanced receptor-mediated endocytosis.

3. Hierarchical topography

   The addition of secondary structures reduces HUVEC transfection efficiency. From our studies, all hierarchical topographies reduced HUVEC transfection as compare to the primary structure topography, flatten 2 μm gratings topography. Although different topographies such as 250 nm pillars, 250 nm gratings were used for the secondary structures, no significant difference was observed for different secondary structures.

4. Spatial orientation (anisotropic versus isotropic)

   Isotropic topography enhanced endocytosis more as compared to anisotropic topography. For COS 7 and hMSCs, higher FITC-dextran internalization was observed on 200 nm pillars as compared to 250 nm gratings.

In this thesis, new knowledge was also generated in the patterning of materials and new novel topography for studying cell responses were fabricated. 2D patterning of PVA hydrogels via casting, NIL and novel 3D patterning of tubular PVA via dip-coating were developed. With the patterning techniques developed, patterning of aqueous-based hydrogel can be done at ease with high yield and pattern fidelity. This further develops the use of PVA for vascular engineering. The 3D patterning techniques also open doors to new development to use topographical modification in the field of tissue engineering and vascular grafts.

The fabrication of novel structures such as the collapse pillars enable the use of topography as a modulator and the vehicle for drug and gene delivery. As a proof of concept, hMSCs was able to endocytose the underlying 2 μm collapsed pillars on the culturing substrate.

In conclusion, various topographies on biomaterials can modulate cell adhesion, proliferation, endocytosis and transfection of different cell types such as EAhy.926, HUVEC, COS 7 and hMSCs. Through the study of cell adhesion, proliferation and transfection on various topographies, topographical design such as topography with RC in z direction, feature size of anisotropic topography and hierarchical topography can modulate part or all EC behaviours studied in this thesis. In addition, topographical design such as feature size and spatial orientation can modulate endocytosis and transfection of hMSCs. Our findings in this thesis generated new information for the use of topographica modification in the application towards vascular engineering and drug and non-viral gene delivery. Once again, from our findings and

observation in this thesis, the importance of the role of topography in the modulation of different cellular behaviours is substantiate.

Chapter 7 Future work

In this thesis, new knowledge was generated in the patterning of materials and cell responses on various topographies. These include 2D and 3D patterning of hydrogel materials and various topographical designs to modulate cell adhesion, proliferation and transfection. Additional development in some areas could be further pursued to provide more insight on the usage of topography for medical application as well as the effect of topography on more cell responses.

7.1 Patterning of PVA hydrogel

In Chapter 3, 2D and 3D patterning of PVA hydrogel was achieved with high yield and shape fidelity. However, there are issues on pattern shrinkage and limitations in patterning resolution. Casting and dip-coating patterning techniques are limited to micron-size feature. In addition, dimension fidelity was not achieved in the patterned PVA via casting. Better understanding of the crosslinking mechanism of PVA hydrogels and the physical changes during the crosslinking process may be critical for the improvement of the pattern resolution and dimension fidelity. For example, a rheology study to investigate the changes in the physical properties of PVA during crosslinking process may give useful information for the development of different strategies to overcome the materials shrinkage and to improve patterning resolution. This further develops the application of PVA for soft tissue applications.

7.2 The effect of curvature structure on cell morphology and adhesion behaviour

In Chapter 4, cell adhesion had been shown to be significantly reduced on various lenses topographies. These topographies are anisotropic topographies with RC in z direction. The effect of topographical design was attributed to the cell morphology observed. Rounded and dendritic-like cell morphology could increase cell apoptosis or inhibition of myosin II activities, leading to reduced EC adhesion. These cells responses can also correlate to cell proliferation and transfection. There is a need to establish the influence of these topographies on cell apoptosis rate, FA distribution and maturation as well as the expression of myosin light-chain kinase. These studies provide more insight to understand the mechanism behind topography-mediated cells responses.

In addition, the detailed design of topography with curvature could be further examined. More investigation can be done to understand the effect of the degree of curvature on cell responses. This information is necessary to predict and control the effect of these topographies on cell behaviour.

7.3 The effect of hierarchical topography on cellular behaviours

In Chapter 4, hierarchical topographies had been shown to modulate cell transfection, indicating that the presence of secondary structures can modulate cellular behaviours. However, no significant different in transfection efficiency were observed in the 3 hierarchical topographies used in the study.

In the native environment that cells resides in, the surface of the basement membrane consists of multilayered topographical design. Hence, it is important to understand the effect of multilayered topography on cellular

behaviour. Further studies using the hierarchical topography can be carried to identify the topographical design in the secondary structures to modulate cellular behaviour. They are a good systematic representation of the nature multi-layered topography to investigate the effect of various secondary structures on cellular behaviours.

7.4 The effect of topography on cell endocytosis and cell transfection

In Chapters 4 and 5, various topographies have been shown to modulate the endocytosis and transfection of different cells. Although some topographical designs were identified, more information on the topographical designs could be investigated to gain more insight on the topographical designs in modulating cell endocytosis and transfection. For example, the range of feature size or degree of topography curvature could be further investigated to determine their limitation in modulating cell endocytosis and transfection. Further research on the effect of topography on cell endocytosis and transfection would benefit the field of drug and non-viral gene delivery and gene therapy by providing another method to increase delivery efficiency.

The mechanism on how topography modulate cell endocytosis should also be further studied. The effect of topography on the internalization of FITC-dextran molecules and DNA-lipoplexes complexes could be due to the activation of different endocytosis pathway on different topographies. Thus, by conducting endocytosis pathway inhibition studies on these topographies, the effect of topography on endocytosis pathway activation can be understood. Previously, Gratton *et al.* [127] or Agarwal *et al.* [128] conducted an endocytosis pathway inhibition study to understand the effect of different

particles on endocytosis. Similar experiments may be carried out to explore the effect of topography on endocytosis pathway activation.

The enhancement in cell transfection can also be contributed by the subsequent process that followed after delivery cargo was endocytosed into the cells. These processes include the pathway out of the endosomal compartment, entry into the cell nucleus and gene transcription inside the cell nucleus. Membrane trafficking studies can be conducted to track the transfection process and to investigate the effect of topography on the 3 processes after vehicle has been endocytosed by the cells that could lead to increase transfection efficiency.

7.5 New drug and non-viral gene delivery platform

In Chapter 5, the internalization of cargo through the baso-lateral membrane of the cells was demonstrated as a proof-of-concept. Out of the 3 cell types studied, hMSCs was the only cell type that internalizes the residual free pillars and the collapsed pillars. This indicates the potential of such a platform for targeted cell delivery. To develop this platform into useful delivery system, the effect of topography on reverse transfection needs to be further studied. For example, gene or delivery cargo can be immobilised on different topography surfaces to study the efficiency of cell endocytosis or transfection on the topography from the baso-lateral membrane of the cells. Understanding the effect of topography on the baso-lateral membrane aid in the development of new delivery system using topographical cue to enhance delivery efficiency.

Chapter 8 **Patents and publications**

8.1 List of patents

1. US Patent (No. 13/602,616) "Construct for promoting absorption of molecules by a cell and methods of using the construct" Yim EKF, Low HY, Kustandi TS, Teo BKK, Goh SH
2. US Provisional Application (No. 61/871,640) " Bioactive modification of poly(vinyl alcohol) with surface topography and biochemical cues for vascular graft" Yim EKF, Le Visage C, Cutiongco MFA, Tan MH, Low HY, Goh SH

8.2 List of publications

1. Goh SH*, Teo BKK*, Kastandi TS, Loh WW, Low HY, Yim EK, The effect of micro and nanotopography on endocytosis in drug and gene delivery systems, Biomaterials, 2011, 32 (36), 9866-75 (* equal first authorship)
2. R. Muhammad, S.H. Lim, S.H. Goh, J.B.K. Law, M.S.S. Saifullah, G.W. Ho and E.K.F. Yim, Sub-100 nm patterning of TiO2 film for the regulation of endothelial and smooth muscle cell function, Biomaterials science, 2014, 2, 1740-49
3. Kenneth K.B.Tan, Jason T. Tann, Sharvari R. Sathe, Seok Hong Goh, Dongliang Ma, Eyleen L.K Goh, Evelyn K.F. Yim, Enhanced differentiation of neural progenitor cells into neurons of the mesencephalic dopaminergic subtype on topographical patterns, Biomaterials, 2015, 43, 32-43

4. Cutiongco MFA*, Goh SH*, Aid R, Le Visage C, Low HY, Yim EKF, Planar and tubular patterning of micro and nano-topographies on poly(vinyl alcohol) hydrogel for improved endothelial cell responses (Resubmission in process) (* equal first authorship)
5. Goh SH, Low HY, Yim EKF " High-throughput screening for the effect of topography on endothelial cells transfection" (in preparation)
6. Kukumberg M*, Goh SH*, Yim EKF " Multi-Architecture (MARC) chip as a screening platform to study and identify various topographies for endothelial cell adhesion and proliferation (in preparation)

Bibliography

1. Martínez, E., et al., *Effects of artificial micro- and nano-structured surfaces on cell behaviour.* Annals of Anatomy - Anatomischer Anzeiger, 2009. **191**(1): p. 126-135.
2. Flemming, R.G., et al., *Effects of synthetic micro- and nano-structured surfaces on cell behavior*. Biomaterials, 1999. **20**(6): p. 573-88.
3. Curtis, A. and C. Wilkinson, *Topographical control of cells.* Biomaterials, 1997. **18**(24): p. 1573-83.
4. van Hinsbergh, V.W., *The endothelium: vascular control of haemostasis.* Eur J Obstet Gynecol Reprod Biol, 2001. **95**(2): p. 198-201.
5. Pawlowski, K.J., et al., *Endothelial cell seeding of polymeric vascular grafts.* Front Biosci, 2004. **9**: p. 1412-21.
6. Melchiorri, A.J., N. Hibino, and J.P. Fisher, *Strategies and Techniques to Enhance the In Situ Endothelialization of Small-Diameter Biodegradable Polymeric Vascular Grafts.* Tissue Engineering. Part B, Reviews, 2013. **19**(4): p. 292-307.
7. Liliensiek, S.J., et al., *Modulation of human vascular endothelial cell behaviors by nanotopographic cues.* Biomaterials, 2010. **31**(20): p. 5418-5426.
8. Thomas, C.E., A. Ehrhardt, and M.A. Kay, *Progress and problems with the use of viral vectors for gene therapy.* Nat Rev Genet, 2003. **4**(5): p. 346-58.
9. Duvall, C.L., et al., *Chapter 35 - Gene Delivery into Cells and Tissues*, in *Principles of Tissue Engineering (Fourth Edition)*, R.L.L. Vacanti, Editor. 2014, Academic Press: Boston. p. 687-723.
10. Nitta, S.K. and K. Numata, *Biopolymer-based nanoparticles for drug/gene delivery and tissue engineering.* Int J Mol Sci, 2013. **14**(1): p. 1629-54.
11. Duan, X. and Y. Li, *Physicochemical characteristics of nanoparticles affect circulation, biodistribution, cellular internalization, and trafficking.* Small, 2013. **9**(9-10): p. 1521-32.
12. Solanki, A., et al., *Nanotopography-mediated Reverse Uptake for siRNA Delivery into Neural Stem Cells to Enhance Neuronal Differentiation.* Sci. Rep., 2013. **3**.
13. Cao, H., et al., *The Effects of Nanofiber Topography on Astrocyte Behavior and Gene Silencing Efficiency.* Macromolecular Bioscience, 2012. **12**(5): p. 666-674.
14. Adler, A.F., et al., *High-throughput screening of microscale pitted substrate topographies for enhanced nonviral transfection efficiency in primary human fibroblasts.* Biomaterials, 2011. **32**(14): p. 3611-3619.
15. Totzeck, M., et al., *Semiconductor fabrication: Pushing deep ultraviolet lithography to its limits.* Nat Photon, 2007. **1**(11): p. 629-631.
16. Vieu, C., et al., *Electron beam lithography: resolution limits and applications.* Applied Surface Science, 2000. **164**(1): p. 111-117.
17. Xia, Y. and G.M. Whitesides, *Soft Lithography.* Angewandte Chemie International Edition, 1998. **37**(5): p. 550-575.

18. Whitesides, G.M., et al., *Soft lithography in biology and biochemistry.* Annu Rev Biomed Eng, 2001. **3**: p. 335-73.
19. Guo, L.J., *Nanoimprint lithography: methods and material requirements.* Advanced Materials, 2007. **19**(4): p. 495-513.
20. Schift, H., *Nanoimprint lithography: An old story in modern times? A review.* Journal of Vacuum Science & Technology B, 2008. **26**(2): p. 458-480.
21. Menon, R., et al., *Maskless lithography.* Materials Today, 2005. **8**(2): p. 26-33.
22. Kane, R.S., et al., *Patterning proteins and cells using soft lithography.* Biomaterials, 1999. **20**(23–24): p. 2363-2376.
23. Geissler, M., *4.03 - Sub-Micrometer Patterning Using Soft Lithography*, in *Comprehensive Nanoscience and Technology*, D.L.A.D.S.P. Wiederrecht, Editor. 2011, Academic Press: Amsterdam. p. 63-81.
24. Xia, Y., et al., *Complex Optical Surfaces Formed by Replica Molding Against Elastomeric Masters.* Science, 1996. **273**(5273): p. 347-9.
25. Zhao, X.-M., Y. Xia, and G.M. Whitesides, *Fabrication of three-dimensional micro-structures: Microtransfer molding.* Advanced Materials, 1996. **8**(10): p. 837-840.
26. Gates, B.D., et al., *New Approaches to Nanofabrication: Molding, Printing, and Other Techniques.* Chemical Reviews, 2005. **105**(4): p. 1171-1196.
27. Chou, S.Y., P.R. Krauss, and P.J. Renstrom, *Imprint of sub‐25 nm vias and trenches in polymers.* Applied Physics Letters, 1995. **67**(21): p. 3114-3116.
28. Krauss, P.R. and S.Y. Chou. *Sub-10 nm imprint lithography and applications*. in *Device Research Conference Digest, 1997. 5th*. 1997.
29. Austin, M.D., et al., *Fabrication of 5nm linewidth and 14nm pitch features by nanoimprint lithography.* Applied Physics Letters, 2004. **84**(26): p. 5299-5301.
30. Kooy, N., et al., *A review of roll-to-roll nanoimprint lithography.* Nanoscale Research Letters, 2014. **9**(1): p. 320-320.
31. Chong, K.S.L., Y.-Y. Lee, and H. Yee Low, *Recessed area patterning via nanoimprint lithography.* Journal of Vacuum Science & Technology B, 2011. **29**(6): p. -.
32. Zhang, F. and H.Y. Low, *Ordered three-dimensional hierarchical nanostructures by nanoimprint lithography.* Nanotechnology, 2006. **17**(8): p. 1884.
33. Benedetto, F.D., et al., *Patterning polyacrylamide hydrogels by soft lithography.* Nanotechnology, 2005. **16**(5): p. S165.
34. Kobel, S., et al., *Micropatterning of Hydrogels by Soft Embossing†.* Langmuir, 2009. **25**(15): p. 8774-8779.
35. Revzin, A., et al., *Fabrication of Poly(ethylene glycol) Hydrogel Microstructures Using Photolithography.* Langmuir, 2001. **17**(18): p. 5440-5447.
36. Shah, S.S., et al., *Micropatterning of bioactive heparin-based hydrogels.* Soft Matter, 2011. **7**(7): p. 3133-3140.

37. Yu, T. and C.K. Ober, *Methods for the Topographical Patterning and Patterned Surface Modification of Hydrogels Based on Hydroxyethyl Methacrylate.* Biomacromolecules, 2003. **4**(5): p. 1126-1131.
38. Lee, B.K., et al., *Stepwise Self-Assembly of a Protein Nanoarray from a Nanoimprinted Poly(Ethylene Glycol) Hydrogel.* Small, 2008. **4**(3): p. 342-348.
39. Rodriguez Vilches, S., et al., *Nanostructuration of soft hydrogels: synthesis and characterization of saccharidic methacrylate gels.* Colloid and Polymer Science, 2011. **289**(13): p. 1437-1449.
40. Pourciel, M.L., et al., *Development of photo-polymerisable polyvinyl alcohol for biotechnological applications.* Sensors and Actuators B: Chemical, 2003. **94**(3): p. 330-336.
41. Cheng, C.-M. and P.R. LeDuc, *Micropatterning polyvinyl alcohol as a biomimetic material through soft lithography with cell culture.* Molecular BioSystems, 2006. **2**(6-7): p. 299-304.
42. Jensen, B.E.B., et al., *Poly(vinyl alcohol) Physical Hydrogels: Noncryogenic Stabilization Allows Nano- and Microscale Materials Design.* Langmuir, 2011. **27**(16): p. 10216-10223.
43. Kawabe, T.T., D.K. MacCallum, and J.H. Lillie, *Variation in basement membrane topography in human thick skin.* Anat Rec, 1985. **211**(2): p. 142-8.
44. Abrams, G.A., et al., *Electron Microscopy of the Canine Corneal Basement Membranes.* Cells Tissues Organs, 2002. **170**(4): p. 251-257.
45. Abrams, G.A., et al., *Nanoscale topography of the basement membrane underlying the corneal epithelium of the rhesus macaque.* Cell and Tissue Research, 2000. **299**(1): p. 39-46.
46. Brody, S., et al., *Characterizing nanoscale topography of the aortic heart valve basement membrane for tissue engineering heart valve scaffold design.* Tissue Eng, 2006. **12**(2): p. 413-21.
47. Liliensiek, S.J., P. Nealey, and C.J. Murphy, *Characterization of Endothelial Basement Membrane Nanotopography in Rhesus Macaque as a Guide for Vessel Tissue Engineering.* Tissue Engineering. Part A, 2009. **15**(9): p. 2643-2651.
48. Geiger, B., J.P. Spatz, and A.D. Bershadsky, *Environmental sensing through focal adhesions.* Nat Rev Mol Cell Biol, 2009. **10**(1): p. 21-33.
49. Wozniak, M.A. and C.S. Chen, *Mechanotransduction in development: a growing role for contractility.* Nat Rev Mol Cell Biol, 2009. **10**(1): p. 34-43.
50. Yamamoto, S., et al., *Effect of Honeycomb-Patterned Surface Topography on the Adhesion and Signal Transduction of Porcine Aortic Endothelial Cells.* Langmuir, 2007. **23**(15): p. 8114-8120.
51. Lu, J., et al., *Improved endothelial cell adhesion and proliferation on patterned titanium surfaces with rationally designed, micrometer to nanometer features.* Acta biomaterialia, 2008. **4**(1): p. 192-201.
52. Thapa, A., T.J. Webster, and K.M. Haberstroh, *Polymers with nano-dimensional surface features enhance bladder smooth muscle cell adhesion.* Journal of Biomedical Materials Research Part A, 2003. **67A**(4): p. 1374-1383.

53. Wong, S., et al., *Anisotropic rigidity sensing on grating topography directs human mesenchymal stem cell elongation.* Biomechanics and Modeling in Mechanobiology, 2014. **13**(1): p. 27-39.
54. Uttayarat, P., et al., *Topographic guidance of endothelial cells on silicone surfaces with micro- to nanogrooves: Orientation of actin filaments and focal adhesions.* Journal of Biomedical Materials Research Part A, 2005. **75A**(3): p. 668-680.
55. Muhammad, R., et al., *Sub-100 nm patterning of TiO2 film for the regulation of endothelial and smooth muscle cell functions.* Biomaterials Science, 2014. **2**(12): p. 1740-1749.
56. Tan, K.K.B., et al., *Enhanced differentiation of neural progenitor cells into neurons of the mesencephalic dopaminergic subtype on topographical patterns.* Biomaterials, 2015. **43**(0): p. 32-43.
57. Moe, A.A.K., et al., *Microarray with Micro- and Nano-topographies Enables Identification of the Optimal Topography for Directing the Differentiation of Primary Murine Neural Progenitor Cells.* Small, 2012. **8**(19): p. 3050-3061.
58. Ankam, S., et al., *Substrate topography and size determine the fate of human embryonic stem cells to neuronal or glial lineage.* Acta Biomaterialia, 2013. **9**(1): p. 4535-4545.
59. Shi, Z., et al., *Enhanced endothelial differentiation of adipose-derived stem cells by substrate nanotopography.* Journal of Tissue Engineering and Regenerative Medicine, 2014. **8**(1): p. 50-58.
60. Jeon, H., et al., *The effect of micronscale anisotropic cross patterns on fibroblast migration.* Biomaterials, 2010. **31**(15): p. 4286-4295.
61. Then, K.Y., et al., *Effect of Microtopographical Cues on Human Keratocyte Orientation and Gene Expression.* Current Eye Research, 2011. **36**(2): p. 88-93.
62. Al-Haque, S., et al., *Hydrogel Substrate Stiffness and Topography Interact to Induce Contact Guidance in Cardiac Fibroblasts.* Macromolecular Bioscience, 2012. **12**(10): p. 1342-1353.
63. Du, X., et al., *Guiding the behaviors of human umbilical vein endothelial cells with patterned silk fibroin films.* Colloids and Surfaces B: Biointerfaces, 2014. **122**(0): p. 79-84.
64. Singh, A.V., et al., *Astrocytes Increase ATP Exocytosis Mediated Calcium Signaling in Response to Microgroove Structures.* Scientific Reports, 2015. **5**: p. 7847.
65. Klymov, A., et al., *Nanogrooved Surface-Patterns induce cellular organization and axonal outgrowth in neuron-like PC12-Cells.* Hearing Research, 2015. **320**(0): p. 11-17.
66. Mobasseri, S.A., G. Terenghi, and S. Downes, *Schwann cell interactions with polymer films are affected by groove geometry and film hydrophilicity.* Biomedical Materials, 2014. **9**(5): p. 055004.
67. Trichet, L., et al., *Evidence of a large-scale mechanosensing mechanism for cellular adaptation to substrate stiffness.* Proceedings of the National Academy of Sciences, 2012. **109**(18): p. 6933-6938.
68. Kim, E., et al., *Response of bone marrow derived connective tissue progenitor cell morphology and proliferation on geometrically modulated microtextured substrates.* Biomedical Microdevices, 2013. **15**(3): p. 385-396.

69. Kim, E.J., et al., *Post microtextures accelerate cell proliferation and osteogenesis.* Acta Biomaterialia, 2010. **6**(1): p. 160-169.
70. Wu, Y.-N., et al., *Substrate topography determines the fate of chondrogenesis from human mesenchymal stem cells resulting in specific cartilage phenotype formation.* Nanomedicine: Nanotechnology, Biology and Medicine, 2014. **10**(7): p. 1507-1516.
71. Turner, A.M.P., et al., *Attachment of astroglial cells to microfabricated pillar arrays of different geometries.* Journal of Biomedical Materials Research, 2000. **51**(3): p. 430-441.
72. Kidambi, S., et al., *Cell Adhesion on Polyelectrolyte Multilayer Coated Polydimethylsiloxane Surfaces with Varying Topographies.* Tissue engineering, 2007. **13**(8): p. 2105-2117.
73. Dickinson, L.E., et al., *Endothelial cell responses to micropillar substrates of varying dimensions and stiffness.* Journal of Biomedical Materials Research. Part a, 2012. **100**(6): p. 1457-1466.
74. Gallagher, J.O., et al., *Interaction of animal cells with ordered nanotopography.* NanoBioscience, IEEE Transactions on, 2002. **1**(1): p. 24-28.
75. Schmidt, J.A. and A.F. von Recum, *Texturing of polymer surfaces at the cellular level.* Biomaterials, 1991. **12**(4): p. 385-389.
76. Wan, Y., et al., *Adhesion and proliferation of OCT-1 osteoblast-like cells on micro- and nano-scale topography structured poly(l-lactide).* Biomaterials, 2005. **26**(21): p. 4453-4459.
77. Berry, C.C., et al., *The influence of microscale topography on fibroblast attachment and motility.* Biomaterials, 2004. **25**(26): p. 5781-5788.
78. Meehan, S. and Amrinder S. Nain, *Role of Suspended Fiber Structural Stiffness and Curvature on Single-Cell Migration, Nucleus Shape, and Focal-Adhesion-Cluster Length.* Biophysical Journal, 2014. **107**(11): p. 2604-2611.
79. Hosseini, V., et al., *Fiber-Assisted Molding (FAM) of Surfaces with Tunable Curvature to Guide Cell Alignment and Complex Tissue Architecture.* Small, 2014. **10**(23): p. 4851-4857.
80. Park, J.Y., et al., *Study of cellular behaviors on concave and convex microstructures fabricated from elastic PDMS membranes.* Lab Chip, 2009. **9**(14): p. 2043-9.
81. Meyle, J., K. Gultig, and W. Nisch, *Variation in contact guidance by human cells on a microstructured surface.* J Biomed Mater Res, 1995. **29**(1): p. 81-8.
82. Engler, A.J., et al., *Matrix Elasticity Directs Stem Cell Lineage Specification.* Cell, 2006. **126**(4): p. 677-689.
83. Kong, H.J., et al., *Non-viral gene delivery regulated by stiffness of cell adhesion substrates.* Nat Mater, 2005. **4**(6): p. 460-4.
84. Sakakura, K., et al., *Pathophysiology of atherosclerosis plaque progression.* Heart Lung Circ, 2013. **22**(6): p. 399-411.
85. Rubanyi, G.M., *The role of endothelium in cardiovascular homeostasis and diseases.* J Cardiovasc Pharmacol, 1993. **22 Suppl 4**: p. S1-14.
86. Campbell, J.B., J.L. Glover, and B. Herring, *The influence of endothelial seeding and platelet inhibition on the patency of ePTFE*

grafts used to replace small arteries--an experimental study. Eur J Vasc Surg, 1988. **2**(6): p. 365-70.

87. Sauvage, L.R., et al., *Current arterial prostheses. Experimental evaluation by implantation in the carotid and circumflex coronary arteries of the dog.* Arch Surg, 1979. **114**(6): p. 687-91.
88. Herring, M., A. Gardner, and J. Glover, *A single-staged technique for seeding vascular grafts with autogenous endothelium.* Surgery, 1978. **84**(4): p. 498-504.
89. Mazzucotelli, J.P., et al., *A new device for endothelial cell seeding of a small-caliber vascular prosthesis.* Artif Organs, 1993. **17**(9): p. 787-90.
90. van Wachem, P.B., et al., *Vacuum cell seeding: a new method for the fast application of an evenly distributed cell layer on porous vascular grafts.* Biomaterials, 1990. **11**(8): p. 602-6.
91. Bowlin, G.L. and S.E. Rittgers, *Electrostatic endothelial cell seeding technique for small-diameter (<6 mm) vascular prostheses: feasibility testing.* Cell Transplant, 1997. **6**(6): p. 623-9.
92. Fields, C., et al., *Evaluation of electrostatically endothelial cell seeded expanded polytetrafluoroethylene grafts in a canine femoral artery model.* J Biomater Appl, 2002. **17**(2): p. 135-52.
93. Poirier-Quinot, M., et al., *High-resolution 1.5-Tesla magnetic resonance imaging for tissue-engineered constructs: a noninvasive tool to assess three-dimensional scaffold architecture and cell seeding.* Tissue Eng Part C Methods, 2010. **16**(2): p. 185-200.
94. Rosenman, J.E., et al., *Kinetics of endothelial cell seeding.* J Vasc Surg, 1985. **2**(6): p. 778-84.
95. Kempczinski, R.F., et al., *Thrombogenicity of a fibronectin-coated, experimental polytetrafluoroethylene graft.* Surgery, 1987. **101**(4): p. 439-44.
96. Yates, S.G., et al., *The preclotting of porous arterial prostheses.* Ann Surg, 1978. **188**(5): p. 611-22.
97. Schmedlen, R.H., et al., *Tissue engineered small-diameter vascular grafts.* Clin Plast Surg, 2003. **30**(4): p. 507-17.
98. Berglund, J.D. and Z.S. Galis, *Designer blood vessels and therapeutic revascularization.* British Journal of Pharmacology, 2003. **140**(4): p. 627-636.
99. Jaganathan, S.K., et al., *Biomaterials in Cardiovascular Research: Applications and Clinical Implications.* BioMed Research International, 2014. **2014**: p. 459465.
100. Tan, A., et al., *Surface modification of a polyhedral oligomeric silsesquioxane poly(carbonate-urea) urethane (POSS-PCU) nanocomposite polymer as a stent coating for enhanced capture of endothelial progenitor cells.* Biointerphases, 2013. **8**(1): p. 23.
101. Edlund, U., T. Sauter, and A.C. Albertsson, *Covalent VEGF protein immobilization on resorbable polymeric surfaces.* Polymers for Advanced Technologies, 2011. **22**(1): p. 166-171.
102. Conklin, B.S., et al., *Basic Fibroblast Growth Factor Coating and Endothelial Cell Seeding of a Decellularized Heparin-coated Vascular Graft.* Artificial Organs, 2004. **28**(7): p. 668-675.

103. Shin, Y.M., et al., *Mussel-Inspired Immobilization of Vascular Endothelial Growth Factor (VEGF) for Enhanced Endothelialization of Vascular Grafts.* Biomacromolecules, 2012. **13**(7): p. 2020-2028.
104. Cooke, J.P., *Flow, NO, and atherogenesis.* Proceedings of the National Academy of Sciences, 2003. **100**(3): p. 768-770.
105. Förstermann, U. and T. Münzel, *Endothelial Nitric Oxide Synthase in Vascular Disease: From Marvel to Menace.* Circulation, 2006. **113**(13): p. 1708-1714.
106. Di Rienzo, C., et al., *Unveiling LOX-1 receptor interplay with nanotopography: mechanotransduction and atherosclerosis onset.* Sci. Rep., 2013. **3**.
107. Palmaz, J.C., A. Benson, and E.A. Sprague, *Influence of Surface Topography on Endothelialization of Intravascular Metallic Material.* Journal of Vascular and Interventional Radiology, 1999. **10**(4): p. 439-444.
108. Ganta, S., et al., *A review of stimuli-responsive nanocarriers for drug and gene delivery.* Journal of Controlled Release, 2008. **126**(3): p. 187-204.
109. De Jong, W.H. and P.J.A. Borm, *Drug delivery and nanoparticles: Applications and hazards.* International Journal of Nanomedicine, 2008. **3**(2): p. 133-149.
110. Yin, R.-X., D.-Z. Yang, and J.-Z. Wu, *Nanoparticle Drug- and Gene-eluting Stents for the Prevention and Treatment of Coronary Restenosis.* Theranostics, 2014. **4**(2): p. 175-200.
111. Adler, A.F. and K.W. Leong, *Emerging links between surface nanotechnology and endocytosis: impact on nonviral gene delivery.* Nano Today, 2010. **5**(6): p. 553-569.
112. Wiethoff, C.M. and C.R. Middaugh, *Barriers to nonviral gene delivery.* Journal of Pharmaceutical Sciences, 2003. **92**(2): p. 203-217.
113. Doherty, G.J. and H.T. McMahon, *Mechanisms of endocytosis.* Annu Rev Biochem, 2009. **78**: p. 857-902.
114. Le Roy, C. and J.L. Wrana, *Clathrin-and non-clathrin-mediated endocytic regulation of cell signalling.* Nature reviews Molecular cell biology, 2005. **6**(2): p. 112-126.
115. Cohen, A.W., et al., *Role of caveolae and caveolins in health and disease.* Physiological reviews, 2004. **84**(4): p. 1341-1379.
116. Orlandi, P.A. and P.H. Fishman, *Filipin-dependent Inhibition of Cholera Toxin: Evidence for Toxin Internalization and Activation through Caveolae-like Domains.* The Journal of Cell Biology, 1998. **141**(4): p. 905-915.
117. Pelkmans, L., J. Kartenbeck, and A. Helenius, *Caveolar endocytosis of simian virus 40 reveals a new two-step vesicular-transport pathway to the ER.* Nat Cell Biol, 2001. **3**(5): p. 473-483.
118. Rejman, J., A. Bragonzi, and M. Conese, *Role of clathrin- and caveolae-mediated endocytosis in gene transfer mediated by lipo- and polyplexes.* Mol Ther, 2005. **12**(3): p. 468-74.
119. Rejman, J., et al., *Size-dependent internalization of particles via the pathways of clathrin- and caveolae-mediated endocytosis.* Biochem J, 2004. **377**(Pt 1): p. 159-69.

120. Hess, G.T., et al., *Cellular binding, motion, and internalization of synthetic gene delivery polymers.* Biochim Biophys Acta, 2007. **1773**(10): p. 1583-8.
121. Almofti, M.R., et al., *Lipoplex size determines lipofection efficiency with or without serum.* Mol Membr Biol, 2003. **20**(1): p. 35-43.
122. He, C., et al., *Effects of particle size and surface charge on cellular uptake and biodistribution of polymeric nanoparticles.* Biomaterials, 2010. **31**(13): p. 3657-66.
123. Almofti, M.R., et al., *Cationic liposome-mediated gene delivery: biophysical study and mechanism of internalization.* Arch Biochem Biophys, 2003. **410**(2): p. 246-53.
124. Rolland, J.P., et al., *Direct fabrication and harvesting of monodisperse, shape-specific nanobiomaterials.* J Am Chem Soc, 2005. **127**(28): p. 10096-100.
125. Glangchai, L.C., et al., *Nanoimprint lithography based fabrication of shape-specific, enzymatically-triggered smart nanoparticles.* Journal of Controlled Release, 2008. **125**(3): p. 263-272.
126. Agarwal, R., et al., *Scalable Imprinting of Shape-Specific Polymeric Nanocarriers Using a Release Layer of Switchable Water Solubility.* ACS Nano, 2012. **6**(3): p. 2524-2531.
127. Gratton, S.E., et al., *The effect of particle design on cellular internalization pathways.* Proc Natl Acad Sci U S A, 2008. **105**(33): p. 11613-8.
128. Agarwal, R., et al., *Mammalian cells preferentially internalize hydrogel nanodiscs over nanorods and use shape-specific uptake mechanisms.* Proceedings of the National Academy of Sciences, 2013. **110**(43): p. 17247-17252.
129. Yoo, J.W., N. Doshi, and S. Mitragotri, *Endocytosis and Intracellular Distribution of PLGA Particles in Endothelial Cells: Effect of Particle Geometry.* Macromol Rapid Commun, 2010. **31**(2): p. 142-8.
130. Zhang, Y., et al., *Permission to Enter Cell by Shape: Nanodisk vs Nanosphere.* ACS Applied Materials & Interfaces, 2012. **4**(8): p. 4099-4105.
131. Barua, S., et al., *Particle shape enhances specificity of antibody-displaying nanoparticles.* Proc Natl Acad Sci U S A, 2013. **110**(9): p. 3270-5.
132. Sharma, G., et al., *Polymer particle shape independently influences binding and internalization by macrophages.* J Control Release, 2010. **147**(3): p. 408-12.
133. Dalby, M.J., et al., *Attempted endocytosis of nano-environment produced by colloidal lithography by human fibroblasts.* Exp Cell Res, 2004. **295**(2): p. 387-94.
134. Teo, B.K.K., et al., *The effect of micro and nanotopography on endocytosis in drug and gene delivery systems.* Biomaterials, 2011. **32**(36): p. 9866-9875.
135. Yim, E.K.F., et al., *Nanopattern-induced changes in morphology and motility of smooth muscle cells.* Biomaterials, 2005. **26**(26): p. 5405-5413.

136. Miller, D.C., et al., *Endothelial and vascular smooth muscle cell function on poly(lactic-co-glycolic acid) with nano-structured surface features.* Biomaterials, 2004. **25**(1): p. 53-61.
137. Bourke, S., et al., *A photo-crosslinked poly(vinyl alcohol) hydrogel growth factor release vehicle for wound healing applications.* AAPS PharmSci, 2003. **5**(4): p. 101-111.
138. Jiang, Y., et al., *In-vivo studies on intraperitoneally administrated poly(vinyl alcohol).* Journal of Biomedical Materials Research Part B: Applied Biomaterials, 2010. **93B**(1): p. 275-284.
139. Chaouat, M., et al., *A Novel Cross-linked Poly(vinyl alcohol) (PVA) for Vascular Grafts.* Advanced Functional Materials, 2008. **18**(19): p. 2855-2861.
140. Krumova, M., et al., *Effect of crosslinking on the mechanical and thermal properties of poly(vinyl alcohol).* Polymer, 2000. **41**(26): p. 9265-9272.
141. Mansur, H.S., et al., *FTIR spectroscopy characterization of poly (vinyl alcohol) hydrogel with different hydrolysis degree and chemically crosslinked with glutaraldehyde.* Materials Science and Engineering: C, 2008. **28**(4): p. 539-548.
142. Ino, J.M., et al., *Evaluation of hemocompatibility and endothelialization of hybrid poly(vinyl alcohol) (PVA)/gelatin polymer films.* Journal of Biomedical Materials Research Part B: Applied Biomaterials, 2013. **101**(8): p. 1549-1559.
143. Ino, J.M., et al., *Plasma functionalization of poly(vinyl alcohol) hydrogel for cell adhesion enhancement.* Biomatter, 2013. **3**(4): p. e25414.
144. Suh, K.Y. and H.H. Lee, *Capillary Force Lithography: Large-Area Patterning, Self-Organization, and Anisotropic Dewetting.* Advanced Functional Materials, 2002. **12**(6-7): p. 405-413.
145. Schulte, V.A., et al., *Surface Topography Induces Fibroblast Adhesion on Intrinsically Nonadhesive Poly(ethylene glycol) Substrates.* Biomacromolecules, 2009. **10**(10): p. 2795-2801.
146. de Mel, A., et al., *Development of cardiovascular bypass grafts: endothelialization and applications of nanotechnology.* Expert Review of Cardiovascular Therapy, 2008. **6**(9): p. 1259-1277.
147. Lovmand, J., et al., *The use of combinatorial topographical libraries for the screening of enhanced osteogenic expression and mineralization.* Biomaterials, 2009. **30**(11): p. 2015-2022.
148. Unadkat, H.V., et al., *An algorithm-based topographical biomaterials library to instruct cell fate.* Proceedings of the National Academy of Sciences of the United States of America, 2011. **108**(40): p. 16565-16570.
149. Peng, L., et al., *The effect of TiO2 nanotubes on endothelial function and smooth muscle proliferation.* Biomaterials, 2009. **30**(7): p. 1268-1272.
150. Giacca, M. and S. Zacchigna, *VEGF gene therapy: therapeutic angiogenesis in the clinic and beyond.* Gene Ther, 2012. **19**(6): p. 622-9.
151. Nečas, D. and P. Klapetek, *Gwyddion: an open-source software for SPM data analysis.* Open Physics, 2012. **10**(1): p. 181-188.

152. Mann, H.B. and D.R. Whitney, *On a test of whether one of two random variables is stochastically larger than the other.* The annals of mathematical statistics, 1947: p. 50-60.
153. Berrier, A.L. and K.M. Yamada, *Cell–matrix adhesion.* Journal of Cellular Physiology, 2007. **213**(3): p. 565-573.
154. Kanchanawong, P., et al., *Nanoscale architecture of integrin-based cell adhesions.* Nature, 2010. **468**(7323): p. 580-584.
155. Choi, C.K., et al., *Actin and α-actinin orchestrate the assembly and maturation of nascent adhesions in a myosin II motor-independent manner.* Nature cell biology, 2008. **10**(9): p. 1039-1050.
156. Cai, Y., et al., *Cytoskeletal coherence requires myosin-IIA contractility.* Journal of Cell Science, 2010. **123**(3): p. 413-423.
157. Watt, F.M., P.W. Jordan, and C.H. O'Neill, *Cell shape controls terminal differentiation of human epidermal keratinocytes.* Proceedings of the National Academy of Sciences, 1988. **85**(15): p. 5576-5580.
158. Chen, C.S., et al., *Micropatterned Surfaces for Control of Cell Shape, Position, and Function.* Biotechnology Progress, 1998. **14**(3): p. 356-363.
159. Cutiongco, M.F.A., et al., *Composite Scaffold of Poly(Vinyl Alcohol) and Interfacial Polyelectrolyte Complexation Fibers for Controlled Biomolecule Delivery.* Frontiers in Bioengineering and Biotechnology, 2015. **3**: p. 3.
160. Fuard, D., et al., *Optimization of poly-di-methyl-siloxane (PDMS) substrates for studying cellular adhesion and motility.* Microelectron. Eng., 2008. **85**(5-6): p. 1289-1293.
161. Wang, Z., A.A. Volinsky, and N.D. Gallant, *Crosslinking effect on polydimethylsiloxane elastic modulus measured by custom-built compression instrument.* Journal of Applied Polymer Science, 2014. **131**(22): p. n/a-n/a.
162. Irwin, E., et al., *Modulus-dependent macrophage adhesion and behavior*. Journal of Biomaterials Science, Polymer Edition, 2008. **19**(10): p. 1363-1382.
163. Saunders, R.L. and D.A. Hammer, *Assembly of Human Umbilical Vein Endothelial Cells on Compliant Hydrogels.* Cellular and molecular bioengineering, 2010. **3**(1): p. 60-67.
164. Heng, B.C., et al., *Effect of cell-seeding density on the proliferation and gene expression profile of human umbilical vein endothelial cells within ex vivo culture.* Cytotherapy, 2011. **13**(5): p. 606-617.
165. Dalby, B., et al., *Advanced transfection with Lipofectamine 2000 reagent: primary neurons, siRNA, and high-throughput applications.* Methods, 2004. **33**(2): p. 95-103.
166. Medina-Kauwe, L.K., J. Xie, and S. Hamm-Alvarez, *Intracellular trafficking of nonviral vectors.* Gene Ther, 2005. **12**(24): p. 1734-51.
167. Fasbender, A., et al., *A low rate of cell proliferation and reduced DNA uptake limit cationic lipid-mediated gene transfer to primary cultures of ciliated human airway epithelia.* Gene therapy, 1997. **4**(11): p. 1173-1180.
168. Kustandi, T.S., et al., *Mimicking Domino-Like Photonic Nanostructures on Butterfly Wings.* Small, 2009. **5**(5): p. 574-578.

169. Kerr, M.C. and R.D. Teasdale, *Defining macropinocytosis.* Traffic, 2009. **10**(4): p. 364-71.
170. Miaczynska, M. and H. Stenmark, *Mechanisms and functions of endocytosis.* J Cell Biol, 2008. **180**(1): p. 7-11.
171. Rejman, J., M. Conese, and D. Hoekstra, *Gene transfer by means of lipo- and polyplexes: role of clathrin and caveolae-mediated endocytosis.* J Liposome Res, 2006. **16**(3): p. 237-47.
172. Cai, J., et al., *Effect of Chain Length on Cytotoxicity and Endocytosis of Cationic Polymers.* Macromolecules, 2011. **44**(7): p. 2050-2057.
173. Maniak, M., *Conserved features of endocytosis in Dictyostelium*, in *International Review of Cytology*, W.J. Kwang, Editor. 2002, Academic Press. p. 257-287.
174. Caswell, P.T., et al., *Rab25 associates with alpha5beta1 integrin to promote invasive migration in 3D microenvironments.* Dev Cell, 2007. **13**(4): p. 496-510.
175. Cheng, K.W., et al., *The RAB25 small GTPase determines aggressiveness of ovarian and breast cancers.* Nat Med, 2004. **10**(11): p. 1251-6.
176. Kim, D.H., et al., *Mechanosensitivity of fibroblast cell shape and movement to anisotropic substratum topography gradients.* Biomaterials, 2009. **30**(29): p. 5433-44.
177. Lamers, E., et al., *The influence of nanoscale topographical cues on initial osteoblast morphology and migration.* Eur Cell Mater, 2010. **20**: p. 329-43.
178. Yim, E.K., et al., *Nanotopography-induced changes in focal adhesions, cytoskeletal organization, and mechanical properties of human mesenchymal stem cells.* Biomaterials, 2010. **31**(6): p. 1299-306.
179. Chao, W.T. and J. Kunz, *Focal adhesion disassembly requires clathrin-dependent endocytosis of integrins.* FEBS Lett, 2009. **583**(8): p. 1337-43.
180. Gu, Z., et al., *Integrins traffic rapidly via circular dorsal ruffles and macropinocytosis during stimulated cell migration.* J Cell Biol, 2011. **193**(1): p. 61-70.
181. Lee, J.W., et al., *Effects of surface nano-topography on human osteoblast filopodia.* Anal Sci, 2011. **27**(4): p. 369.
182. Haleem-Smith, H., et al., *Optimization of high-efficiency transfection of adult human mesenchymal stem cells in vitro.* Mol Biotechnol, 2005. **30**(1): p. 9-20.
183. Lord, M.S., et al., *The effect of silica nanoparticulate coatings on serum protein adsorption and cellular response.* Biomaterials, 2006. **27**(28): p. 4856-62.
184. Tseng, S.j., C.-J. Chuang, and S.-C. Tang, *Electrostatic immobilization of DNA polyplexes on small intestinal submucosa for tissue substrate-mediated transfection.* Acta Biomaterialia, 2008. **4**(4): p. 799-807.
185. Yim, E.K., S.W. Pang, and K.W. Leong, *Synthetic nanostructures inducing differentiation of human mesenchymal stem cells into neuronal lineage.* Exp Cell Res, 2007. **313**(9): p. 1820-9.
186. Dalby, M.J., et al., *Fibroblast signaling events in response to nanotopography: a gene array study.* IEEE Trans Nanobioscience, 2002. **1**(1): p. 12-7.

187. Dalby, M.J., N. Gadegaard, and C.D. Wilkinson, *The response of fibroblasts to hexagonal nanotopography fabricated by electron beam lithography.* J Biomed Mater Res A, 2008. **84**(4): p. 973-9.
188. Liu, A.P., et al., *Global and local regulation of clathrin-coated pit dynamics detected on patterned substrates.* Biophys J, 2009. **97**(4): p. 1038-47.
189. Mattila, P.K. and P. Lappalainen, *Filopodia: molecular architecture and cellular functions.* Nat Rev Mol Cell Biol, 2008. **9**(6): p. 446-54.
190. Davenport, R.W., et al., *A sensory role for neuronal growth cone filopodia.* Nature, 1993. **361**(6414): p. 721-4.